MONTE CARLO METHODS, MODELS, AND APPLICATIONS FOR THE ADVANCED NEUTRON SOURCE

by

EVERETT LEE REDMOND II

SUBMITTED TO THE DEPARTMENT OF
NUCLEAR ENGINEERING
IN PARTIAL FULFILLMENT OF THE REQUIREMENTS
FOR THE DEGREES OF
BACHELOR OF SCIENCE
AND
MASTER OF SCIENCE
IN NUCLEAR ENGINEERING

at the

MASSACHUSETTS INSTITUTE OF TECHNOLOGY
June 1990

Signature of Author _____
Department of Nuclear Engineering
May 20, 1990

Certified by _____
Dr. Allan Henry
Professor of Nuclear Engineering
Thesis Supervisor

Accepted by _____
Dr. Allan Henry, Chairman
Committee on Graduate Students
Department of Nuclear Engineering

MONTE CARLO METHODS, MODELS, AND APPLICATIONS FOR THE ADVANCED NEUTRON SOURCE

by

EVERETT L. REDMOND II

Submitted to the Department of Nuclear Engineering
on May 1, 1990 in partial fulfillment of the
requirements for the Degrees of
Bachelor of Science and Master of Science in
Nuclear Engineering

ABSTRACT

A three-dimensional continuous-energy coupled neutron-gamma Monte Carlo model of the Advanced Neutron Source final preconceptual reference core design has been developed using MCNP Version 3b. This model contains the reactor core with control rods, the heavy water reflector tank with shutdown rods and some beam tubes, and the outer light water pool. Eighty homogenized fuel zones per fuel element are used to represent the radial and axial U-235 fuel grading. This model is the most sophisticated, physically accurate reactor physics model of the Advanced Neutron Source currently available. The purpose of this thesis is to demonstrate the MCNP methods and applications for the Advanced Neutron Source. Beam tube studies, coolant voiding studies, and many criticality studies have already been performed. Studies with variance reduction techniques have also been performed. In comparison to deterministic methods, MCNP proves superior in calculating the core multiplication factor and neutron fluxes in the reflector. MCNP offers the Advanced Neutron Source project the capability of performing complicated reactor physics calculations not currently possible with most deterministic methods.

Thesis Supervisor: Dr. Allan Henry
Title: Professor of Nuclear Engineering

ACKNOWLEDGMENTS

I would like to thank Dr. John Ryskamp of the Idaho National Engineering Laboratory for his guidance and thoughtful comments during my employment with EG&G Idaho and during the preparation of this thesis. I am also thankful to Dr. Ryskamp for performing all PDQ calculations and providing the general description of the Advanced Neutron Source, which is found in Chapter 1.

I am very grateful to Joanie Reseigh for typing this thesis and my many corrections. Without her help and understanding I would not have been able to complete this document.

I would like to thank Professor Allan Henry for being my thesis supervisor at MIT. I also thank Professor Jacquelyn Yanch for permitting me to use her computers to finish my MCNP runs.

The Los Alamos National Laboratory X-6 Group provided valuable assistance in the use MCNP. They also made several suggestions to reduce the variances in the Advanced Neutron Source models.

The Advanced Neutron Source Project Office at Oak Ridge National Laboratory provided the funding to support this research. Most of this work was performed under the auspices of the U. S. Department of Energy under DOE Contract No. DE-AC07-76ID01570.

Finally I would like to thank EG&G Idaho, Inc. for participating in the MIT Engineering Internship Program.

SUMMARY

A three-dimensional, continuous-energy, coupled neutron-gamma Monte Carlo model of the Advanced Neutron Source (ANS) final preconceptual reference core design[1] has been developed using MCNP Version 3b.[2] This model contains the reactor core with control rods, the heavy water reflector tank with shutdown rods and representative beam tubes, and the outer light water pool. Eighty homogenized fuel zones per fuel element are used to represent the radial and axial U-235 fuel grading.

A major advantage of MCNP over other neutronics codes is the continuous-energy cross section data available for each isotope. This energy representation eliminates the errors in formulating few-group cross sections. MCNP also offers a transport solution that is more accurate than diffusion theory. Earlier studies with S_n transport theory demonstrated some diffusion theory inadequacies.[3] The MCNP results reinforce the multigroup S_n transport theory trends.

Table 1 presents the results of various neutronic studies performed with MCNP models and PDQ-7[4] two-dimensional, four-group, diffusion theory models. The MCNP models contain four hafnium control rods in the central hole of the ANS. The rods are homogenized in the r-z geometry of PDQ. These rods are withdrawn upward during normal operation and inserted downward during scram.

The Monte Carlo versus diffusion theory discrepancies are illustrated in Table 1. MCNP is 3.5% lower on its prediction of the core multiplication factor compared to PDQ-7 for the base case models. PDQ predicts the change in core multiplication factors due to full control rod insertion and insertion to core midplane to be -0.1307 and -0.2235, respectively. MCNP predicts the same values to be -0.1169 and -0.2191. These results indicate that PDQ estimates reasonable control rod bank worths, even though the absolute core multiplication factors are too high.

TABLE 1. ADVANCED NEUTRON SOURCE CHARACTERISTICS AT BEGINNING OF CYCLE

Description[a]	Core Multiplication Factor	
	PDQ-7	MCNP-3b
Base case without control or reflector shutdown rods	1.1608	1.1205 ± 0.0045[b]
Control rods fully withdrawn to 100 mm above top element		1.1162 ± 0.0040
Control rods inserted to core midplane	1.0301	1.0036 ± 0.0040
Control rods fully inserted	0.9373	0.9014 ± 0.0032
8 reflector shutdown rods fully inserted, no control rods		0.8568 ± 0.0030
	Peak Thermal Neutron Flux[c] (10^{19} m^{-2} s^{-1})	
	PDQ-7	MCNP-3b
Control rods inserted to core midplane	7.3527	7.9225 ± 0.1426
		Coupled-Neutron Gamma Heating[d] (W/g)
Peak heating in Al-6061 core pressure boundary tube for control rods fully inserted		29.8559 ± 0.4060
Average heating in the hafnium portion of the control rods for control rods fully inserted		48.8016 ± 0.3807

a. All results are for a reactor power of 350 MW fission.
b. The statistical uncertainties reported with all MCNP calculations represent one standard deviation.
c. Thermal flux energy boundaries are 0.0 eV < E < 0.683 eV.
d. Since this is a fresh core, fission product gammas are not accounted for.

Table 1 also presents the peak thermal neutron flux in the D_2O reflector as calculated by MCNP and PDQ. MCNP predicts a flux peak 7.7% higher than PDQ. Flux predictions within the fuel elements also differ between MCNP and PDQ. MCNP consistently predicts higher fast and thermal fluxes and lower epithermal fluxes than PDQ. These differences may be large enough to warrant concern for some reactor parameters calculated with PDQ.

The flux values in the target irradiation positions, which are next to the upper and lower fuel elements, differ when calculated with PDQ and MCNP. In the upper target region, PDQ predicts a thermal flux value 48% lower than MCNP. The fast flux is also depressed by 31%. In the lower target region PDQ predicts the thermal flux value 24% lower than MCNP. The fast flux value is depressed by 12%. These results indicate that diffusion theory has its most difficult times when the fluxes are changing very rapidly, such as from the fuel to the heavy water reflector, as expected at boundaries between very high and very low absorbing materials.

MCNP has also been used to compute the microscopic U-235 cross sections as a function of position in the fuel. The cross sections are quite different from those used in PDQ, which were calculated for earlier ANS designs. The MCNP-generated cross sections were used to modify the PDQ U-235 cross section sets. This modification slightly improved the MCNP versus PDQ comparisons, indicating the importance of accurate cross sections within PDQ.

MCNP performs coupled neutron-gamma heating calculations in any material for which heating information is available. Table 1 lists the combined neutron-gamma heat in the peak region of the Al-6061 core pressure boundary tube (CPBT), as well as the average heating of the hafnium portion of a fully inserted control rod. The primary heating in both cases is caused by gammas. These values are at beginning of cycle without fission product gammas. When these gammas are accounted for, the values are expected to increase significantly.

Beam tube studies, coolant voiding studies, and many criticality studies have also been performed.

Variance reduction techniques have been used in an attempt to improve the run time efficiency. The primary tools in this effort were energy and spatially dependent weight windows. These weight windows were calculated with the weight window generator within MCNP.[2,5,6] A 45% increase in the run time efficiency was realized when the weight windows were employed. However, some discrepancies in the D_2O reflector flux values were noticed when a comparison was made to the base case without weight windows. Further study will have to be performed to determine the cause of these discrepancies.

TABLE OF CONTENTS

LIST OF TABLES

LIST OF FIGURES

CHAPTER 1. INTRODUCTION

The general description of the Advanced Neutron Source presented in this chapter is a summary of the description presented by Dr. John Ryskamp, Idaho National Engineering Laboratory (INEL), in an article submitted to Nuclear Technology. Dr. Ryskamp also performed all non-MCNP calculations cited within this thesis.

An Advanced Neutron Source (ANS) with a peak thermal neutron flux of about 8.5×10^{19} $m^{-2}s^{-1}$ is being designed for condensed matter physics, materials science, isotope production, and fundamental physics research. The ANS is a new reactor-based research facility being planned by Oak Ridge National Laboratory (ORNL) to meet the need for an intense steady-state source of neutrons.[7,8] The design effort is currently in the conceptual phase. A reference reactor design has been selected in order to examine the safety, performance, and costs associated with this one design. Modifications to this design will be made during this conceptual design phase as our research and development effort identifies further improvements and verifies some of the calculated parameters through experiments.

The purpose of this thesis is to demonstrate the advantages that the Monte Carlo Neutron and Photon transport code MCNP-3b[2] offers for the analysis of the Advanced Neutron Source. The Monte Carlo methodology in modelling the ANS is fully discussed and comparisons with diffusion theory are made where appropriate.

Monte Carlo offers a full three-dimensional modelling. Continuous-energy cross section data is used for the coupled neutron-gamma transport. These advantages make Monte Carlo superior to diffusion theory in the reactor physics modelling of the ANS. Monte Carlo is a statistical method of neutron transport and therefore, some calculational problems exist. In order to obtain reasonably low standard deviations for calculated values, it is necessary to use up to five hours of CRAY time per problem. This can easily be cost

prohibitive. Therefore some variance reduction techniques have been employed. Their effectiveness is discussed in this thesis.

The three dimensional capability permits physically accurate modelling of the control rods, reflector shutdown rods, and beam tubes. Various studies have been performed with these models. These include the following areas: control rod worth studies, reflector shutdown rod worth studies, preliminary beam tube transport studies, and D_2O coolant voiding studies.

1.1 Reference Reactor Characteristics

The neutron scattering community requires an extremely high thermal neutron flux over a volume large enough to be accessible to beam tubes and spectrum-modifying cold neutron sources. This leads to core designs that minimize internal neutron moderation and enhance neutron leakage into a heavy water reflector outside the core.[9,10] Heavy water (D_2O) was selected because it has the highest core-to-reflector flux-ratio of any moderator, and the beam tubes can be oriented in heavy water with greater flexibility than in solid moderators such as graphite and beryllium. The use of heavy water places the peak thermal neutron flux further out in the reflector than most other moderators and results in a much broader high flux distribution. However, even with the use of heavy water, high neutron fluxes in the reflector cannot be produced without high power densities in the core. Small core volumes are, therefore, highly desirable to keep the total reactor power as low as possible. The required high core power density results in high heat fluxes, which present a major challenge to cooling the core. This challenge can be met by using thin fuel plates to produce a large fuel plate surface area per unit core volume, a high coolant flow velocity, short heated flow paths, and efficient hydraulic geometries.

The reference reactor consists of two fuel elements containing hundreds of thin involute fuel plates with highly-enriched uranium

silicide (U_3Si_2) fuel meat.[1] As shown in Figures 1-1 and 1-2, the elements are radially and axially offset. Thus we call this the "offset split core design". Radially offset fuel elements allow the same low coolant inlet temperature for each element. This greatly improves the thermal hydraulic safety margins over an aligned concept in which the heated coolant out of the first element flows into the second element. The fuel elements are offset axially to create greater neutron leakage, which increases the reflector volume with a high thermal neutron flux. The neutron and gamma heating effects on reactor and reflector components are smaller with axially separated fuel elements. The axial offset also increases the available worth of the control rods in the central hole region and provides additional space next to the fuel for irradiation targets.

The entire reactor and core pressure boundary tube (CPBT) sit in a large, low-pressure and low-temperature tank of heavy water, as illustrated in Figure 1-3. Because fast neutrons produced in the fuel leak through the CPBT, the thermal neutron flux peaks outside the reactor in the reflector tank. Heavy water in this region slows the neutrons to thermal energies (< 1 eV). Beam tubes placed in the tank will permit access to the resulting high flux environment with minimum high-energy-neutron and gamma contamination from the core. The D_2O reflector is contained in a large 3.5-mm-diameter Al-6061 vessel surrounded by H_2O as illustrated in Figure 1-4. The light water pool provides biological shielding and accessibility and reduces the amount of D_2O required to maintain the desired core reactivity.

The CPBT is placed close to the core for several reasons. It allows the hot, high pressure core coolant to be isolated from the reflector tank so that the beam tubes can be operated in a low-temperature, low-pressure environment. This greatly facilitates operation and maintenance of the cold source, beam tubes, and other items in the tank and provides greater flexibility for modifications. A small CPBT costs much less than a large pressure vessel with beam tube

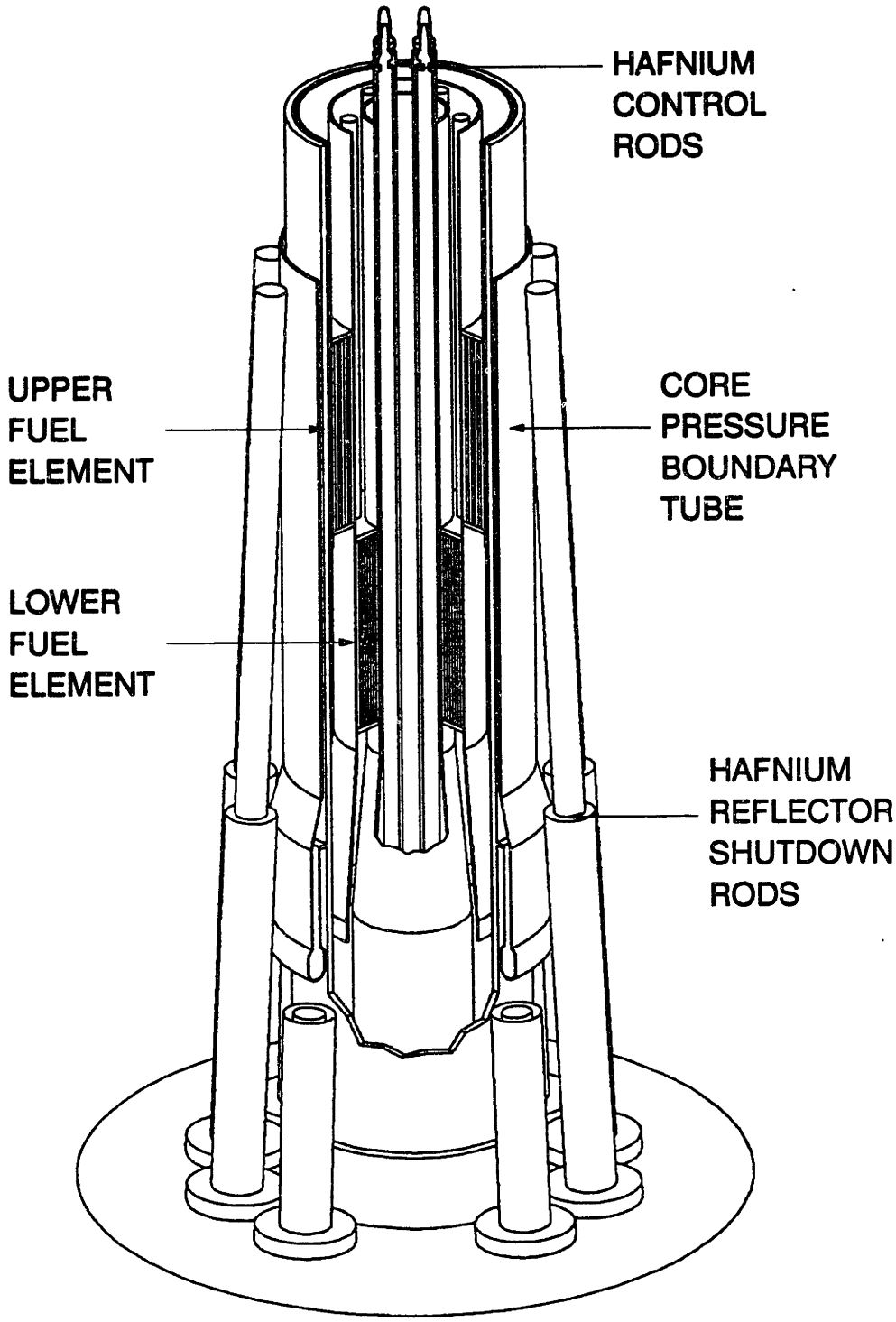

Figure 1-1. The Advanced Neutron Source reference offset split core with control rods and reflector shutdown rods inserted. A D_2O reflector completely surrounds these assemblies.

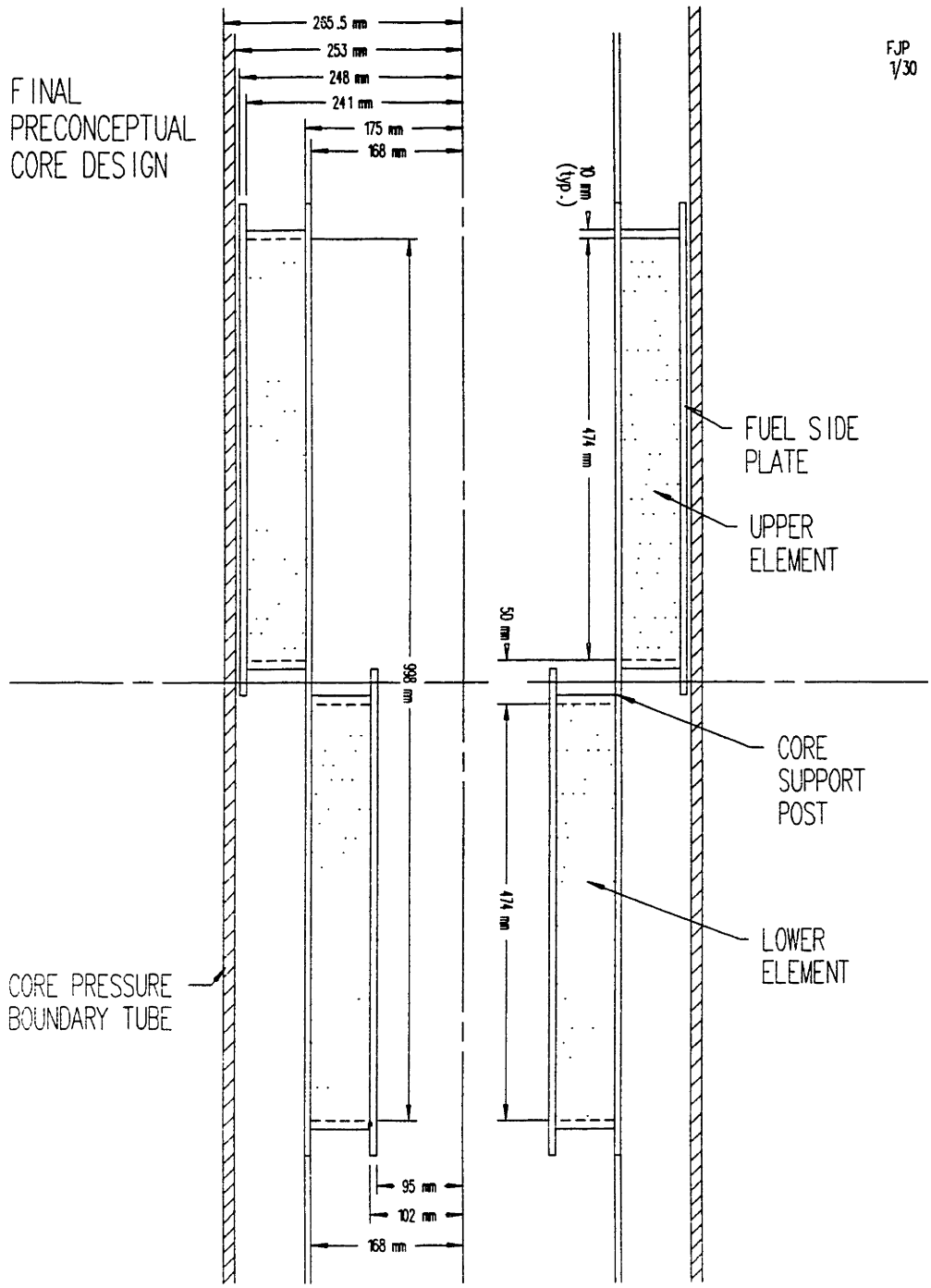

Figure 1-2. The Advanced Neutron Source reference offset split core. The reactor dimensions within the core pressure boundary tube are shown.

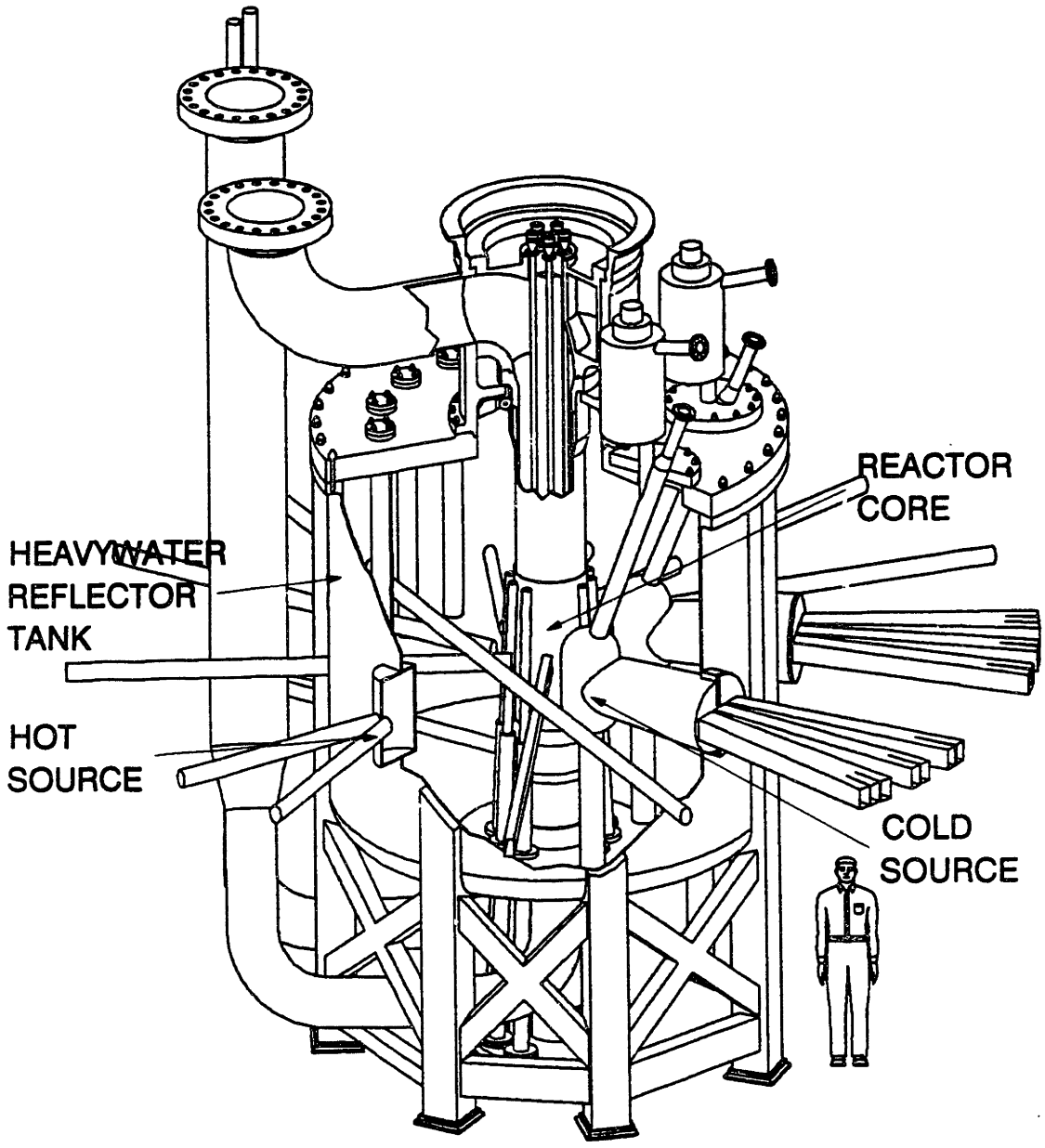

Figure 1-3. The reactor, beam tubes, and cold sources are shown sitting inside the heavy water tank. The thermal neutron flux peaks inside this heavy water tank near the beam tubes and cold sources.

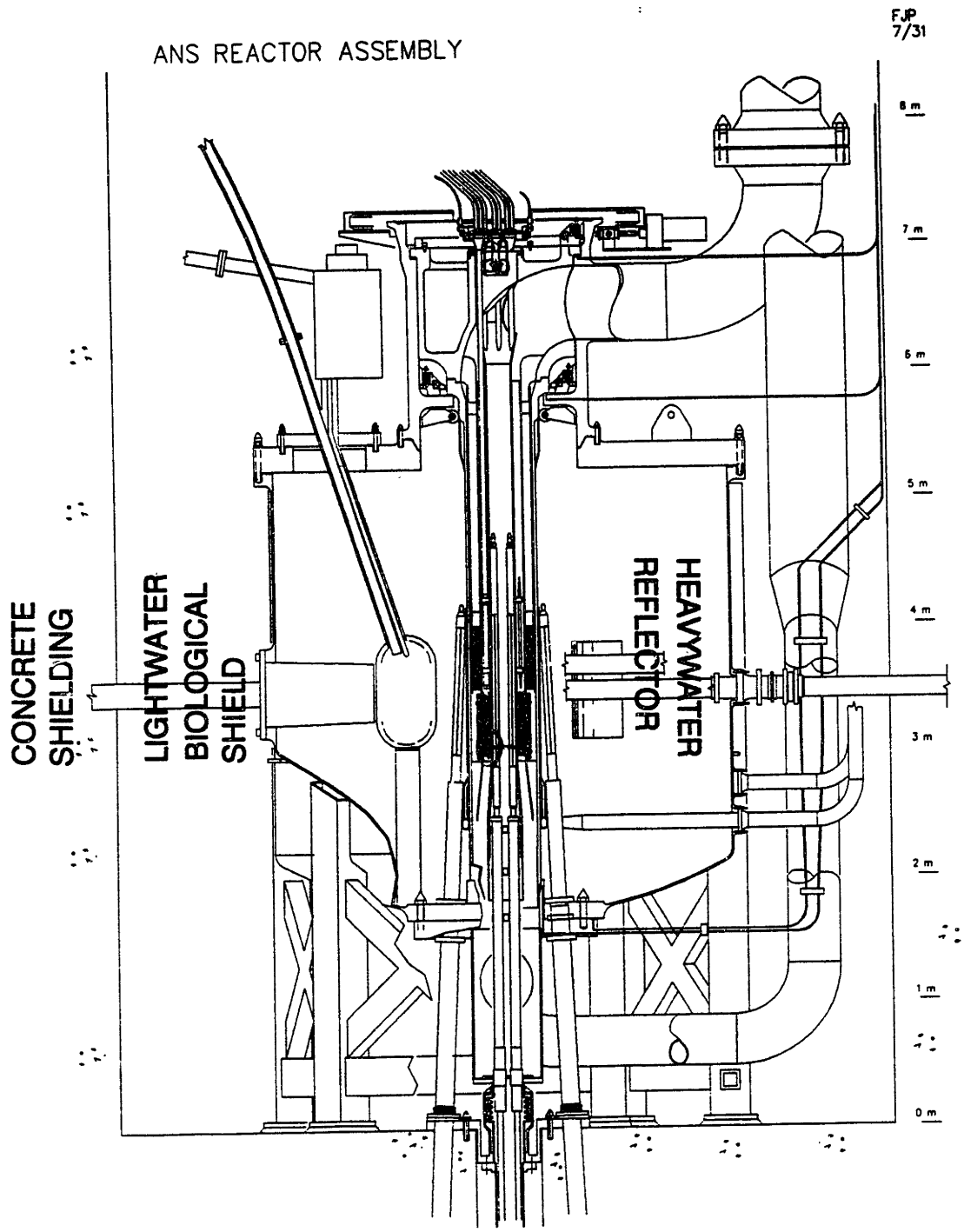

Figure 1-4. The entire reactor and heavy water tank are shown sitting inside the light water biological shield surrounded by concrete.

penetrations, although the small, close-in CPBT must be replaced periodically because of radiation damage. Beam tubes and cold sources in a low-temperature, low-pressure tank, which is not part of the primary reactor coolant pressure boundary, can be designed with thin windows, which minimize neutron transmission losses, and thin walls, which minimize activation heating. The reference design is proposed to have an Al-6061 CPBT. Data are being gathered to support an American Society of Mechanical Engineers code case for use of Al-6061 for this application.

The characteristics of the reference reactor are presented in Table 1-1. The reactor operates for 14 days at a power of 350 MW-fission to achieve a peak thermal neutron flux of about 8.5 x 10^{19} $m^{-2}s^{-1}$ in the reflector at the end of cycle (EOC). Here we define MW-fission (MWf) as the total power (heat rate) deposited in the reactor and reflector tank. MW-core (MWc) is the power deposited in the fuel plates and coolant channels (MW-core is assumed to be 0.95 x MW-fission). The fuel plates are highly enriched (93% U-235) U_3Si_2/Al, 0.762-mm-thick, and clad with 0.25-mm-thick Al-6061. The U-235 loading varies continuously, axially and radially, throughout the fuel to reduce the local power peaking. Burnable boron poison is provided in the end caps of the fuel to reduce the excess reactivity at the beginning of cycle and to help flatten the power distribution. The plates are cooled with D_2O flowing up 1.27-mm-wide coolant channels. The upper element has 432 involute fuel plates containing a total of 9.36 kg U-235; the lower element has 252 plates with 5.65 kg U-235. The involute plates are welded to cylindrical Al-6061 side plates, similar to the High Flux Isotope Reactor (HFIR) fuel elements. Heavy water flowing through a coolant bypass annulus between the outer side plates and the CPBT cools the side plates and CPBT. Figure 1-5 is a cross sectional view of an earlier core design illustrating the involute fuel plate.

TABLE 1-1. DESIGN CHARACTERISTICS OF THE REFERENCE OFFSET SPLIT CORE MODEL

Core Dimensions	
Fuel element height (mm)	474
with Al end tips	494
Upper fuel element	
Inner diameter (mm)	350
Outer diameter (mm)	482
Radial thickness (mm)	66
Lower fuel element	
Inner diameter (mm)	204
Outer diameter (mm)	336
Radial thickness (mm)	66
Core volume (litres)	67.42
Core total height (mm)	1038
Volume of fuel meat (litres)	20.23
Axial distance between active fuel elements (mm)	50
Coolant bypass annulus width (mm)	5
Al-6061 core pressure boundary tube thickness (mm)	12.5
Al-6061 central support pipe thickness (mm)	7.0
Fuel plate surface area in core (m^2)	53.0
Central hole diameter (mm)	190
Fuel	
Material	U_3Si_2/Al
Uranium enrichment (weight % U-235)	93
Maximum volume fraction (U in fuel meat)	0.45
Maximum fuel density (kg U/L fuel meat)	2.25
Fuel plate thickness (mm)	1.27
Coolant channel width (mm)	1.27
Fuel meat thickness (mm)	0.76
Cladding and side plate material	Al-6061
Cladding thickness (mm)	0.254
Al-6061 plate tip length (mm)	10.0
Number of fuel plates	
Upper element	432
Lower element	252
Total	684
Side plate thickness (mm)	7.0
Fuel span between side plates (mm)	
Upper element	78.4
Lower element	87.4
Fuel volume fraction in core	0.30
Coolant volume fraction in core	0.50
Cladding volume fraction in core	0.20

TABLE 1-1 (CONTINUED)

Physics Characteristics

Reactor power (constant) (MW-fission)	350.0
(MW-core)	332.5
Cycle length (days at full power)	14.0
Core average power density (MWf/L)	5.19
Peak reflector thermal neutron flux,	
$E < 0.625$ eV ($m^{-2}s^{-1}$) Beginning-of-cycle	7.95×10^{19}
Middle-of-cycle	8.37×10^{19}
End-of-cycle	8.57×10^{19}
Fast neutron contamination at thermal flux peak location at BOC ($m^{-2}s^{-1}$)	7.95×10^{17}
Core fissile loading at BOC (kg U-235)	15.01
Fuel burnup (kg U-235)	6.07
average (fissions/m^3 meat)	6.3×10^{26}
peak (fissions/m^3 meat)	1.0×10^{27}
Core burnable poison loading (kg B^{10}) at BOC	0.0134
Core burnable poison loading (kg B^{10}) at EOC	0.0002
Maximum k excess (%Δk/k)	24.2
Efficiency factor at EOC ($m^{-2}s^{-1}$ MWf^{-1})	2.45×10^{17}
Axial distance of thermal flux peak relative to core midplane	
at BOC (m)	-0.15
at EOC (m)	0.07
Radial distance of thermal flux peak	
at BOC (m)	0.38
at EOC (m)	0.38
Fast-to-thermal flux ratio at flux peak at EOC at location of peak thermal flux	0.010

Fluxes at Target Irradiation Positions at BOC

Group energy boundaries	
Group 1 (fast)	0.1 MeV < E < 17 MeV
Group 2	100 eV < E < 0.1 MeV
Group 3 (epithermal)	0.625 eV < E < 100 eV
Group 4 (thermal)	0.0 eV < E < 0.625 eV

Fast flux irradiation position - above lower element	
Average group 1 flux ($m^{-2}s^{-1}$)	3.58×10^{19}
Average group 2 flux ($m^{-2}s^{-1}$)	5.37×10^{19}
Average group 3 flux ($m^{-2}s^{-1}$)	1.88×10^{19}
Average group 4 flux ($m^{-2}s^{-1}$)	1.05×10^{19}
Epithermal flux irradiation position-below upper element	
Average group 1 flux ($m^{-2}s^{-1}$)	2.88×10^{19}
Average group 2 flux ($m^{-2}s^{-1}$)	4.35×10^{19}
Average group 3 flux ($m^{-2}s^{-1}$)	1.79×10^{19}
Average group 4 flux ($m^{-2}s^{-1}$)	3.08×10^{19}

TABLE 1-1 (CONTINUED)

Thermal flux irradiation position - at r = 1.5 m in tank	
Average group 1 flux ($m^{-2}s^{-1}$)	~2 x 10^{10}
Average group 2 flux ($m^{-2}s^{-1}$)	~3 x 10^{12}
Average group 3 flux ($m^{-2}s^{-1}$)	~5 x 10^{14}
Average group 4 flux ($m^{-2}s^{-1}$)	~4 x 10^{18}
Thermal Hydraulic Conditions	
Reflector tank temperature (^{o}C)	27.0
Coolant inlet pressure (MPa)	3.7
Core outlet pressure (MPa)	2.0
Core pressure drop (MPa)	1.7
Available flow area (m^2)	
in upper element coolant channels	0.0431
in lower element coolant channels	0.0280
in coolant bypass annulus	0.00787
in control rod channel	0.025
Coolant flow rate (kg/s)	
in upper element coolant channels	1196
in lower element coolant channels	770
in coolant bypass annulus	236
in control rod channel	274
Coolant velocity (m/s)	
in core channels	27.4
in coolant bypass annulus	27.4
in control rod channel	10.0
Coolant bulk inlet temperature (^{o}C)	49
Coolant bulk outlet temperature (^{o}C)	83
Average surface heat flux (MWc/m^2)	6.27
Average heat transfer area per plate	
upper element (m^2)	0.0743
lower element (m^2)	0.0828
Energy conversion factor (%)	
(MW-core/MW-fission)	95.0
Average power density in fuel meat (MWc/L)	16.44

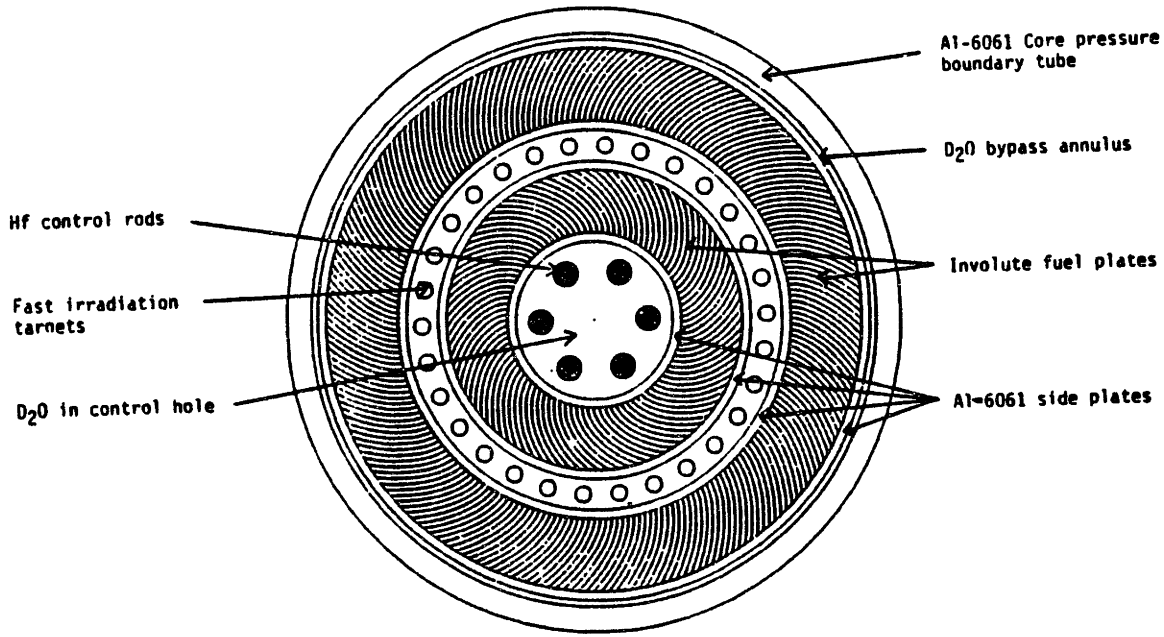

Figure 1-5. Cross section of the February 1988 radially split core model with involute fuel.

A shim/regulating/safety control rod system is located in the central hole, and a safety control rod system is located in the reflector just outside the CPBT. Approximately 20% Δk/k excess reactivity is required at the beginning of cycle (BOC) to maintain a reactor power of 350 MWf for 14 days. About 11% of the core excess reactivity at the beginning of cycle is shimmed with 13.4 g of burnable boron poison. The remaining excess reactivity at BOC is controlled by four hafnium rods in the central hole. Hafnium is used because it has higher epithermal absorption cross sections than boron, providing higher worth in the epithermal spectrum of the central hole region. In addition, the high strength of hafnium reduces the amount of structural material required for the control system. Under irradiation hafnium isotopes generally produce other highly absorbing hafnium isotopes, whereas neutron capture in boron leads to helium production, which causes rod swelling and has a higher nuclear heating effect. Hafnium also has a relatively high melting temperature and does not require cladding. In the present concept, the four shim rods are driven from below the core, with each rod having a separate scram capability.

Removal of the control shim rods over the cycle causes shifts in the power and flux distributions, with larger shifts near the central hole.

The location of the peak thermal neutron flux in the reflector is perturbed somewhat when the control rods in the central hole move. The peak thermal neutron flux in the reflector increases over the cycle.

The high power densities require as flat a power distribution as possible. The power shape is flattened by burnable boron poison and by grading the fuel, radially and axially, placing higher U-235 content near the center of the fuel zone and lower U-235 content in the core periphery. Each involute plate in either element has the same U-235 distribution as the other plates in that element.

The region of peak thermal neutron flux occurs in the D_2O reflector about 120 mm outside the core pressure boundary tube, covering a large volume, which also has low fast-neutron and gamma-ray contamination. Because experimenters desire a high thermal neutron flux with minimum contamination, the tips of the beam tubes will be located as close as possible to the peak thermal flux. Because gamma heating of the cold source is a problem, the cold source will be positioned at a radial distance greater than the location at which the peak thermal neutron flux occurs.

Most of the gammas and fast neutrons are produced in the fuel. Hence, the amount of gammas and fast neutrons that stream down the tubes and contaminate the experiments depends on the tube orientation with respect to the core. The tubes can be placed with orientations ranging from radial to tangential with respect to the core. Radially-orientated beam tubes have slightly shorter beam tube lengths and less impact on core reactivity than tangential beam tubes; however, radial tubes allow more fast neutron streaming than other orientations. Tangential tubes have a greater impact on core reactivity because they displace more heavy water and have more aluminum next to the core. Rotating a radial beam tube so that its line of sight just misses the core creates what we call the no-line-of-sight tube orientation. This configuration combines the features of tangential and radial beam tubes and produces only a small reactivity impact with about half the fast neutron contamination of radial tubes.[11] Thus, no-line-of-sight tubes will be used because they retain the best features of each orientation.

Operationally, the effect of beam tubes, cold sources, and targets on the core reactivity is significant. A 1% reduction in the core reactivity reduces the cycle length by about one day. We have accounted for this reactivity deficit in our unperturbed core model by adding enough U-235 in the fuel to achieve about 5% excess reactivity at the end of cycle (EOC).

The materials irradiation and isotope production capabilities and associated design trade-offs of the current ANS conceptual design have been examined.[12] The ANS will be capable of producing ultra-high flux levels for a wide variety of users. A region of high epithermal neutron flux is needed for production of transuranic isotopes, and an area of high fast flux is needed for engineering materials irradiation. The fuel region has a hard spectrum (more fast neutrons), and the reflector has a soft spectrum (more slow neutrons). Thus this reactor design can accommodate targets in a wide variety of spectra. The fast spectrum target irradiation positions are located adjacent to the inside of the upper element. The epithermal positions are adjacent to the outside of the lower fuel element. The fluxes in these positions are given in Table 1-1. This reactor concept produces both flux and spectrum values that surpass the goals set for the irradiation positions.

Some thermal hydraulic conditions are also presented in Table 1-1. The bulk outlet coolant temperature is maintained below 100°C to avoid steam flashing in the event of rapid core depressurization. Thin fuel plates, producing a large fuel plate surface area per unit core volume, a high coolant flow velocity, and short heated flow paths improve the safety margins. The proposed ANS fuel meat thickness of 0.76 mm is currently used in the High Flux Isotope Reactor. The coolant velocity of 27.4 m/s is well above that of existing reactors. Thus, the critical velocity to fuel plate collapse will be determined by experiments to ensure fuel element integrity at this high velocity. Aluminum cladding erosion is not expected to be a problem at coolant velocities below 30 m/s.[13] The reactor coolant inlet pressure of 3.7 MPa drives the coolant flow against the core pressure drop, prevents hydraulic instability from occurring at the fuel element exit, and allows sufficient critical heat flux (CHF) margin at the peak heat flux location.

Hydraulic instability occurs when the enthalpy rise in a flow channel reaches a certain fraction of the enthalpy rise to saturation at the local conditions. Because the power distribution changes over the cycle, the coolant hot streak location varies during the cycle. Also, the limiting hot streak may not have the highest peak fuel temperature because aluminum oxide builds up on the cladding at different rates along the channel. For the statistical safety margin calculations, several hot streaks located at different radii are being examined in order to determine the limiting locations at BOC and EOC. The radial and axial fuel grading is still being modified to flatten the power distribution over the cycle, which will improve the margins to CHF, incipient nucleate boiling (INB), hydraulic instability, and the fuel temperature limit.

1.2 Analytical Methodology

For the reactor analysis, ground rules were established that form the bases on which all calculations were performed. The ground rules include some design requirements, core operating conditions, thermal hydraulic correlations, safety limits, and other constraints. This allowed ORNL and INEL to analyze different core designs on a consistent basis in order to illuminate the fundamental physical differences in the performance of the various designs.

1.2.1 Neutronics

Prior to June 1989, when the MCNP work began, most neutronics calculations were performed with diffusion theory codes. S_n transport theory codes were also used to verify results in the early stages of this project. The methodology behind this work is presented and provides the foundation for the Monte Carlo work performed.

Reactor physics analyses were performed with ENDF/B-V cross section data. INEL processed 28-group cross section libraries with the

COMBINE[14] code using the calculated flux and current spectra from different unit cells as weighting functions. INEL used one-dimensional (1D) cylindrical transport models (SCRABL) to collapse cross sections to four groups. These models were iterated with two-dimensional (2D) four-group diffusion theory calculations to make sure the axial leakage in each group was estimated correctly for the 1D transport model.

Oak Ridge National Laboratory utilized both 227- and 27-group cross sections.[15] Checks were made to verify that the 27-group library retained enough detail to yield relatively accurate neutron flux calculations. One-dimensional spherical and cylindrical transport models were used with the computer program XSDRNPM[16] to collapse cell-averaged cross sections to four energy groups. Conservation of radial thicknesses or volumes of fuel zones was required for cylindrical or spherical models, respectively.

Four-group cross sections were calculated in different regions.[17] In particular, the one-thermal-group U-235 capture and fission cross sections vary significantly depending on the distance from the core periphery. This occurs because the flux spectra are very hard in the center of each fuel element but are considerably softer in the fuel regions adjacent to the heavy water. Spatially-dependent cross sections permit the use of inexpensive computations using one thermal group and three fast groups. Additional thermal groups reduce the need for spatially-dependent cross sections but increase computer costs because the treatment of neutron upscattering in the thermal range requires an iterative procedure. Cross section exposure dependence was also examined and included for some nuclides.

Both laboratories primarily analyzed 2D (r,z) core models with four-group diffusion theory, PDQ-7[4] for INEL and BOLD-VENTURE[18] for ORNL. The fuel was modeled with up to 192 regions. This is a reasonable way to represent the continuously-graded, highly-enriched uranium silicide fuel. The mesh structure in each model was examined

and modified to account for the very steep flux gradients near the fuel-water interface.

INEL compared a four-group diffusion theory axially split core model with a 2D 11-group transport theory benchmark (TPT). Compared with the transport calculation, PDQ underestimates the core multiplication factor by less than 1% and the peak thermal neutron flux by 3%. However, differences in the core power distributions are typically 10% and even greater at the fuel-water interfaces where diffusion theory fails because a high absorbing region is next to a very low absorbing region. Analyses with four-group transport theory and 11-group diffusion theory were also conducted. Results indicate that the 11-group to four-group differences are larger than, but partially corrected by, the transport to diffusion differences.

ORNL reached similar conclusions using a 1D spherical 26-group transport (XSDRNPM) model and a 2D six-group transport model (DORT) of a radially split core design. Some of the discrepancies seem related to mesh size effects rather than to the underlying theory.[19]

The differences between four-group diffusion theory and multigroup transport theory are small enough to permit the use of four-group diffusion theory for preconceptual design and comparative studies. Four-group cross section sets generated for specific regions of the reactor reduce these differences.

ORNL verified their methodology by comparison with measurements from existing research reactors, specifically the High Flux Isotope Reactor and the Institute Laue-Langevin reactor. Calculated cycle length, peak thermal flux in the reflector, and local power densities agree well with measured values.

Excellent agreement was achieved on most reactor physics parameters calculated by ORNL and INEL for different reactor concepts.[3] The

parameters computed are accurate enough for different preconceptual reactor designs to be compared on a consistent basis.

The diffusion theory and transport theory methods discussed contain approximations that introduce errors into the reactor physics calculations. Therefore, a Monte Carlo neutron and photon transport code, MCNP-3b[2], is used to benchmark these methodologies and results. MCNP-3b is also used to perform three-dimensional, continuous-energy, coupled neutron-gamma calculations, which are not possible with the other reactor physics methods currently being used. The development and use of the MCNP neutronics model is discussed in detail in the following chapters.

1.2.2 Thermal Hydraulics

The INEL analyzed the core thermal hydraulics with the INEL codes TOODEE, MACABRE, and SAMPLE, which are used for Advanced Test Reactor (ATR) core evaluations. TOODEE is a two-dimensional time-dependent heat conduction code.[20] TOODEE models one fuel plate and coolant channel. TOODEE computed the temperature distributions throughout each fuel plate position of interest. MACABRE is a one-dimensional heat conduction and thermal hydraulics code.[21] It analyzes the thermal hydraulics for up to 19 fuel plates and associated flow channels and is used to compute the pressure drop across the core.

SAMPLE computes statistical margins by Monte Carlo sampling and is used to evaluate the margins to critical heat flux, incipient nucleate boiling, and flow instability. The parameter to be evaluated is a function of specified variables that have a distribution about their mean, which is specified as a variance. A sample is chosen from each distribution, and the corresponding sample is evaluated. This is repeated several times to obtain the confidence limits and distribution for the evaluated parameter.

The ORNL analyzed the core thermal hydraulics with a fuel element steady-state heat transfer code previously developed for HFIR [22] that has been modified considerably to account for the ANS geometry and to include the physical and thermodynamic properties of D_2O. Further modifications were made to include updated thermal and flow correlations.[23] ORNL is currently developing a burnout heat flux correlation to add to the code.[24]

CHAPTER 2. MCNP MODELLING OF THE ANS

MCNP permits full three-dimensional modelling. Various surfaces (i.e., cylinder, planes, etc.) are used to represent the bounding surfaces of an object. It was possible to model all parts of the ANS reactor core explicitly except the fuel plates. MCNP does not have the capability to model involute surfaces.

The modelling of the ANS was performed in two phases. During the first phase a very simplified model was constructed. This model was used to experiment with various aspects of MCNP. Some preliminary comparisons to PDQ-7 were also made to verify that MCNP was in the right ballpark in its calculations. During the second phase, the model was expanded to include the more sophisticated physical description incorporated in the PDQ models. All of the MCNP studies were performed with this model, and some variance reduction techniques were also employed.

A sample input deck for an ANS MCNP problem is included in Appendix A. The geometry description and surface specifications are shown as well as the various control cards and tally choices for an MCNP run.

2.1 Preliminary MCNP Model

The first MCNP model of the ANS contained only the D_2O coolant, D_2O reflector, core pressure boundary tube, and two homogenized fuel zones representing the fuel elements. The fuel, cladding, and D_2O coolant of the fuel elements were homogenized to produce the homogeneous fuel zones. All Al-6061 was modelled as Al-27 since no cross sections were available for Al-6061.

No control rods or burnable poisons were modelled. The uranium loadings used in the preliminary and final MCNP runs were representative of a fresh, beginning of cycle core. No fission products were

modelled. Currently, MCNP does not offer adequate fission product lump cross sections for reactor applications. Therefore, it is not possible to model accurately a depleted core. There are, however, cross sections available for the fission products such as Xe-135 and Sm-149, making it possible to approximate a depleted case. Some studies will be performed with this approximation at a later date. Two D_2O densities were used in this model. The reflector and cold D_2O regions of the core have densities evaluated at 300 K. The hot D_2O regions, such as coolant outlet channels, have densities evaluated at 350 K. MCNP offers D_2O $S(\alpha,\beta)$ thermal libraries, evaluated at 300 and 400 K, which represent the molecular effects at thermal temperatures. Ideally, the 300 K $S(\alpha,\beta)$ library would be used in the D_2O cold regions and the 400 K $S(\alpha,\beta)$ library would be used in the D_2O hot regions. However, a bug in MCNP version 3b permits only a single D_2O $S(\alpha,\beta)$ library to be used problem- wide. Therefore, the 300 K D_2O $S(\alpha,\beta)$ library is used for all D_2O regions.

For all preliminary runs the default MCNP settings were used. The neutron energy ranges were chosen to be 0.0 eV to 17.0 MeV. No geometry or energy splitting was performed. These preliminary results, when compared to PDQ, were very encouraging and the core multiplication factors were within a few percent.

2.2 Final MCNP Model

Once a good understanding of MCNP and the preliminary ANS model was obtained, the final, detailed, physically accurate model of the ANS was set up. Al-6061 was correctly represented by modelling each of its constituents: Si, Fe, Cr, Cu, Al-27, Mg, Mn. Al-6061 fuel side plates were added as well as Al fuel end caps. Boron-10 was modelled in the fuel end caps during some of the runs as a burnable poison to control the excess reactivity at the beginning of the cycle. The inner Al-6061 support pipe was modelled as well as the Al-6061 tank separating the D_2O reflector and the H_2O biological shield. Four

hafnium control rods and eight hafnium reflector shutdown rods were modelled. Four circular beam tubes were also modelled to simply demonstrate some of MCNP's capabilities. Elliptical beam tubes will be modelled in future ANS work.

Figure 2-1 shows the reactor core, control rods, core pressure boundary tube, D_2O reflector, Al-6061 tank, and the H_2O biological shield. Various surfaces in the reflector are identical to some surfaces in the PDQ-7 model in order to compare region-averaged fluxes with PDQ. Other surfaces were added to MCNP for neutron importance modelling.

Figure 2-2 is similar to Figure 2-1 except that the D_2O reflector and the reactor central hole are divided into more cells. This was done to permit neutron flux maps to be calculated. This segmentation was also used in weight window generation runs.

Figure 2-3 is a close-up view of the reactor core and control rods. Each fuel element has 80 cells through which 5 materials are distributed, each with a different U-235 loading. The different materials are used to represent the axial and radial U-235 grading. The D_2O region next to each fuel element is divided into two cells. One cell is D_2O and the other cell represents target irradiation positions.

These regions are a homogeneous mixture of D_2O and Al-27 structural material. The control rods shown in these figures were modelled according to information received from Dr. Felix Difilippo at ORNL. These control rods are inserted from the top of the reactor into the central hole and are essentially hollow cylinders with a layer of hafnium on the outside. Figure 2-4 is a view of the reactor central hole along the core midplane with control rods inserted. The gap between the control rods and the inner Al-6061 tube is 4 mm. The dashed line in Figure 2-4 splits one control rod to represent the two halves in which heating calculations were performed.

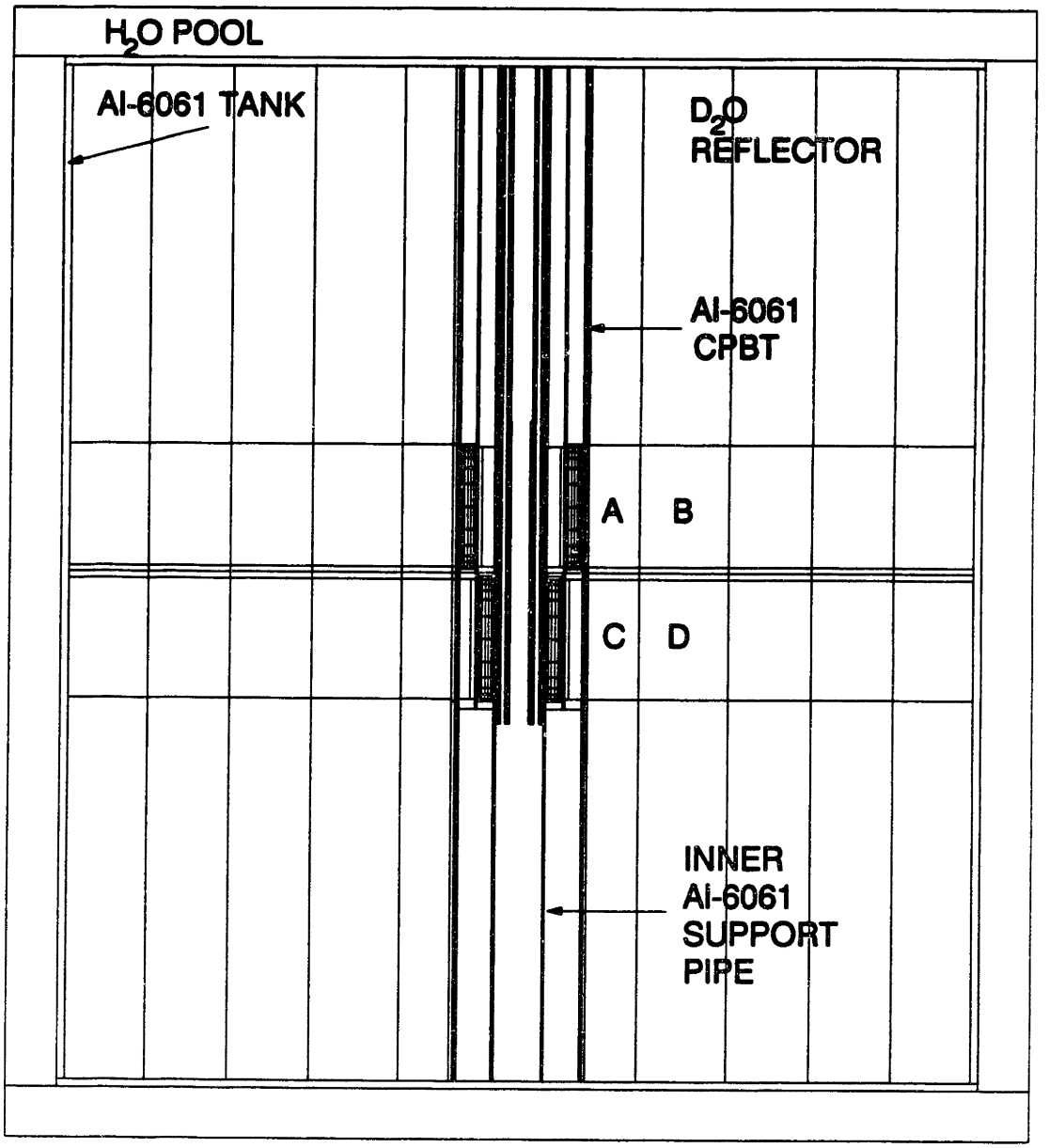

Figure 2-1. Final MCNP model of the ANS shown with control rods fully inserted. The view represented is a cut along the core centerline. (A, B, C, and D identify specific regions.)

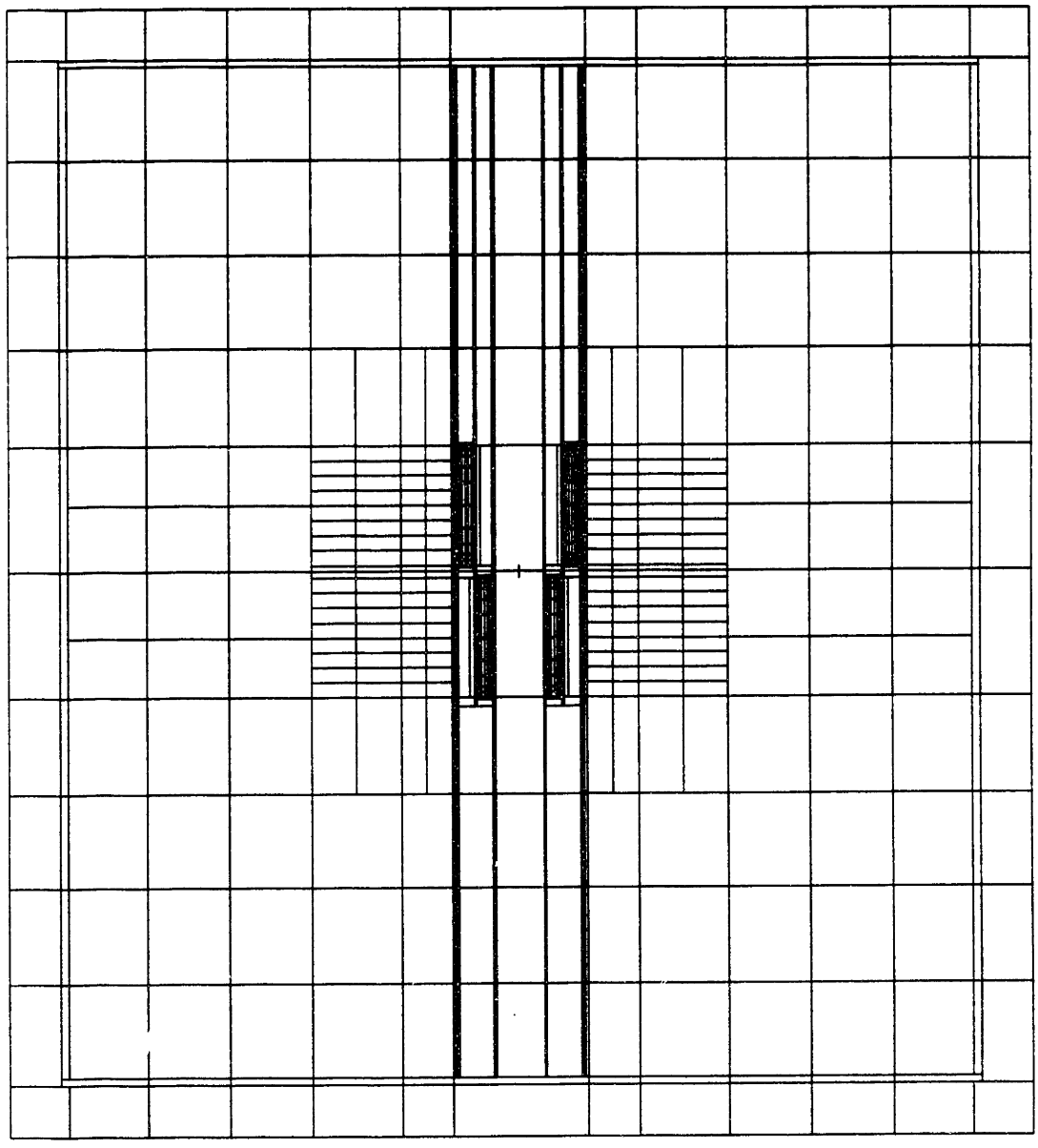

Figure 2-2. Final MCNP model of the ANS shown without control rods. The view represented is a cut along the core centerline. The D_2O reflector and reactor central hole are divided into many cells for use in flux mapping and variance reduction efforts.

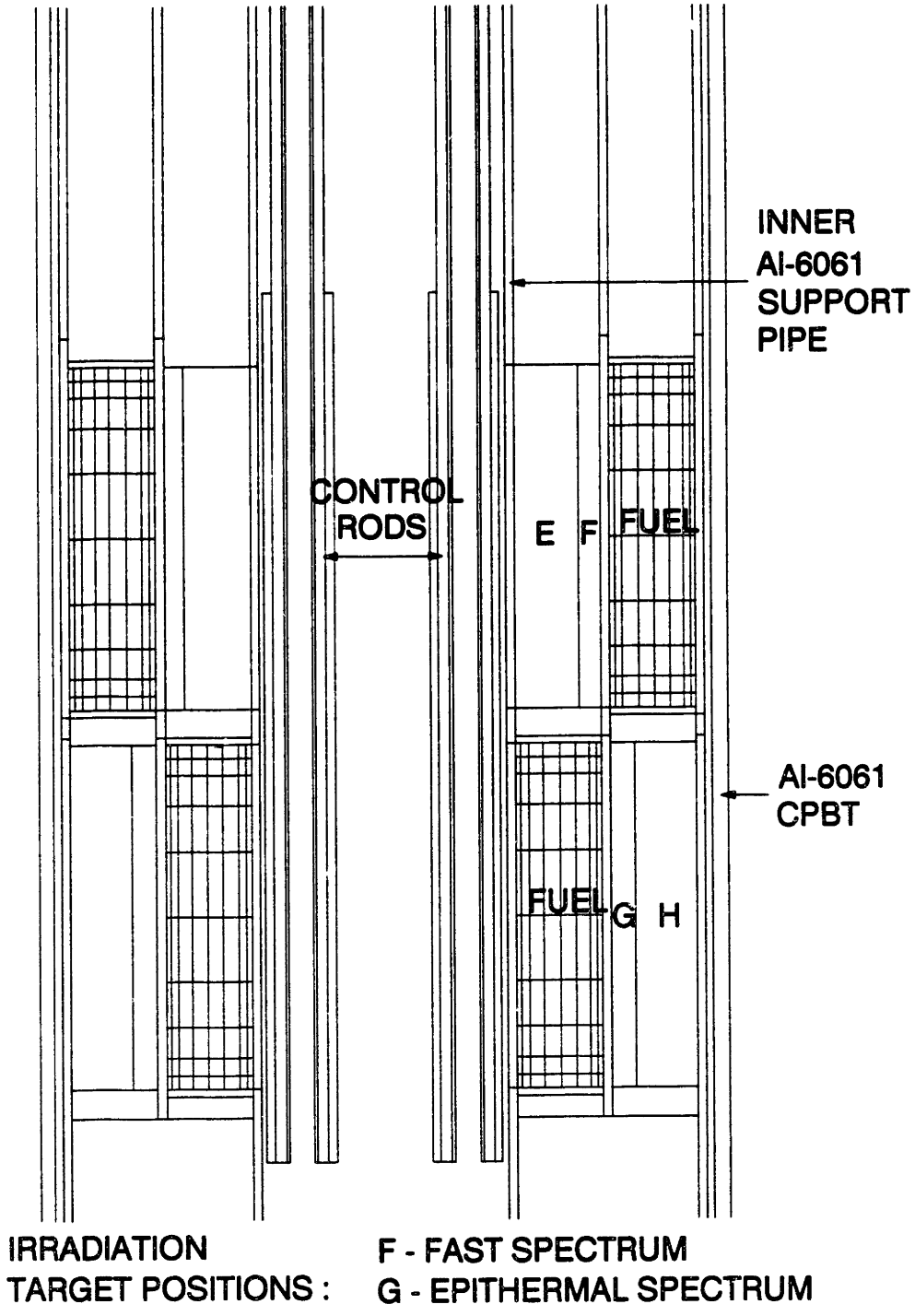

Figure 2-3. An expanded view of the MCNP ANS reactor core with two control rods fully inserted. The view represented is a cut along the core centerline. (E, F, G, and H identify specific regions).

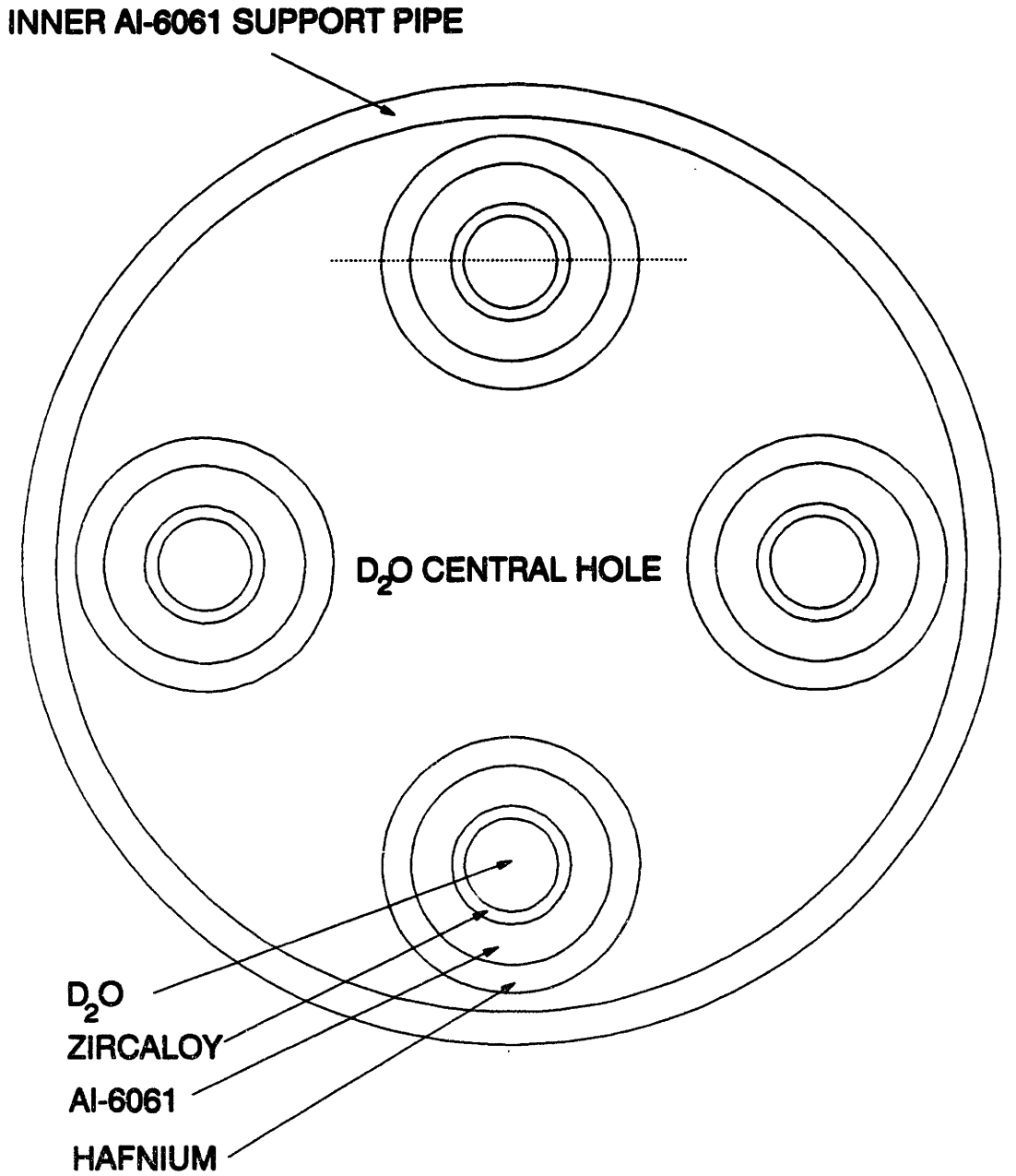

Figure 2-4. Horizontal view of the ANS reactor central hole at the core midplane with four control rods inserted.

Figure 2-5 shows the reactor core pressure boundary tube and reactor internals surrounded by 8 shutdown rods, also modelled according to information received from ORNL. In this figure, four Al-6061 beam tubes with a 100-mm outside diameter and a 5-mm-thick shell surrounding a void are represented.

Figure 2-6 is an expanded view of the upper and lower fuel regions showing the material numbers used in each fuel regions. Material 1 has the highest U-235 density while material 5 has the lowest U-235 density. When the U-235 density is decreased, the Al-27 density is increased to compensate. The U-235 density is varied both axially and radially to try to flatten the power distribution. The fuel in the outer regions is of lower U-235 density than the fuel in the center. This is done to force the power production inward and minimize the power peaking in the outer regions.

Most production runs used the default MCNP parameters; implicit capture over the entire energy range, default weight cutoffs, neutron and photon importances of 1 in all cells. The neutron energy range used was 0.0 eV to 17.0 MeV. All runs were k-effective calculation runs (kcode), and usually had 3000 neutrons/cycle with 4 settle cycles and a total of 20 cycles. MCNP tracks a user-specified number of neutrons in each cycle, after which all parameters requested are tallied and calculated. MCNP repeats this process a user specified number of times. Each new cycle has a source generation distribution based on the previous cycle. The settle cycles are cycles in which no tallies are performed. The purpose of these cycles is to permit the source generation to settle and converge before performing the computations. Source distributions from previous runs can be used to begin new runs thereby minimizing the number of settle cycles. This technique was used in all MCNP runs performed, when possible. The 300 K D_2O $S(\alpha,\beta)$ libraries was used for all D_2O regions, since 300 K is close to the average D_2O temperature throughout the reactor.

All studies performed with MCNP are presented in the next chapter.

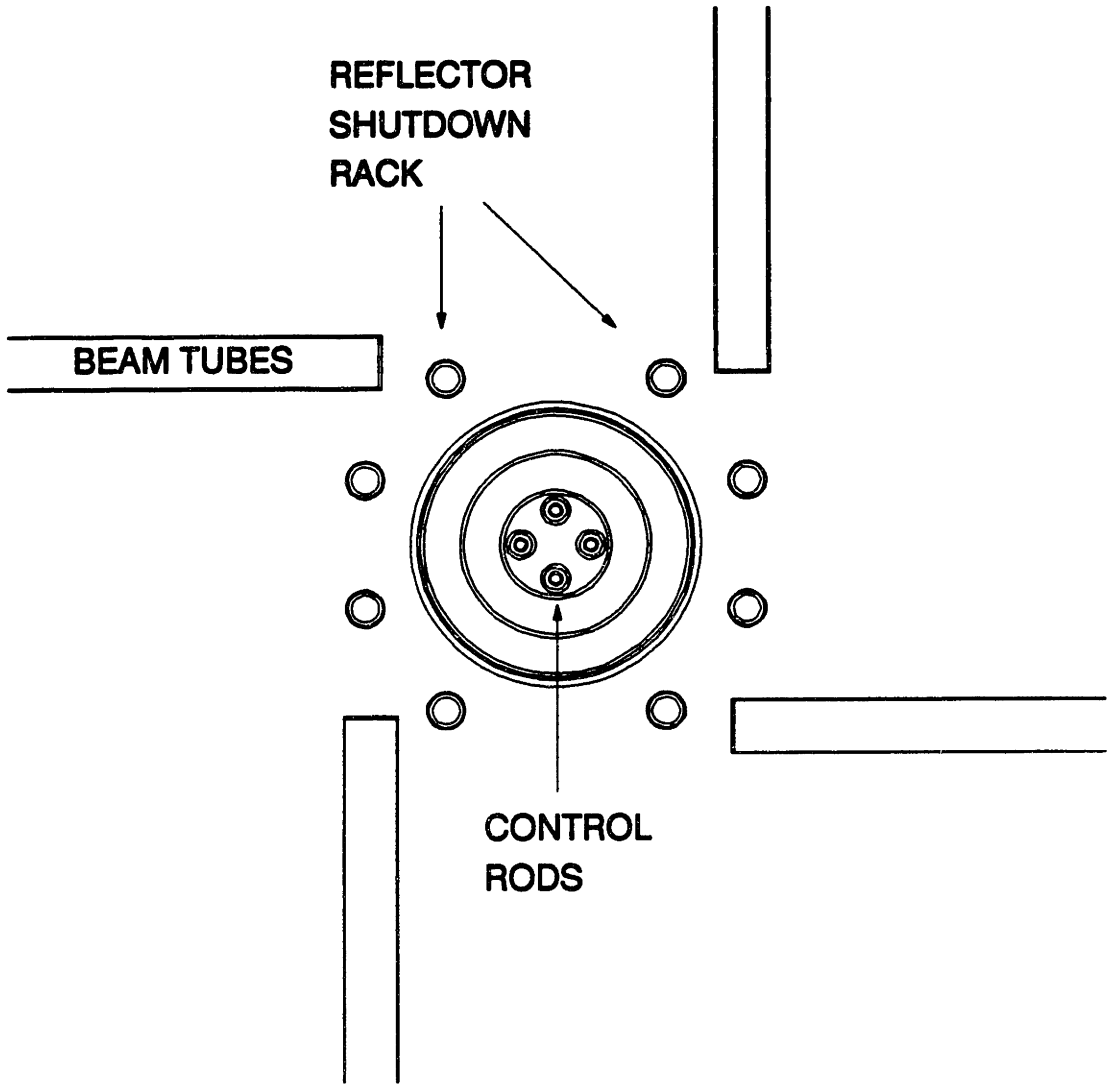

Figure 2-5. Horizontal view of the ANS at the core midplane. Control rods, reflector shutdown rack and beam tubes are depicted.

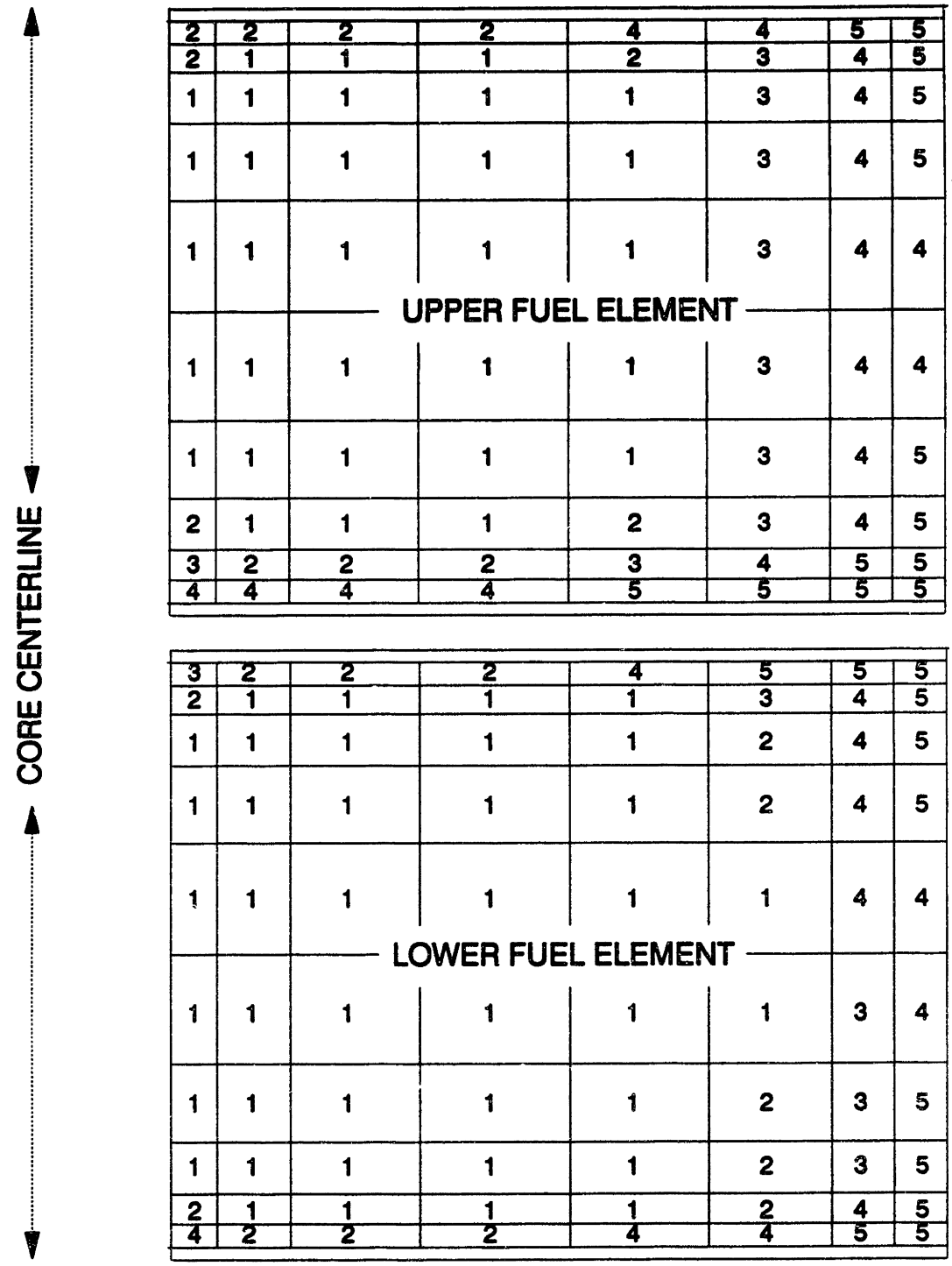

Figure 2-6. An expanded view of the upper and lower fuel elements of the ANS. Material numbers are shown in the 160 fuel zones to represent the axial and radial U-235 density changes. (1 = highest U-235 density, 5 = lowest U-235 density.)

CHAPTER 3. MCNP CALCULATIONS

The primary focus of the Monte Carlo work was to provide calculations in support of the ORNL design decisions on the ANS. These studies were performed with the default MCNP techniques since studies on improving Monte Carlo efficiency had not been completed at that time.

Prior to these calculations the MCNP ANS model was benchmarked against the PDQ-7 model. These results were very encouraging and are presented in Chapter 4. Appendix B contains a list of all MCNP and PDQ studies referenced in this thesis.

3.1 Control Rod Studies

Control rod studies were performed with MCNP, PDQ-7, and VENTURE. The MCNP calculations were the most accurate since the control rods were correctly modelled. The PDQ model contained a homogeneous mixture of hafnium and D_2O in the central hole that represented control rods. The VENTURE calculations had a solid ring of hafnium in the central hole to represent the four control rods. The MCNP calculations were assumed to be more accurate than the PDQ and VENTURE calculations since the theoretical foundation of MCNP is superior to that of either PDQ or VENTURE. Using the MCNP calculations as a reference, VENTURE predicts the rod worths better than PDQ.

3.1.1 Reactivity Effects of Control Rods

The control rod studies contained the four proposed control rods. The first study had no control rods modeled, the second study had the four control rods modeled at the fully removed position, the third study modeled the control rods at the fully inserted position and the fourth study modeled the control rods parked at the core midplane. All of these studies were performed with graded fuel core models containing boron in the end caps. Table 3-1 presents these results.

TABLE 3-1. REACTIVITY EFFECTS OF CENTRAL CONTROL RODS

Description	Run Number	Core Multiplication Factor
Base Case - No control rods	ANS39[a]	1.1205 ± 0.0045[b]
Control rods fully removed (100 mm above top element)	ANS45	1.1162 ± 0.0040
Control rods fully inserted	ANS36	0.9014 ± 0.0032
Control rods inserted to core midplane	ANS50	1.0036 ± 0.0040

a. Appendix B contains a detailed description of each run number referenced.
b. The statistical uncertainties reported with all MCNP calculations represent one standard deviation.

These results indicate that the current configuration of four control rods in the central hole is adequate to shut down the reactor. The control rods also have negligible reactivity effect when in the fully removed position. These results also indicate that four control rods inserted to core midplane are sufficient to reach criticality.

The hafnium cross sections used for these studies were natural hafnium cross sections evaluated at 300 K. Natural hafnium cross sections evaluated at 0 K were also available. The 300 K cross sections do not contain gamma production data. The 0 K cross sections, however, do contain gamma production data. Therefore the 0 K cross sections were used when coupled neutron-gamma heating calculations were required. The resulting increase in the core multiplication factor was less than one percent.

Since individual hafnium isotope cross sections are not currently available it is not possible to model depleted control rods with MCNP. Advanced Test Reactor data, however, indicates that the

control rod worths can decrease as much as 50% when depleted. This estimate will have to be verified by future work.

3.1.2 Neutron Flux Calculations

During all MCNP calculations cell-averaged neutron fluxes were calculated. These fluxes were tallied over two, four-group energy structures. One energy structure is identical to the group structure used in the PDQ calculations. The second is the Advanced Neutron Source energy structure, which is used for reported results. Table 3-2 lists the PDQ and ANS energy group structures. The ANS energy structure is also listed in Table 1-1.

TABLE 3-2. GROUP ENERGY BOUNDARIES

Group	PDQ		ANS	
Number	Upper	Lower	Upper	Lower
1	17 MeV	0.821 MeV	17 MeV	0.1 MeV
2	0.821 MeV	5531 eV	0.1 MeV	100 eV
3	5531 eV	0.683 eV	100 eV	0.625 eV
4	0.683 eV	0.0 eV	0.625 eV	0.0 eV

MCNP cannot calculate fluxes at a single point, but rather calculates fluxes averaged over a cell of user-chosen volume. As the cell becomes smaller, fewer neutrons enter the cell, and therefore less information concerning the flux value is obtained. The result is an increase in the standard deviation of the calculated value. The D_2O reflector was broken into many cells as shown in Figure 2-2. Each of the cells next to the fuel elements was further segmented radially. The maximum relative error in these cells during any calculation was 0.05. The relative error is defined as the standard deviation divided by the mean.

Figure 3-1 shows the radial group fluxes in the reflector for a beginning-of-cycle case with control rods parked at core midplane. The axial location is between 143 mm and 203 mm below the core midplane (see Figure 1-2). This is the location of the peak thermal neutron flux. The thermal flux remains high after peaking, while the fast flux rapidly decreases. The axial location of the peak is expected to change as the core is depleted, however, the radial shape should remain constant.

The volume-averaged peak thermal neutron flux between 0.0 and 0.625 eV was calculated to be $7.8945 \pm 0.1429 \times 10^{19}$ $m^{-2}s^{-1}$. The peak occurs between 340.5 mm and 365.5 mm from the core centerline.

Fluxes were also calculated for the two incore irradiation positions, regions F and G in Figure 2-3. These fluxes were calculated when control rods were fully withdrawn, inserted to core midplane, and fully inserted. This data is presented in Table 3-3. No targets were present and the beginning-of-cycle fuel loading was used in these runs.

The effect of control rod movement on fluxes in the irradiation positions was considerable. When control rods are fully inserted, the upper target region has higher total fluxes than the lower target region. However, when control rods are inserted only to core midplane the lower target region has a higher total flux. This indicates the neutron flux is forced axially downward with control rod insertion until the rods pass the core midplane. After the rods are fully inserted, the effect on the target fluxes is absent since the absorbing material is uniformly distributed through the axial length of the core.

The transplutonium target region has a higher thermal flux than the material irradiations region. This occurs because neutrons leaving the bottom element have a better opportunity to thermalize both inside the CPBT and the D_2O reflector prior to returning to the target locations. Neutrons leaving the top element do not have the

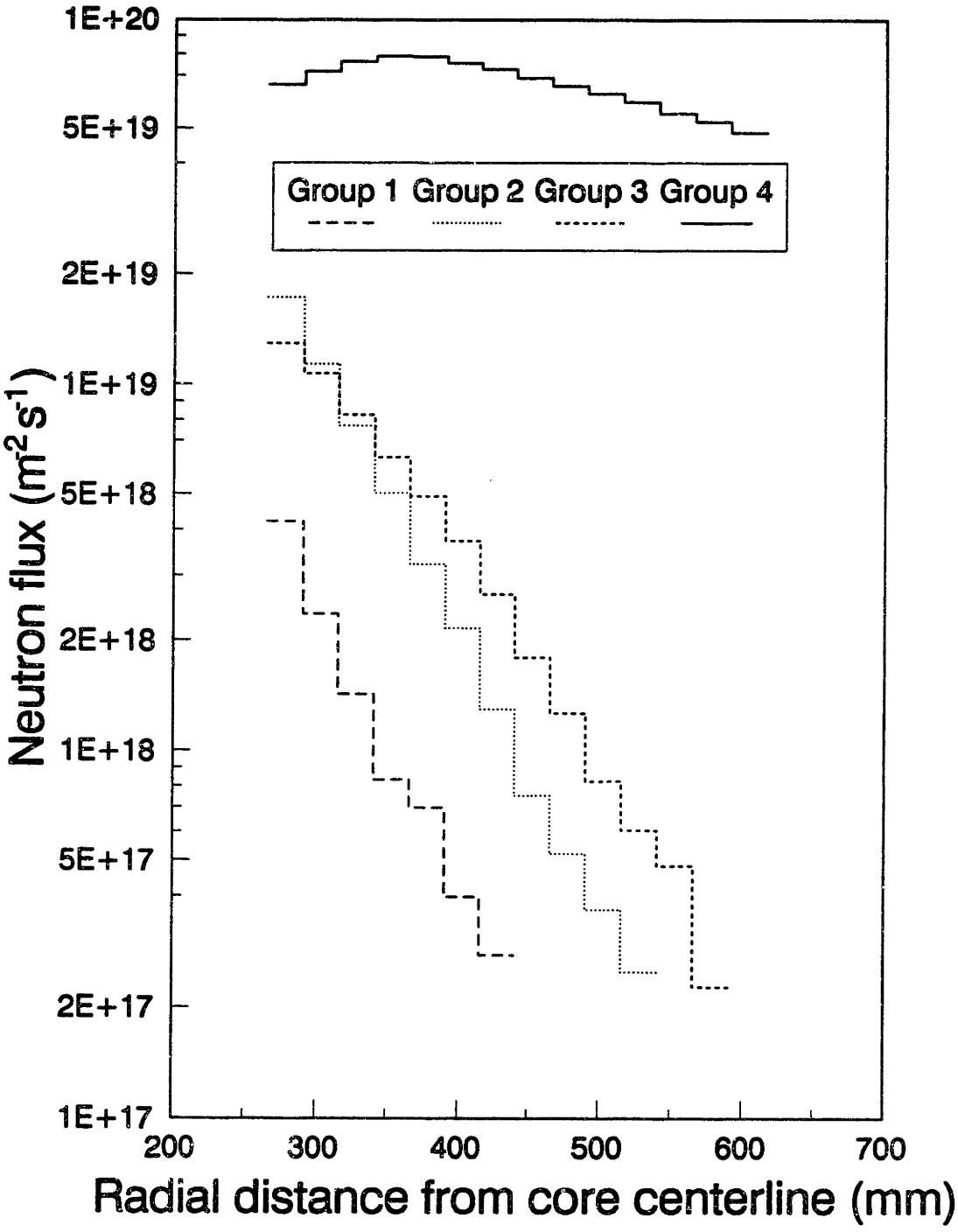

Figure 3-1. MCNP calculated neutron fluxes versus radial distance along the axial location of the peak thermal neutron flux at beginning of cycle. The ANS group structure was used in this calculation.

TABLE 3-3. MCNP FLUXES IN THE TARGET LOCATIONS WITHOUT TARGETS PRESENT FOR DIFFERENT CONTROL ROD POSITIONS

ANS Energy Group	Material Irradiation Positions Adjacent to Top Fuel Element (Region F in Figure 2-3) (10^{19} $m^{-2}s^{-1}$)	Transplutonium Target Positions Adjacent to Bottom Fuel Element (Region G in Figure 2-3) (10^{19} $m^{-2}s^{-1}$)
	Control Rods Fully Withdrawn	
1	2.840[a]	1.855
2	4.018	2.823
3	1.560	1.219
4	1.743	2.305
Total	10.161	8.202
	Control Rods Parked at Core Midplane	
1	2.239	2.879
2	3.484	4.350
3	1.277	1.787
4	0.739	3.080
Total	7.739	12.096
	Control Rods Fully Inserted	
1	3.575	1.967
2	5.366	2.956
3	1.881	1.121
4	1.046	2.233
Total	11.868	8.277

a. The relative error for these values is between 0.7 and 2.0 %.

opportunity to thermalize completely in the D_2O central hole before returning to the upper target region. When control rods are inserted, the thermal flux in the upper region decreases since the probability that thermal neutrons will return from the central hole is further reduced.

These data indicate that the current ANS design achieves a high peak thermal neutron flux in the reflector with minimal fast neutron

contamination. The target regions also have high epithermal and fast flux profiles that provide good material and transplutonium irradiation capabilities. The values presented are at beginning of cycle. These good characteristics should be maintained through the life of the core with possible change in some of the flux values as a function of U-235 burnup.

3.1.3 Coupled Neutron-Gamma Heating

As indicated earlier, one of MCNP's major advantages is its ability to perform coupled neutron-gamma transport. During this transport process, both neutron and gamma heating can be calculated. Not all isotopes, however, contain gamma production cross section data. For these isotopes, the neutron-heating values have been artificially increased to assume that all gammas created are deposited locally. Therefore, the neutron heating value calculated is substantially increased, while the photon heating calculated will be substantially reduced. This can lead to an incorrect interpretation of the results, as will be shown.

During a run where the control rods were fully inserted, a coupled neutron-gamma heating calculation was performed. Heating rates were calculated in the control rods, Al-6061 inner support pipe, and the Al-6061 CPBT. Each of these objects was segmented axially. This segmentation was identical with the axial segmentation of the fuel elements. In addition, a control rod had heating rates calculated for half its volume. The control rod was split along its diameter as shown by the dotted line in Figure 2-4.

Initially, the heating values were calculated using the 300 K Hf cross sections, which do not contain gamma production. Figure 3-2 presents the heating of the hafnium portion of an average control rod as calculated with the 300 K Hf cross sections. The peak heating, of approximately 150 W/g, occurs next to the top fuel element. Neutrons in the top half of the core thermalize to a greater extent than those

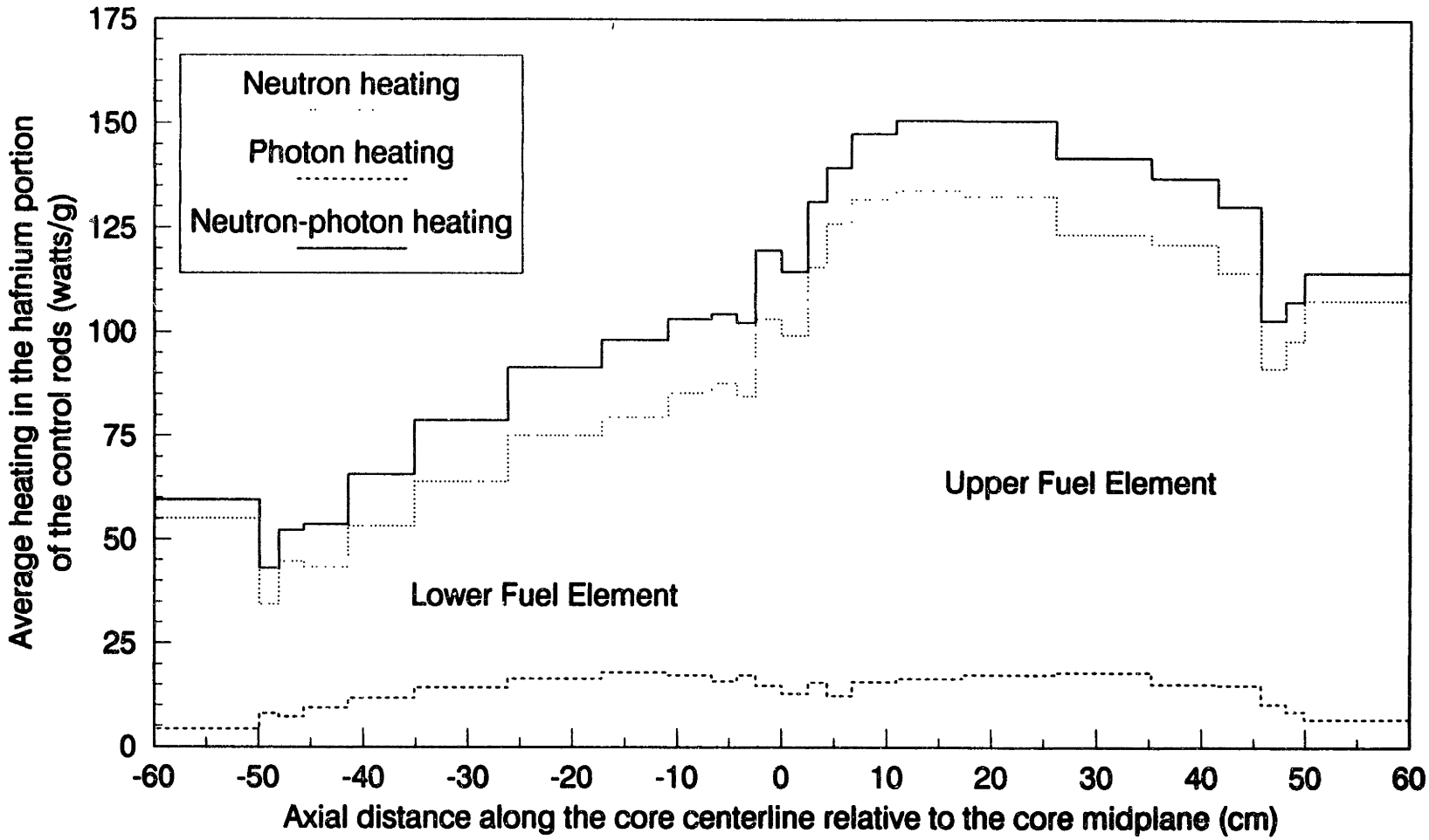

Figure 3-2. Heating rates calculated by MCNP for the hafnium portion of an average control rod. All gammas created from neutron absorptions within the Hf were assumed to be deposited locally.

in the bottom half. This leads to a higher neutron and gamma heating in the top half because the thermal absorption cross section of hafnium is very high. The drop in the heating at the top of the upper element and the bottom of the lower element correspond to the location of boron in the fuel end caps, which reduces the neutron fluxes in these positions. It was also determined that 60% of the neutron heating was occurring on the half of the control rod facing the inner AL-6061 support pipe. The peak heating on this half of the rod was calculated to be 215 W/g.

These peak heating values seemed to be extremely high. It was assumed that the values would decrease when the gamma production, transport, and heating were simulated correctly. The 0 K Hf cross sections, which contain gamma production, were therefore used to calculate more accurate coupled neutron-gamma heating rates. All further heating rates presented were calculated using the 0 K Hf cross sections.

The temperature effect of the Hf on the heating was assumed to be negligible in these calculations. Since these models contained a fresh beginning-of-cycle core, no fission products were present. Therefore, no gamma and neutron heating from fission products was accounted for. The heating rates are expected to increase greatly when the fission production gammas are accounted for.

Figure 3-3 shows the heating in an average control rod. This is similar to Figure 3-2, however almost all of the heating is due to photon absorption in the hafnium. The peak heating is approximately 65 W/g, with a rod average of 49 W/g.

Figure 3-4 shows the heating for the half of the control rod facing the fuel elements. The results are similar to Figure 3-5. However, the peak heating is now approximately 71 W/g. Approximately 51% of the total heating occurs on this side of the rod.

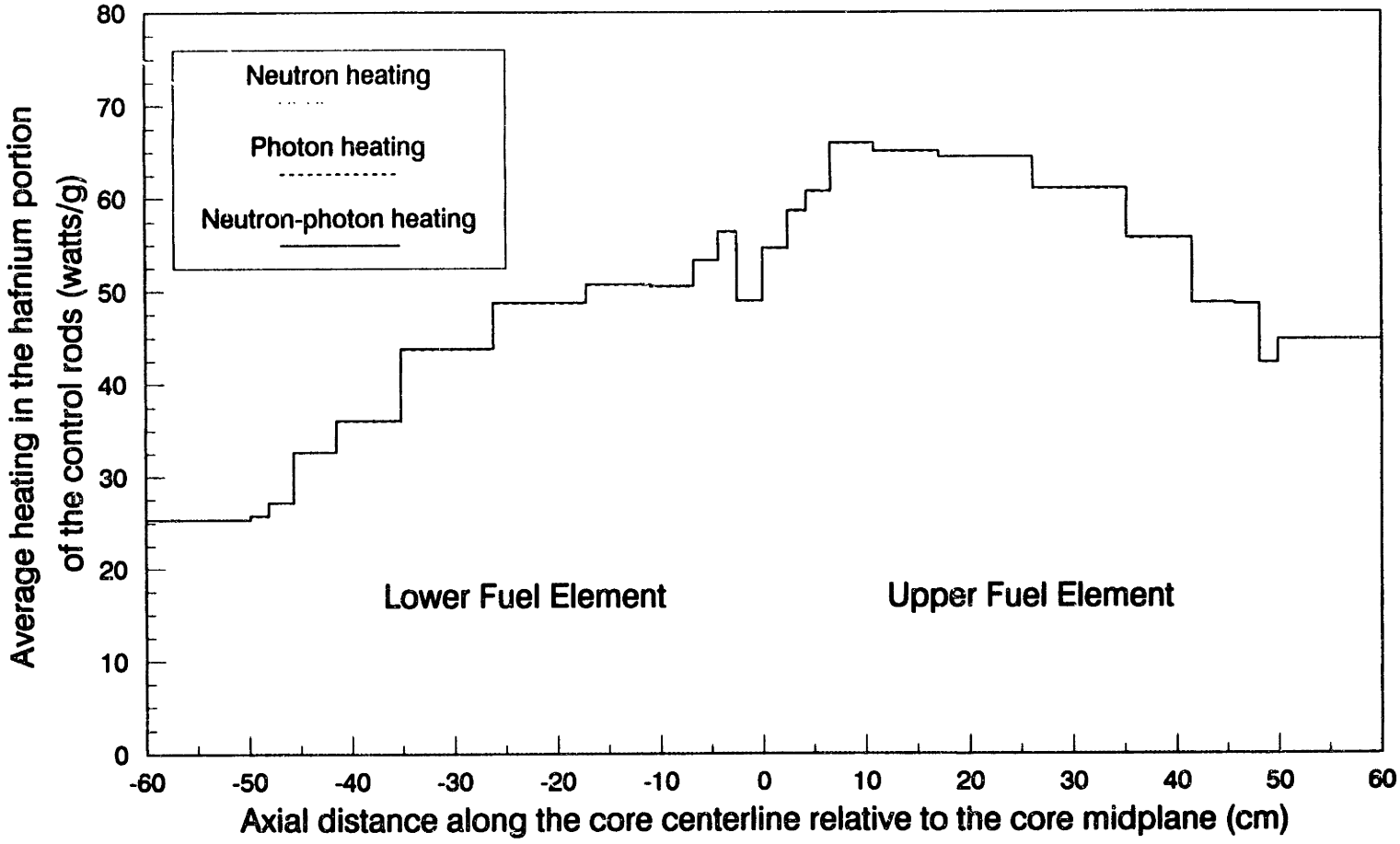

Figure 3-3. Heating rates calculated by MCNP for the hafnium portion of an average control rod.

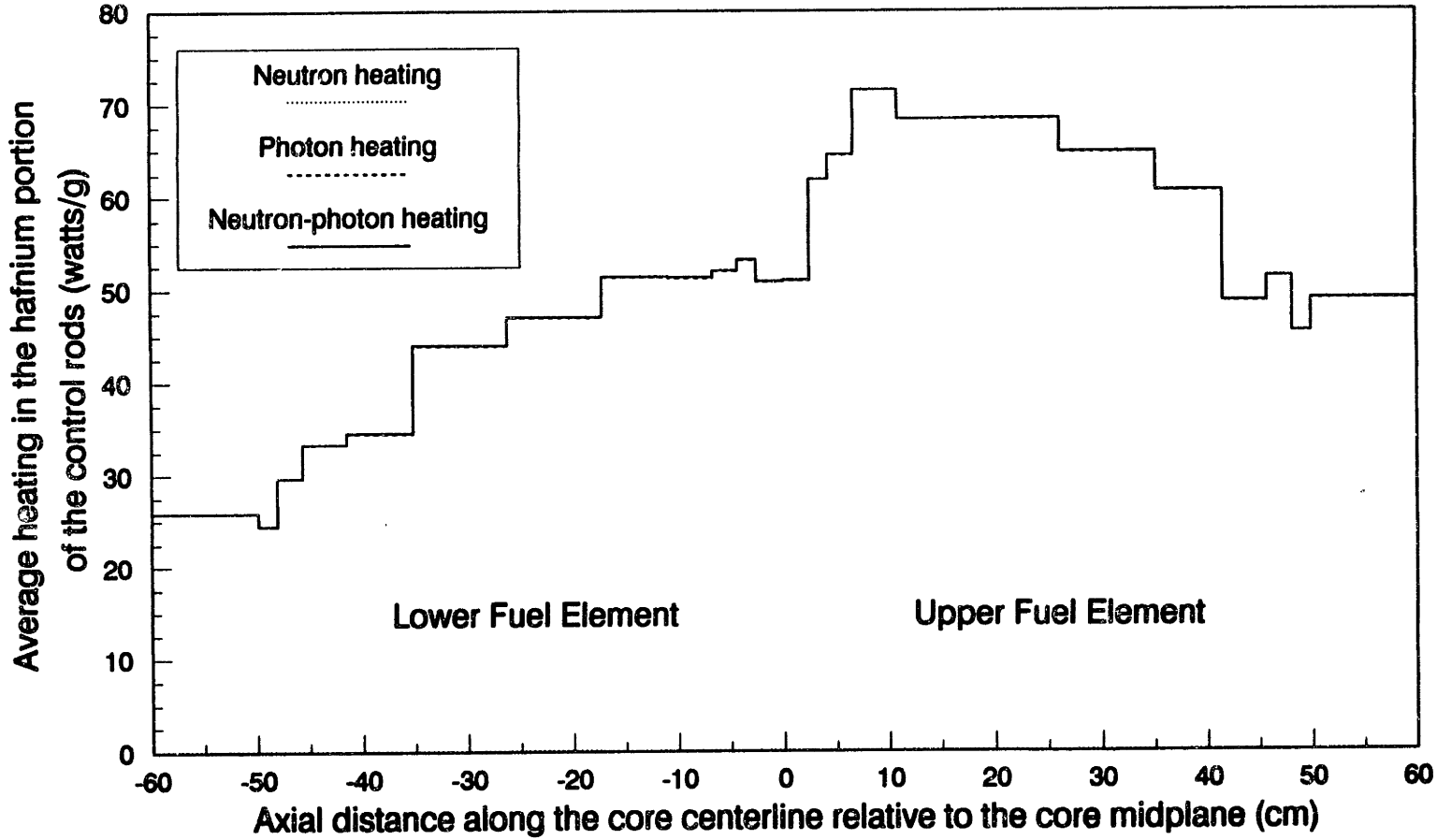

Figure 3-4. Heating rates calculated by MCNP for half a control rod. The half rod is facing the inner Al-6061 support pipe as shown in Figure 2-4.

Figure 3-5 shows the heating in the core pressure boundary tube. As can be seen, the primary heating is due to photons. The peak heating is occurring next to the top fuel element as expected. Neutron heating is a noticeable, but not predominant effect next to the top fuel element. The peak heating of approximately 30 W/g indicates that forced cooling will be required on both sides of the core pressure boundary tube.

Figure 3-6 shows the heating in the inner Al-6061 support pipe. The peak heating occurs next to the upper fuel element. Again the primary heating is due to photons, with neutron heating being more pronounced next to the bottom element. The peak is approximately 37 W/g.

These results indicate that heat removal from the control rods will be a difficult problem. Active cooling will also be required for all reactor components during full power operation, and design changes may be necessary to alleviate this heating problem.

3.1.4 Power Generation in the Fuel Elements

During many MCNP runs, fission heating tallies were performed. These tallies calculate the heat generated in the fuel due to fissioning. It is assumed that all gamma energy created is deposited locally. Therefore this tally can be used to determine the percentage of total power produced in each fuel element. Table 3-4 presents the results of these calculations for three cases: control rods fully withdrawn, control rods inserted to core midplane, and control rods fully inserted.

As this data indicates, the power production shifts to the lower fuel element as control rods are inserted to core midplane. This confirms that a shift in flux is also occurring in the fuel and target irradiation positions as presented earlier.

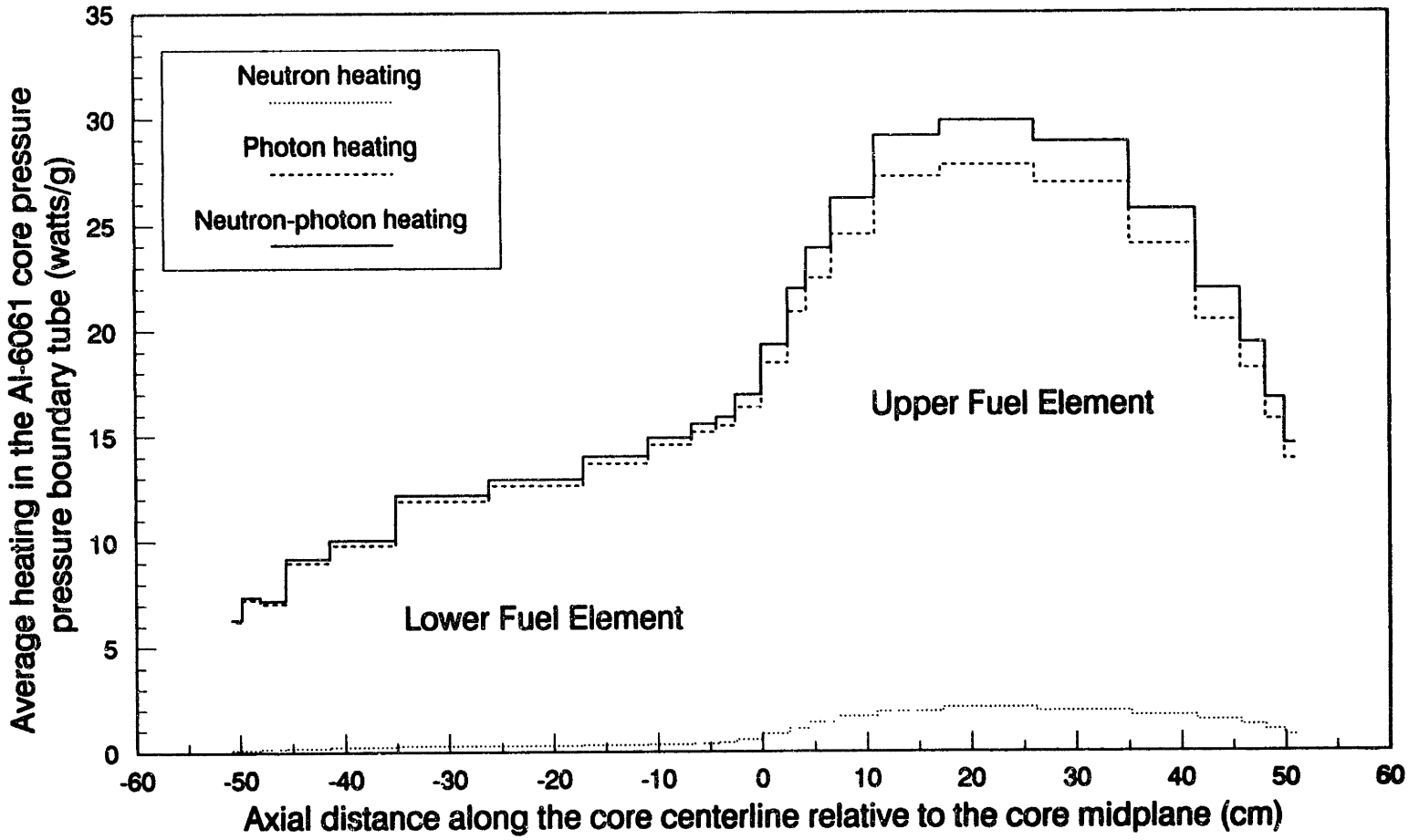

Figure 3-5. Heating rates calculated by MCNP for the Al-6061 core pressure boundary tube.

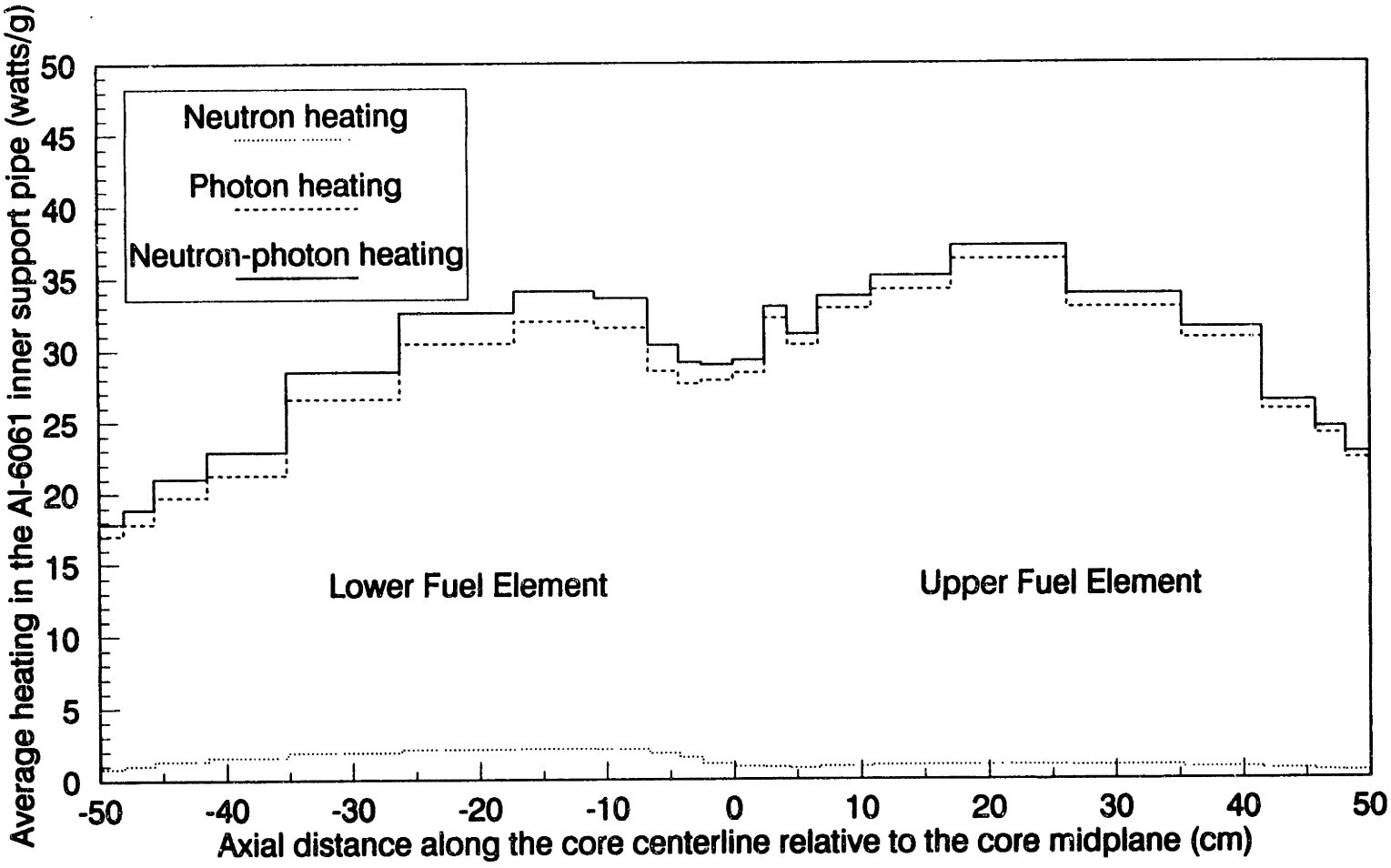

Figure 3-6. Heating rates calculated by MCNP for the inner Al-6061 support pipe.

TABLE 3-4. PERCENTAGE OF TOTAL POWER PRODUCED BY EACH FUEL ELEMENT

	Run Number	Upper Fuel Element	Lower Fuel Element
Control rods fully withdrawn (100 mm above upper element)	ANS45	64.5%	35.5%
Control rods inserted to core midplane	ANS50	49.6%	50.4%
Control rods fully inserted	ANS36	71.8%	28.2%

Relative power densities were also calculated. These values are presented in Chapter 4 in a comparison with PDQ-7.

3.2 Reflector Shutdown Rod Study

A study was performed with the eight proposed reflector shutdown rods at the fully inserted position. Table 3-5 presents the results of this study as compared to a case with no reflector rods present. No control rods were present in either calculation. These results demonstrate that the reflector shutdown rods are capable of safely bringing the ANS to a subcritical state when needed.

TABLE 3-5. REFLECTOR SHUTDOWN RODS CHARACTERIZATION RESULTS

Description	Run Number	Core Multiplication Factor
No shutdown rods	ANS39	1.1205 ± 0.0045
8 reflector shutdown rods fully inserted	ANS46	0.8568 ± 0.0030

3.3 D_2O Voiding Studies

Some D_2O voiding studies were performed with MCNP and PDQ-7. However, unless the cross sections within the PDQ model are altered to account properly for the effect of spectrum changes, the results may be inaccurate. This is especially true when the coolant channels are voided and moderator is removed from the fuel. Also, diffusion theory is not capable of analyzing a pure void properly, whereas MCNP is fully capable of handling a voided geometry. For most D_2O voiding scenarios, a 100% void would not exist.

Three studies were performed. The first study consisted of voiding all coolant channels in both elements. The fuel end caps were not voided. In the second study the outlet plenum above the bottom element and next to the top element was voided. Finally, the entire D_2O central hole was voided while control rods were inserted to core midplane. Table 3-6 presents these results along with the base cases for comparison.

TABLE 3-6. EFFECTS OF D_2O VOIDING ON CORE REACTIVITY

	Run Number	Core Multiplication Factor
Base case without control rods	ANS39	1.1205 ± 0.0045
Coolant channels voided - no control rods	ANS42	1.0661 ± 0.0042
Plenum above lower element voided - no control rods	ANS41	1.0962 ± 0.0044
Base case with control rods inserted to core midplane	ANS50	1.0036 ± 0.0040
Central hole voided - control rods inserted to core mid-plane	ANS49	0.9453 ± 0.0043

All of the voided configurations studied have a negative reactivity impact. When the central hole was voided, the negative effect the control rods have on reactivity was removed, which in itself is a reactivity insertion. However, the predominant effect was the removal of moderator resulting in the large reactivity drop. Further studies should be performed to determine the effect on reactivity of partially voiding the central hole around the control rods.

3.4 Beam Tube Studies

All ANS models currently used do not simulate beam tubes or cold sources. Without modelling these items, their effect on reactivity is unknown. MCNP offers the capability of easily modelling the beam tubes as either elliptical or circular cylinders. As Figure 2-5 shows, four circular voided beam tubes were modelled for preliminary studies to determine the reactivity loss and the flux at the end of a beam tube. Table 3-7 compares two studies, one with and one without the beam tubes.

TABLE 3-7. THE EFFECT ON REACTIVITY DUE TO INSERTING FOUR BEAM TUBES

	Run Number	Core Multiplication Factor
No beam tubes	ANS43	1.1343 ± 0.0044
4 beam tubes	ANS48	1.1302 ± 0.0033

These values indicate that the presence of beam tubes does not have a large effect on reactivity. The effect is expected to become more pronounced when all eight proposed beam tubes are modelled. The total effect, however, is not expected to be much more than one percent in the core multiplication factor.

Another concern is the effect on reactivity of flooding the beam tubes with either D_2O or H_2O. The first case would be a positive

reactivity insertion while the second case would be a negative reactivity insertion. The magnitude of these insertions needs to be determined in future ANS work.

A surface-averaged flux tally was performed over the cross section of a beam tube at four locations along its length. The first and second locations were the faces of the end cap of the beam tube. The third location was the outer edge of the D_2O reflector. The fourth location was the outer edge of the H_2O biological shield. Table 3-8 shows the relative errors for the values calculated at these various locations. The MCNP manual recommends using only values with a relative error less than 0.05. These values are therefore unacceptable. The 0.0 values correspond to no neutrons in those energy groups contributing to the tally. 48,000 neutrons were tallied to produce these values. The primary reason that the relative errors in Table 3-8 are unacceptably large is that the surface area over which the tally is being performed is so small. This problem is further complicated by the fact that the flux of neutrons in the reflector deceases with the increasing radius of the reflector.

These results indicate that some variance reduction techniques will have to be employed before an accurate and efficient calculation of fluxes along the beam tubes can be performed.

3.5 Doppler Broadening of Uranium 235 and 238

The U-235 and U-238 cross sections used in all production calculations were evaluated at 300 K. Cross sections are available at 600 and 900 K. Two runs were made to determine the effect on the core multiplication factor and peak thermal neutron flux of using the higher temperature cross sections. The concentrations were not altered to be representative of the higher temperatures (fuel expansion effects were not considered). The U-235 and U-238 isotope identifiers were simply changed to the higher temperature isotopes. Table 3-9 lists the results.

TABLE 3-8. RELATIVE ERRORS ON AVERAGE SURFACE FLUX CALCULATIONS IN A BEAM TUBE

ANS Energy Group	Relative Error[a]
	Cross Section of Beam Tube Near the CPBT
1	1.000
2	0.5992
3	0.3940
4	0.0886
	Cross Section of Beam Tube at the Edge of the D_2O Reflector
1	0.0000
2	0.0000
3	0.0000
4	0.2263
	Cross Section of Beam Tube at the Edge of the H_2O Biological Shielded
1	0.0000
2	0.0000
3	0.0000
4	0.3579

a. The relative error is defined as the standard deviation divided by the mean.

TABLE 3-9. EFFECT OF HIGH URANIUM TEMPERATURES ON CORE MULTIPLICATION FACTORS AND NEUTRON FLUX

Evaluated Temperature of U-235 and U-238	Core Multiplication Factor	Peak Thermal Neutron Flux (10^{19} $m^{-2}s^{-1}$)
300 K (ANS71)	1.0003 ± 0.0036	7.6088 ± 0.1073
600 K (ANS72)	0.9955 ± 0.0055	7.8218 ± 0.1557
900 K (ANS73)	0.9939 ± 0.0053	7.6819 ± 0.1521

These results effectively indicate no change in the core multiplication factor as the Doppler broadening of the U-235 and U-238 occurs. These results also indicate a slight increase in the peak thermal neutron flux as the U-235 and U-238 temperature increases to 600 K. It may be more accurate to use the higher temperature cross section for future calculations since 600 K is closer to the fuel operating temperature than 300 K.

3.6 Plate Geometry Effects

As stated earlier, MCNP does not offer the capability of modelling involute fuel plates. Therefore, the fuel is modelled as a homogeneous mixture of fuel, cladding, and D_2O coolant.

MCNP, however, can provide some insight into the accuracy of the fuel plate homogenization. MCNP automatically calculates an average mean free path for neutrons and photons in each computational region of the model. MCNP can also calculate macroscopic or microscopic cross sections for any such reason. Since the mean free path is equal to $1/\Sigma_{total}$, MCNP can approximate its value in any energy structure desired. Table 3-10 shows the mean free paths as estimated with the total macroscopic cross section and as automatically calculated by MCNP. These values are representative of the fuel elements. There is very little change in the mean free paths from the center of the fuel to the outside of the fuel.

The fuel plate width is 1.27 mm. These data indicate that any neutron will traverse multiple fuel plates before undergoing an interaction. Therefore, the homogenization of the fuel plates should be quite accurate.

The argument presented above is based on MCNP calculations. However, this argument does not offer much physical insight into the accuracy of the fuel plate homogenization. Therefore, a simple, physical argument is presented to collaborate the MCNP calculations.

TABLE 3-10. NEUTRON MEAN FREE PATHS IN THE CENTER OF THE HOMOGENIZED FUEL ELEMENTS

ANS Energy Group	Neutron Mean Free Path Calculated from Cross Sections (mm)
1	40.933[a]
2	40.032
3	38.388
4	22.437
Total	39.185
Neutron mean free path automatically calculated by MCNP over the total energy range	41.969

a. The standard deviations associated with these values is less than 0.15.

The mean free path of a 6.67 eV neutron in the fuel meat was estimated. The macroscopic cross section was calculated using only the U-238 6.67 eV cross section and the U-238 density within the fuel meat. The 6.67 eV cross section is the largest for U-238 and is also considerably larger than the cross sections, at any energy, of the other fuel materials. This approximation should produce a conservatively low average neutron mean free path since the neutron energies span a wide range of values and the cross sections are considerably lower at other energies.

The 6.67 eV 300 K Doppler-broadened cross section of U-238 is approximately 7000 barns.[26] The U-238 density in the fuel plates, at the location of maximum uranium loading, is 3.984×10^{-4} atoms $barm^{-1}cm^{-1}$. The resulting 6.67 eV neutron mean free path is 3.585-mm. This mean free path spans approximately 2.8 fuel plates.

This simplified physical argument confirms the conclusion that the fuel plate homogenization should be accurate.

CHAPTER 4. MONTE CARLO VERSUS DIFFUSION THEORY

Before MCNP was used for production calculations, the model and methods were benchmarked against the PDQ-7 model. Early studies compared the diffusion theory model to some S_n transport theory models.[3] In general, S_n transport theory predicts lower core multiplication factors and higher flux values. The Monte Carlo results are in the same direction as the S_n results, and the differences with diffusion theory are more pronounced.

During the MCNP-PDQ comparisons it was assumed that a portion of the discrepancy was due to the cross section sets being used in PDQ. These cross sections were generated for an early design of the ANS. The U-235 density was considerably higher than the density in the current preconceptual design. The increased density could have introduced self shielding and other effects inappropriate for the current design. It is generally agreed that the PDQ-7 cross sections should be recalculated when the new design is released. This should improve the accuracy of the diffusion theory model.

4.1 Core Multiplication Factor Comparisons

The first MCNP model contained homogenized fuel zones with a uniform U-235 loading. No boron or hafnium was present in this model. Similar PDQ-7 and VENTURE models were set up. Table 4-1 shows the MCNP, PDQ-7, and VENTURE comparisons for the beginning-of-cycle uniformly-graded U-235 model.

This comparison shows excellent agreement between these codes for this model. The discrepancy is probably due to the different cross section sets used in VENTURE and PDQ.

TABLE 4-1. MONTE CARLO VERSUS DIFFUSION THEORY COMPARISON FOR A UNIFORMLY GRADED U-235 LOADING WITH NO BORON OR HAFNIUM

	Core Multiplication Factor at BOC
PDQ	1.306
VENTURE	1.287
MCNP (ANS25)	1.2762 ± 0.0037

Graded-fuel core models were set up in MCNP and compared to PDQ. Boron was included in the end caps in one model and excluded in another model. The boron was removed in one run in order to determine if the discrepancy between MCNP and PDQ was due primarily to the boron modelling. As the data shows, the discrepancy between MCNP and PDQ is probably due to the cross section sets used in PDQ for the graded-fuel model. Table 4-2 shows the results of the MCNP versus PDQ study.

TABLE 4-2. MCNP VERSUS PDQ COMPARISONS FOR THE GRADED FUEL MODEL

Case	Run Number	Core Multiplication Factor
Boron in the End Caps		
MCNP	ANS39	1.1205 ± 0.0045
PDQ	DD462	1.1608
No Boron in the End Caps		
MCNP	ANS34	1.2595 ± 0.0050
PDQ	DD470	1.2994

MCNP is approximately 3.5% lower on its prediction of the core multiplication factor compared to PDQ for the runs containing boron. The difference between MCNP and PDQ for the runs without boron is only about 3%. This indicates that the primary discrepancy between MCNP

and PDQ is not due to boron and may be due to the spatially-dependent PDQ cross section sets within the fuel.

A comparison of the change in the core multiplication factor as calculated by PDQ and MCNP for control rods inserted to core midplane and rods fully inserted indicates that PDQ does an acceptable job of estimating the control rod bank worths even though PDQ cross sections are homogenized over the central hole. Table 4-3 presents the change in the core multiplication factor as calculated by MCNP and PDQ. The values presented represent the effect of placing control rods inserted to core midplane and rods fully inserted in a model that did not previously contain control rods.

TABLE 4-3. THE CHANGE IN THE CORE MULTIPLICATION FACTOR FOR CONTROL RODS INSERTED TO CORE MIDPLANE AND RODS FULLY INSERTED

	PDQ	MCNP
Base case - no control rods	1.1608	1.1205 $\pm$ 0.0045
Control rods inserted to core midplane	1.0301	1.0036 $\pm$ 0.0040
Change in core multiplication factor	-0.1307	-0.1169
Base case - no control rods	1.1608	1.1205 $\pm$ 0.0045
Control rods fully inserted	0.9373	0.9014 $\pm$ 0.0030
Change in core multiplication factor	-0.2235	-0.2191

4.2 Flux Comparisons

An MCNP model containing control rods inserted to core midplane was run. Incorporated into this model was a reasonably fine segmentation of the D_2O reflector for flux mapping purposes. Figure 4-1 shows the axial thermal neutron flux profile in the reflector as calculated by MCNP and PDQ. Both axial profiles shown contain the peak thermal

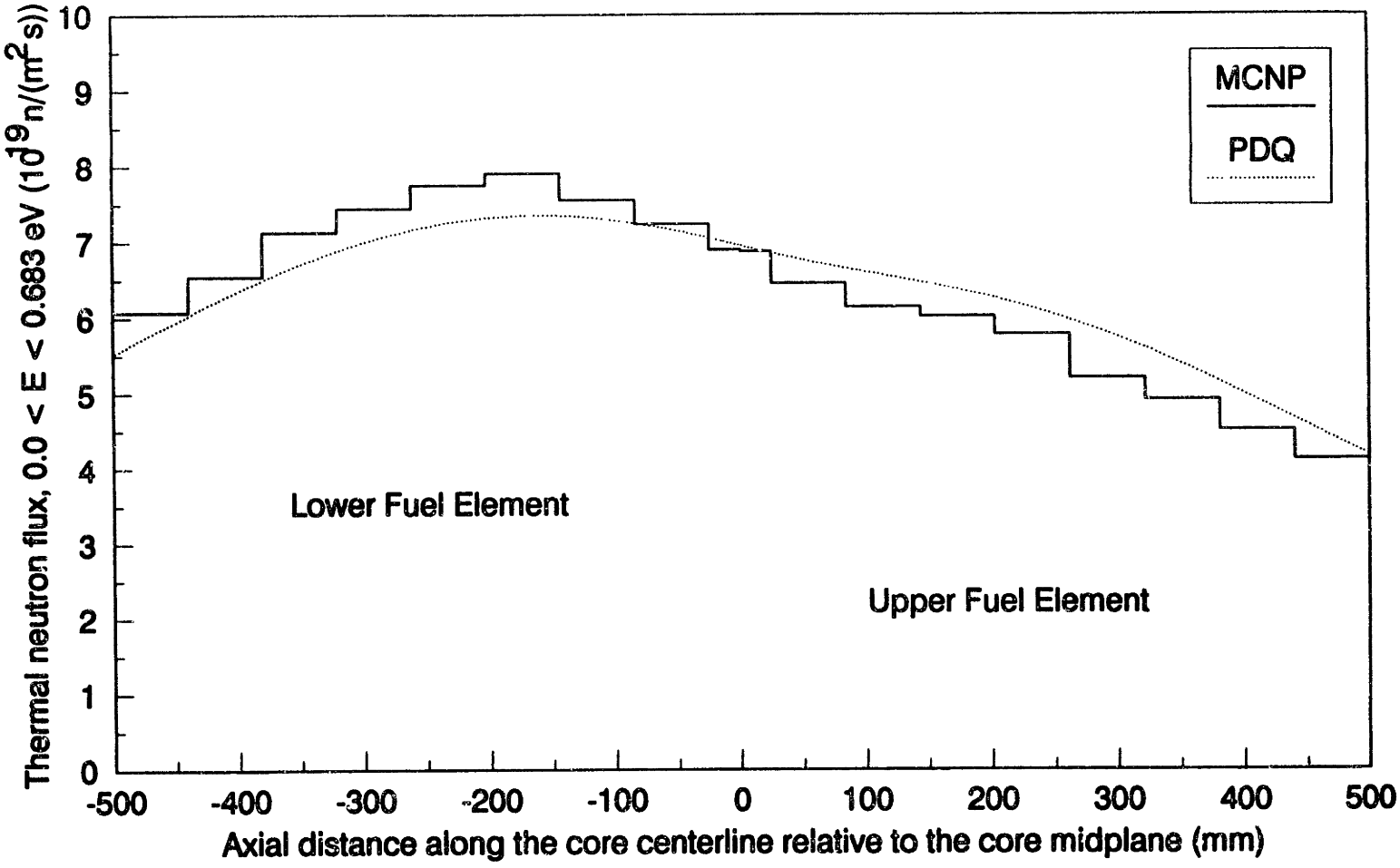

Figure 4-1. Axial thermal neutron flux profile in the reflector as calculated by MCNP and PDQ. Hafnium control rods parked at core midplane were present in these models.

neutron flux as calculated by the respective codes. The MCNP profile presented was calculated between 340.5 and 365.5 mm from the core centerline. The PDQ profile occurs at 358.8 mm from the core centerline. Figure 4-2 shows the radial thermal neutron flux profile as calculated by MCNP and PDQ. Both radial profiles shown contain the peak thermal neutron flux as calculated by the respective codes. The MCNP profile presented was calculated between 143.5 and 202.75 mm below the core midplane. The PDQ profile occurs at 151.0 mm below the core midplane.

The MCNP run used for these figures is ANS50 and the corresponding PDQ run is DD478. MCNP and PDQ calculate the same general flux profile indicating that the PDQ flux profile in the reflector is fairly accurate. However, MCNP predicts a flux peak of 7.5% higher than PDQ (7.9061 x 10^{19} versus 7.3527 x 10^{19} $m^{-2}s^{-1}$ thermal lux). In reality, this difference is more pronounced since the MCNP fluxes are evaluated from tallies averaged over regions while the PDQ fluxes are evaluated pointwise.

The volume-averaged peak thermal neutron flux calculated by MCNP between 0.0 and 0.625 eV is 7.8945 $\pm$ 0.1429 x 10^{19} $m^{-2}s^{-1}$.

PDQ cannot accurately predict the fluxes within the fuel regions. Two comparisons illustrating this failure are presented. The first compares PDQ and MCNP flux calculations in the fuel when control rods are parked at the core midplane. The second case compares PDQ and MCNP flux calculations in the fuel for the graded fuel core models without boron in the end caps. The total flux is compared as well as the fraction of total flux in each group averaged over each fuel element. Table 4-4 shows this comparison for the first case: control rods parked at midplane.

Table 4-5 shows the comparison for the second case: graded fuel model without boron in the end caps. Hafnium control rods were not present.

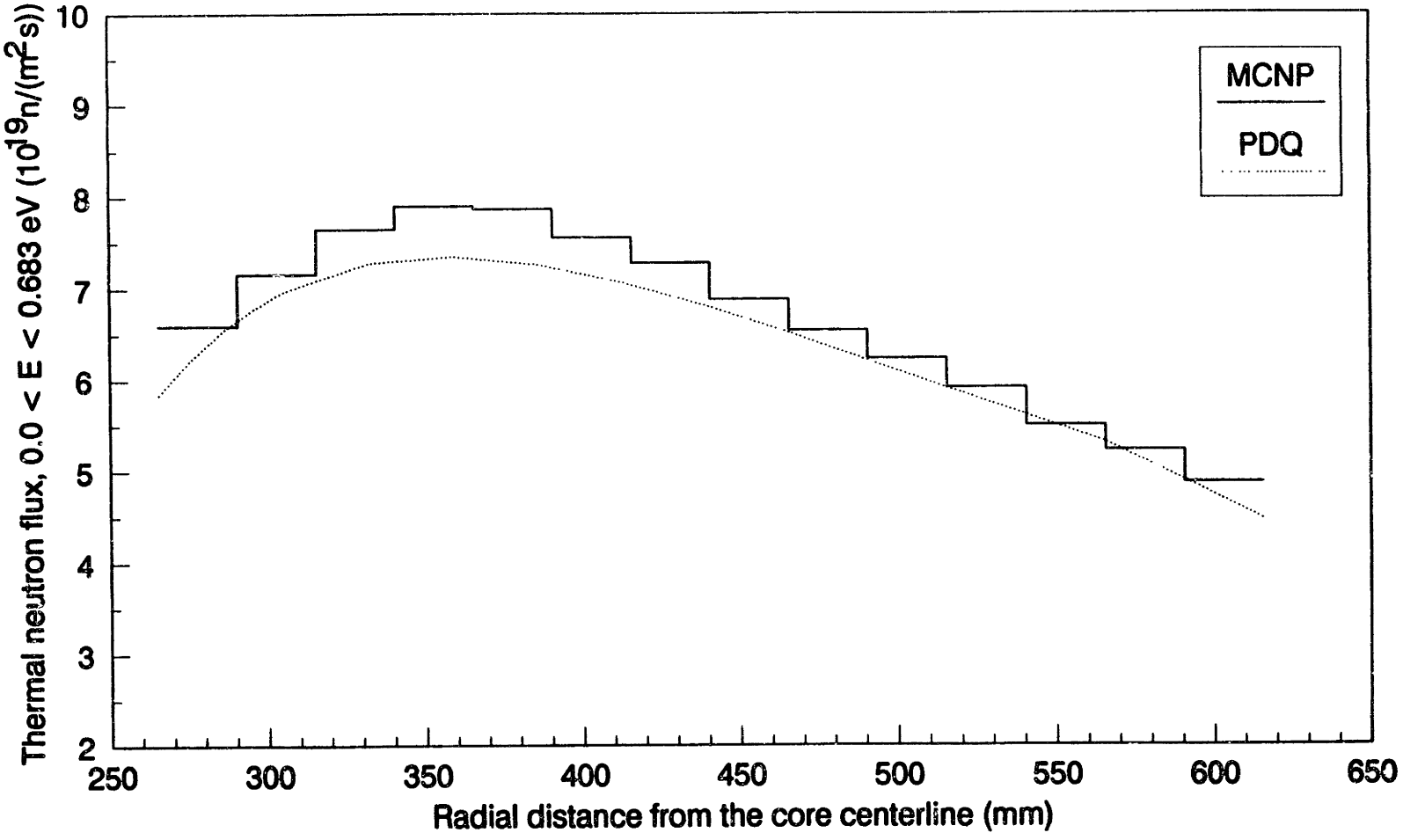

Figure 4-2. Radial thermal neutron flux profile in the reflector as calculated by MCNP and PDQ. Hafnium control rods parked at core midplane were presented in these models.

TABLE 4-4. MCNP AND PDQ FLUX COMPARISONS WHEN CONTROL RODS ARE PARKED AT CORE MIDPLANE

	Upper Fuel Element	
	PDQ (DD478)	MCNP (ANS50)
Total Flux (10^{19} $m^{-2}s^{-1}$)	8.7383	8.8319
Fraction of Total Flux		
Group 1	0.1807	0.2196
Group 2	0.3926	0.4033
Group 3	0.3480	0.2951
Group 4	0.0787	0.0820
	Lower Fuel Element	
	PDQ (DD478)	MCNP (ANS50)
Total Flux (10^{19} $m^{-2}s^{-1}$)	12.024	13.660
Fraction of Total Flux		
Group 1	0.1720	0.2177
Group 2	0.3901	0.4076
Group 3	0.3782	0.3046
Group 4	0.0597	0.0701

TABLE 4-5. MCNP AND PDQ FLUX COMPARISONS FOR THE GRADED FUEL CORE WITHOUT BORON IN THE END CAPS

	Upper Fuel Element	
	PDQ (DD470)	MCNP (ANS34)
Total Flux (10^{19} $m^{-2}s^{-1}$)	8.6214	8.9523
Fraction of Total Flux		
Group 1	0.1739	0.2105
Group 2	0.3713	0.3921
Group 3	0.3564	0.2670
Group 4	0.0984	0.1104
	Lower Fuel Element	
	PDQ (DD470)	MCNP (ANS34)
Total Flux (10^{19} $m^{-2}s^{-1}$)	7.2701	8.1997
Fraction of Total Flux		
Group 1	0.1613	0.2096
Group 2	0.3699	0.3898
Group 3	0.3909	0.3040
Group 4	0.0779	0.0966

As these tables demonstrate, considerable differences exist in the flux representation predicted by PDQ and MCNP. The largest differences consistently occur in Group 3, where MCNP predicts a lower flux. MCNP also predicts a higher thermal and fast neutron flux. Group 2 fluxes seem to be consistent between PDQ and MCNP. These differences may be large enough to warrant concern for some reactor parameters.

4.3 Power Density Comparisons

MCNP was used to calculate the relative power density in the fuel regions for the case with control rods parked at core midplane. Figure 4-3 compares the MCNP and PDQ axial relative power densities for the peak radial regions in the upper and lower fuel elements. Figure 4-4 shows the radial relative power densities calculated by MCNP and PDQ for the peak axial regions in the upper and lower fuel elements. The standard deviation of the MCNP calculations ranges from 10 to 3% of the mean from the outside of the fuel to the inside of the fuel. These figures show that PDQ is predicting more power production in the top element than MCNP, resulting in higher relative power densities in the upper element. MCNP predicts 49.6% of the total power is produced in the upper element, whereas PDQ predicts the value to be 53.8%.

The large variation in region-to-region relative power densities is partially due to changes in the U-235 density. The density is varied in some regions to approximate the proposed fuel grading. If the variations in the U-235 density were smoother, the shape of the relative power density would be smoother. The agreement may also improve with a better PDQ U-235 cross section set assignment in each region.

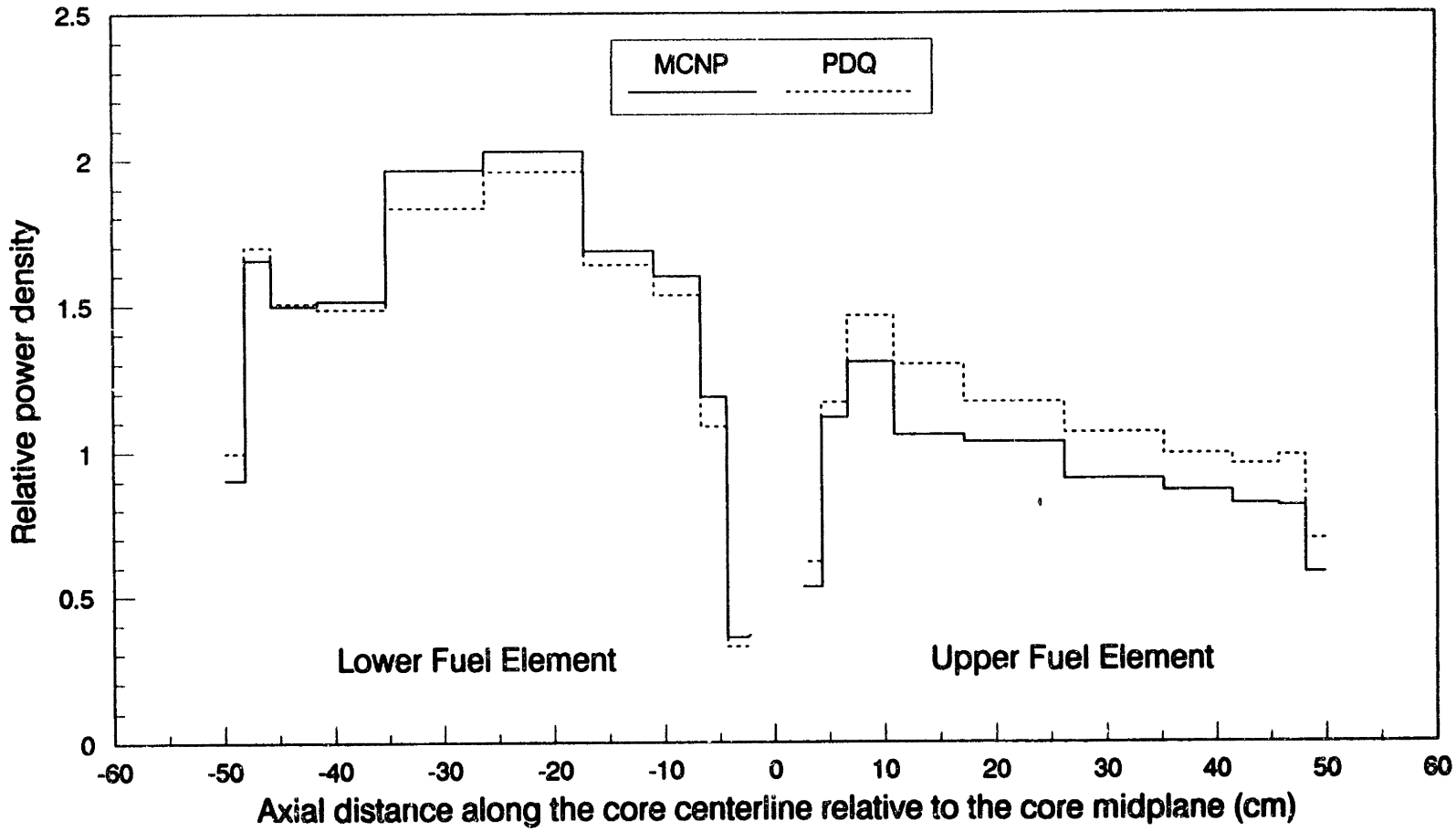

Figure 4-3. Axial relative power densities as calculated by MCNP and PDQ. The radial region of interest in the lower fuel element lies between 148.0 and 158.0 mm from the core centerline. The radial region of interest in the upper fuel element lies between 221.0 and 231.0 m from the core centerline.

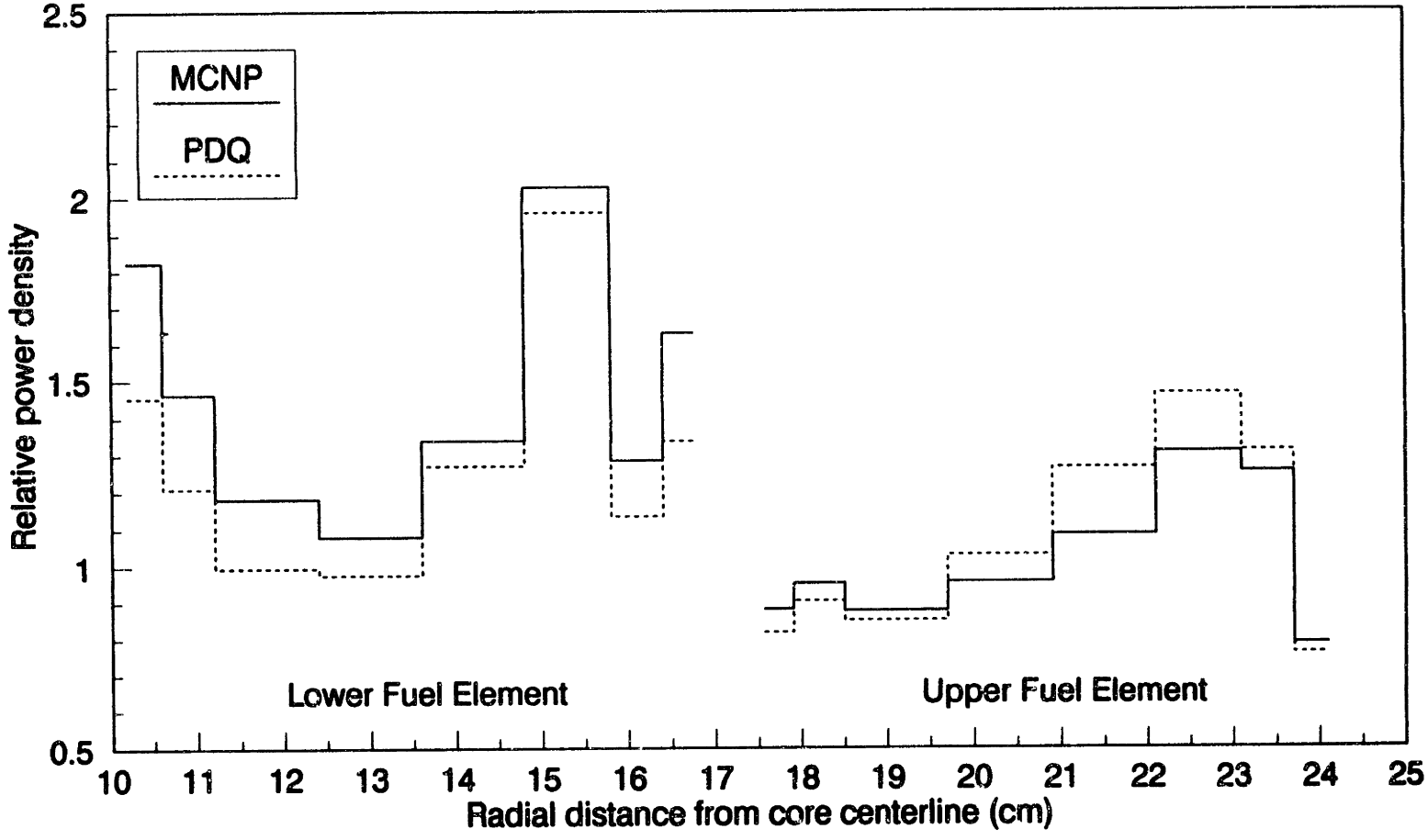

Figure 4-4. Radial relative power densities as calculated by MCNP and PDQ. The axial region of interest in the lower fuel element lies between 172.0 and 262.0 mm below the core midplane. The axial region of interest in the lower fuel element lies between 67.0 and 109.0 mm above the core midplane.

4.4 Uranium-235 Cross Section Comparison

The discrepancies between MCNP and PDQ have been partially blamed on the inaccuracy of the cross section sets in PDQ. MCNP was used to estimate four group U-235 microscopic fission and capture cross sections. This calculation was performed in all 160 fuel regions using the PDQ energy structure. Control rods were inserted to core midplane during this calculation.

The calculated cross sections were then compared to the PDQ microscopic cross sections currently being used. It was discovered that the PDQ and MCNP group-1 and -2 cross sections are extremely close. The group-4 cross sections are noticeably different, and the group-3 cross sections have the largest discrepancies. It is interesting to note that the largest discrepancies in flux values within the fuel are also in group-3.

Dr. John Ryskamp used the MCNP-calculated cross sections to adjust his PDQ U-235 microscopic cross sections to approximately agree with MCNP. This was done in two steps. First the group-4 cross sections were adjusted, then the group-3 cross sections were adjusted. Table 4-6 shows the results of the group-4 adjustment as compared to the base case PDQ values and the MCNP values. Control rods were inserted to core midplane during these runs.

TABLE 4-6. PDQ VERSUS MCNP COMPARISON AFTER THE PDQ GROUP-4 U-235 MICROSCOPIC CROSS SECTIONS WERE CORRECTED

	Core Multiplication Factor	Peak Thermal Neutron Flux (10^{19} $m^{-2}s^{-1}$)
PDQ - Base Case (DD508)	1.0306	7.3466
PDQ - Group 4 U-235 Cross Sections Adjusted (DD509)	0.9991	7.8189
MCNP - Base Case (ANS50)	1.0036 $\pm$ 0.0040	7.9061 $\pm$ 0.1423

Changing the group-4-U-235 microscopic cross sections seemed to eliminate the MCNP-PDQ discrepancies. However, the group-3 cross sections had yet to be altered. After the group-3 cross sections were adjusted, the MCNP-PDQ discrepancies returned. Table 4-7 shows the results of changing both PDQ group-3 and group-4 cross sections.

There is no explanation at this time why the discrepancies returned when the group-3 cross sections were corrected. It is encouraging to note that the MCNP-PDQ discrepancies were not as large as they were originally. It is still expected that the PDQ values will further improve when the cross-sections are recalculated for the current design.

TABLE 4-7. PDQ VERSUS MCNP COMPARISON AFTER THE PDQ GROUP 3 AND 4 U-235 MICROSCOPIC CROSS SECTIONS WERE CORRECTED

	Core Multiplication Factor	Peak Thermal Neutron Flux (10^{19} $m^{-2}s^{-1}$)
Control Rods Inserted to Core Midplane		
PDQ - Base Case (DD508)	1.0306	7.3466
PDQ - Group 3 and 4 U-235 cross sections adjusted (DD510)	1.0235	7.3064
MCNP - Base Case (ANS50)	1.0036 ± 0.0040	7.9061 ± 0.1423
No Control Rods Present		
PDQ - Base Case	1.1608	
PDQ - Group 3 and 4 U-235 cross sections adjusted (DD511)	1.1490	
MCNP - Base Case (ANS39)	1.1205 ± 0.0045	
No Control Rods Present and No Boron in the Fuel End Caps		
PDQ - Base Case (DD470)	1.2994	
PDQ - Group 3 and 4 U-235 cross sections adjusted (DD512)	1.2871	
MCNP - Base Case	1.2595 ± 0.0050	

CHAPTER 5. MCNP TECHNIQUES

Monte Carlo has one major disadvantage compared to deterministic methods. That is the amount of computer time needed to obtain accurate results. This problem is further complicated in a D_2O system where the neutron lifetime is relatively long. Current models need 1-5 hours of CRAY time to achieve adequate results.

The adequacy of a result is dependent upon the relative error, (standard deviation of the mean)/(mean). The relative error is reduced as more information is obtained; however this results in a longer run time. The MCNP manual recommends accepting only relative errors below 0.05. The difficulty in obtaining a relative error is also dependent upon the calculation being performed. It is relatively easy to obtain low relative errors for the core multiplication factors, but it is more difficult to obtain low relative errors for a cell-averaged flux calculation in a small volume.

MCNP has many capabilities, including numerous variance reduction techniques. Some of these features are not applicable to the ANS, while others offer the user more versatility. During many of the MCNP calculations, the default options were used. Some variance reduction techniques were also experimented with in the hopes of improving the problem solving efficiency and reducing the run time.

5.1 Power Normalization Factor

The Monte Carlo technique tracks individual neutrons to obtain the information for the problem solution. The tracking occurs in cycles. Each cycle has an average number of source neutrons, chosen by the user. Therefore the quantity of information from one cycle is dependent upon the number of source neutrons. Each cycle is considered statistically independent of the previous cycle.[25]

During each cycle, the parameters desired are estimated. The estimates from the cycles are then statistically combined to produce the mean value and its standard deviation.

In MCNP all tallies are normalized per fission neutron (a neutron resulting from fission). To normalize to a certain power level, a power normalization constant must be derived so that quantities based on the appearance of one fission neutron can be normalized to the values they would have for the reactor at a given power level. This constant depends on the number of fissions per second, the number of fission neutrons per fission, and the value of k-eff for that run. The normalization factor will be referred to as PN. The value of PN is then the number of fission neutrons per second when the power level is P. PN has the form:

$$PN = P \cdot \bar{\upsilon} \cdot 1/Q \cdot 1/\text{k-eff}$$

where

P = core power level in watts

$\bar{\upsilon}$ = average number of fission neutrons per fission

Q = energy per fission in Joules/fission

k-eff = effective core multiplication factor from the run in which normalization is occurring.

If the equation is rewritten depicting the units of the variables, it becomes a little easier to understand.

$$PN = \left(\frac{\text{Joules}}{\text{s}}\right)\left(\frac{\text{fission neutrons}}{\text{fission}}\right)\left(\frac{\text{fission}}{\text{Joules}}\right)$$

$$\left(\frac{\text{neutrons in generation i}}{\text{neutrons in generation i + 1}}\right) = \frac{\text{fission neutrons}}{\text{s}}$$

Since k-eff is the net number of neutrons created from a certain number of fission neutrons, this is an appropriate definition of PN. All of the tallies are normalized per fission neutron. For example, the cell averaged flux tallies from MCNP have units of $\frac{\text{particles}}{\text{cm}^2}$ and are normalized per fission neutron, resulting in:

$$\phi = \frac{\text{particles}}{(\text{cm}^2)\ (\text{fission neutron})}$$

If ϕ, so normalized, is multiplied by the power normalization factor, the correct units of $\frac{\text{particles}}{\text{cm}^2\ \text{s}}$ are returned.

$\bar{\upsilon}$ is calculated from MCNP by tallying the total number of neutrons from fission as well as the number of fissions occurring and dividing those numbers appropriately.

The Q value used in this normalization is 3.236E-11 Joules/fission or 202 MeV/fission. This is the Q value used in the PDQ calculations.

The form of PN was verified with three quick calculations using the Godiva experiment model. Subcritical, critical, and super critical cases were run. In each run a fission heating tally was performed. This tally assumes all fission energy is deposited locally. Therefore if no energy escapes the system this tally can be normalized and will predict the correct reactor power level. The units of this tally are MeV/(g· fission neutron). If the tally is multiplied by the mass of the cell and the units are changed to Joules, the resulting units for this tally are Joules/(fission neutron). If the value is normalized using the power normalization constant, the resulting units are watts. Table 5-1 shows the power level calculated for the three cases mentioned after normalization to a power level of 350 MW.

TABLE 5-1. REACTOR POWER LEVEL CALCULATED FOR THE GODIVA SPHERE

k-effective	Power Level Calculated (MW)
0.603	348.326
1.000	350.5
1.630	352.867

This data also verifies the necessity of the 1/k-eff term in the normalization constant.

5.2 Reflecting Surfaces

When using deterministic methods, certain simplifications can be made in a reactor model that will increase the efficiency of the calculation. Such an example is the use of a two-dimensional PDQ model, r-z, instead of a three-dimensional model to represent the ANS. The mathematical solution to deterministic calculations becomes more complex as the number of dimensions in the model or the size of the model increases. The efficiency of the calculation is thereby reduced. Therefore it is advantageous for the user to employ symmetry within a model if possible. Modeling a half or a quarter of a reactor core, if appropriate, reduces greatly the complexity of the calculation and will increase the efficiency.

MCNP permits the user to make similar geometric simplifications with the use of reflecting surfaces. A reflecting surface has the effect of specularly (mirror) reflecting any particle that strikes it. The MCNP manual states that "reflecting planes are valuable because they can simplify a geometry setup (and also tracking) in a problem. They can, however, make it difficult (or even impossible) to get the correct answer".[2] The manual further recommends caution in the use of reflecting surfaces.

Since the ANS is rotationally symmetric about the z-axis, the geometry setup could not be simplified with the use of reflecting planes. It was hoped, however, that modeling a quarter of the ANS core with the use of reflecting planes would decrease the run time by permitting fewer neutrons to be tracked while maintaining the same relative error. Table 5-2 shows the result of two MCNP calculations: one with reflecting planes and one without reflecting planes. The reflecting planes represented a quarter of the reactor. 48,000 neutrons were tallied in the full core model calculation and 12,000 neutrons were tallied in the quarter core model calculation.

TABLE 5-2. THE EFFECT OF USING REFLECTING SURFACES ON THE CORE MULTIPLICATION FACTOR

	Neutrons Tallied	Core Multiplication Factor
Base case - full core model	48,000	1.2937 ± 0.0031
Quarter core model utilizing reflecting planes	12,000	1.2880 ± 0.0099

The run time was reduced by approximately one quarter; however, the accuracy of the calculation was not maintained. The reason for this is rather simple. In the base case calculation, 48,000 neutron histories provided a certain amount of information from which the low standard deviation was derived. When reflecting planes were used, no additional information was gained in a neutron history. Therefore, 48,000 histories would still be needed in the quarter core model to produce the same accuracy as the full core model. Since the run time is dependent on the number of neutron histories tracked, there is no increase in the runtime efficiency. As a result, all MCNP calculations are performed with a full three dimensional model.

5.3 Analog and Implicit Capture

MCNP has two basic methods of tracking particles. These methods are analog capture and implicit capture. Analog capture is a physically realistic particle transport method, while implicit capture is a more efficient method of particle transport. Both methods will produce the same answer. However, the standard deviations will be different. Implicit capture is the default MCNP transport method.

"In analog capture, the particle is killed with probability σ_a/σ_T, where σ_a and σ_T are the absorption and total cross sections of the collision nuclide at the incoming neutron energy. The absorption

cross section is specially defined for MCNP as the sum of all (n,x) cross sections where x is anything except neutrons."[2]

In implicit capture, the particle is not terminated in a capture event, rather its weight is reduced by σ_a/σ_T times its original weight and the particle transport is continued. Eventually the particle's weight will fall below the weight cutoff and Russian roulette will be played. The particle is either terminated or its weight is increased and the transport increases.

"For all particles killed by analog capture, the entire particle energy and weight are deposited in the collision cell. For implicit capture, a fraction σ_a/σ_T of the incident particle weight and energy is deposited in the collision cell corresponding to that portion of the particle that was captured."[2]

MCNP has an option to switch the particle transport from implicit capture to analog capture below a certain energy value, usually thermal. This method can be beneficial in regions of low thermal absorptions by reducing the number of tracks being followed. This would save computer time and possibly increase the efficiency. The MCNP manual, however, warns that "analog capture may undesirably kill important particles before they are tallied or participate in physics important to the problem."[2] This method, however, is a problem-wide method. Therefore, in the ANS, analog capture would be performed in the reflector as well as in the fuel. Within the reflector this would be useful because particles undergo a very large number of scatters before being terminated. Within the fuel, however, analog capture is not a good method of transport because the thermal neutrons are very important to the problem solution since the ANS is a thermal reactor. Table 5-3 presents a comparison between a model with all implicit capture and a model with analog capture below 0.683 eV. 48,000 neutron histories were tallied in each run.

TABLE 5-3. IMPLICIT CAPTURE VERSUS ANALOG CAPTURE

	Core Multiplication Factor	Peak Thermal[a] Neutron Flux (10^{19} $m^{-2}s^{-1}$)
All implicit capture (ANS74)	1.0003 ± 0.0037	7.9351 ± 0.1428
Analog capture below 0.683 eV (ANS75)	1.0071 ± 0.0055	7.7862 ± 0.1511

a. The energy range for these flux values is 0.0 eV ≤ E ≤ 0.625 eV.

These results indicate that analog capture within the thermal region does not alter the answer. However, it does result in a higher standard deviation for these calculations.

5.4 D_2O Thermal Treatment

MCNP offers two standard methods for treating thermal neutron interactions: the free gas thermal treatment and the $S(\alpha,\beta)$ thermal library. $S(\alpha,\beta)$ thermal libraries are available for only a few low z materials and are evaluated at various temperatures. The $S(\alpha,\beta)$ treatment, when requested, is used for neutron interactions below 4 eV. The free gas thermal treatment is used when the $S(\alpha,\beta)$ treatment has not been requested.

The free gas "thermal treatment in MCNP assumes that the medium is a free gas and also that in the range of atomic weight and neutron energy where thermal effects are significant, the elastic scattering cross section at zero temperature is nearly independent of the energy of the neutron, and the reaction cross sections are nearly independent of temperature."[2]

The $S(\alpha,\beta)$ scattering model is a "complete representation of thermal neutron scattering by molecules and crystalline solids. This thermal scattering treatment also allows the representation of scattering by multiatomic molecules (for example BeO)."[2]

Heavy water $S(\alpha,\beta)$ thermal libraries are evaluated at 300, 400, 500, 600, and, 800 K. The reflector temperature is approximately 300 K, while the coolant, within the fuel and outlet channels, is approximately 350 K. Therefore, it would be appropriate to use the 300 K $S(\alpha,\beta)$ library for the reflector and the 400 K $S(\alpha,\beta)$ library for most of the D_2O cooling. MCNP-3b, however, has a bug, which does not permit two $S(\alpha,\beta)$ libraries of the same material to be used in a model. Since the average temperature of the entire model is close to 300 K, the 300 K D_2O $S(\alpha,\beta)$ library was used for all regions of the reactor.

A comparison was made between various ANS models to see the effect on the core multiplication factor and the thermal neutron flux of changing the thermal treatment while keeping the D_2O density constant One model contained the 300 K $S(\alpha,\beta)$ library, another model contained the 400 K $S(\alpha,\beta)$ library, while the last model used the free gas thermal treatment. When the free gas treatment was selected, a temperature of 300 K was used for all D_2O except in the fuel and coolant outlet channels, where it was set at 350 K. Table 5-4 presents the results of these comparisons.

TABLE 5-4. THERMAL D_2O LIBRARY EFFECTS

Thermal Library	Run Number	Core Multiplication Factor
No $S(\alpha,\beta)$	ANS53	1.1232 ± 0.0033
300 K $S(\alpha,\beta)$	ANS39	1.1205 ± 0.0045
400 K $S(\alpha,\beta)$	ANS38	1.1368 ± 0.0040

The effect on the core multiplication factor is negligible between the 300 K $S(\alpha,\beta)$ case and no $S(\alpha,\beta)$ case when the temperature

representation for the free gas treatment is approximately 300 K. Currently no explanation can be given for the 1% increase in the core multiplication factor when the 400 K $S(\alpha,\beta)$ library is used. This is not equivalent to a positive void coefficient. This difference, however, emphasizes the importance of correctly representing the thermal temperatures.

Table 5-5 shows the average thermal neutron flux in reflector regions A and C (see Figure 2-1) for the three cases studied.

TABLE 5-5. D_2O $S(\alpha,\beta)$ THERMAL LIBRARY EFFECTS ON THERMAL NEUTRON FLUX

Thermal Library	Thermal Neutron Flux (10^{19} m^{-2} s^{-1})[a]
D_2O Reflector Region A	
No $S(\alpha,\beta)$	4.6813 ± 0.0421
300 K $S(\alpha,\beta)$	5.3062 ± 0.0493
400 K $S(\alpha,\beta)$	5.2864 ± 0.0492
D_2O Reflector Region C	
No $S(\alpha,\beta)$	4.3297 ± 0.0468
300 K $S(\alpha,\beta)$	5.1597 ± 0.0557
400 K $S(\alpha,\beta)$	5.1938 ± 0.0556

a. The energy range for these flux values is $0.0 \text{ eV} \leq E \leq 0.625 \text{ eV}$.

There is little difference in the flux when either the 300 or 400 K $S(\alpha,\beta)$ library is used. However, a 12 to 16% difference is seen

when the $S(\alpha,\beta)$ library is removed. The reason for this is that the free gas thermal treatment does not account for the molecular effects of D_2O.

This results in fewer scattering events and hence less flux. Since less scattering is occurring, more neutrons will penetrate the D_2O reflector and the H_2O biological shield. This is demonstrated when the amount of leakage from the system is analyzed. 0. 0090% of all neutron tracks generated escape the system when the $S(\alpha,\beta)$ is used. This percentage increases to 0.2193% when the $S(\alpha,\beta)$ library is removed and only the free gas thermal treatment is used.

These results further demonstrate the need for an accurate $S(\alpha,\beta)$ thermal library during the calculations.

5.5 Variance Reduction Techniques

Variance reduction techniques are used to increase the efficiency with which a tally is performed. When the techniques are used properly, the mean value of the desired result will not be changed. The objective of variance reduction techniques is to transport important particles (important depends on the tally being performed) to the region of interest while reducing the number of unimportant particles tracked.

During the process a 'fair Monte Carlo game' must be maintained. This is done by altering the particle weights as unimportant particles are killed and important particles are split into more particles. As particles are split, the weights of the new particles are an equal fraction of the weight of the original particle. When unimportant particles are killed, a Russian roulette game is played. The surviving particles have a weight greater than the original particle. This increased weight represents the weight of both the

surviving and rouletted particles. As long as a constant weight is maintained during the transport, a 'fair' game will be maintained.

MCNP offers two variance reduction techniques of interest in the ANS modeling. These are geometry splitting/Russian roulette and weight windows. A detailed description of each method can be found in the MCNP manual. Each method was tried and some moderate success was achieved in increasing the run time efficiency. However, the mean values calculated were not always correct, and the method was abandoned for the present thesis.

CHAPTER 6. CONCLUSIONS AND RECOMMENDATIONS

This thesis has demonstrated the applicability of MCNP to the calculation of reactor physics parameters for the ANS. Monte Carlo offers some computational advantages over diffusion theory and discrete ordinate transport theory. In particular, MCNP offers the Advanced Neutron Source Project the capability of performing complex reactor physics calculations never before possible. The primary disadvantage of Monte Carlo, however, is the amount of computer resources needed to perform the calculations. Therefore, Monte Carlo should be used only to supplement and benchmark other reactor physics computational methods.

Further research needs to be performed with Monte Carlo techniques in the modeling of ANS. Variance reduction techniques should be analyzed in great detail to access their applicability for this difficult computational problem. It is believed that some variance reduction techniques can be incorporated into the ANS model to increase efficiency. However, further research has to be performed before production calculations can be generated with variance reduction techniques incorporated.

REFERENCES

1. G. L. COPELAND et al., "Advanced Neutron Source Final Preconceptual Reference Core Design," ORNL/TM-11234, Oak Ridge National Laboratory (1986).

2. J. F. BRIESMEISTER, Ed., "MCNP - A General Monte Carlo Code for Neutron and Photon Transport (Version 3A)," LA-7396-M, Rev. 2 Los Alamos National Laboratory (1986).

3. J. M. RYSKAMP, F. C. DIFILIPPO, and R. T. PRIMM III, "Reactor Physics Methods for the Preconceptual Core Design of the Advanced Neutron Source," Trans. Am. Nucl. Soc., 57, 290 (1988).

4. C. J. PFEIFER, "PDQ-7 Reference Manual II," WAPD-TM-947(2), Westinghouse Atomic Power Division (1971).

5. T. E. BOOTH and J. S. HENDRICKS, "Importance Estimation in Foreward Monte Carlo Calculations," Nuclear Technology/Fusion, 5, 90 (1984).

6. T. E. BOOTH, "A Sample Problem for Variance Reduction in MCNP," LA-10363-MS, Los Alamos National Laboratory (1985).

7. C. D. WEST, "Overview of the ANS Project," Trans. Am. Nucl. Soc., 57, 288 (1988).

8. C. D. WEST, "The Advanced Neutron Source Facility: A New User Facility for Neutron Research," Proc. Int. Reactor Physics Conf., Jackson, WY, September 18-22, 1988, Vol. II, p. 155 (1988).

9. J. A. LAKE, D. K. PARSONS, J. L. LIEBENTHAL, J. M. RYSKAMP, G. N. FILLMORE, and D. R. DEBOISBLANC, "Ultrahigh Flux Reactor Design--Probing the Limits of Plate Fuel Technology," EGG-EA-7116, Idaho National Engineering Laboratory (1985), Nucl. Inst. Meth., A249, 41 (1986).

10. F. C. DIFILIPPO, W. R. GAMBILL, R. M. MOON, R. T. PRIMM III, and C. D. WEST, "A Preliminary Reactor Design for the Center for Neutron Research," Nucl. Inst. Meth., A249, 58 (1986).

11. W. W. ENGLE, JR., R. A. LILLIE, and C. O. SLATER, "Radiation Transport Calculations for the ANS Beam Tubes," Trans. Am. Nucl. Soc, 57, 294 (1988).

12. J. M. RYSKAMP, "Irradiation Capabilities of the Advanced Neutron Source," Trans. Am. Nucl. Soc., 60, 207 (1989).

13. E. H. HONEYCUTT, Jr., "Erosion of Aluminum," DP-214, Savannah River Site (1957).

14. R. A. GRIMESEY, D. W. NIGG, and R. L. CURTIS, "COMBINE/PC-A Portable ENDF/B Version 5 Neutron Spectrum and Cross Section Generation Program," NRRT-N-89-014, Idaho National Engineering Laboratory (1989).

15. W. E. FORD III et al., "CSRL-V: Processed ENDF/B-V 227-Neutron Group and Pointwise Cross-Section Libraries for Criticality Safety, Reactor and Shielding Studies," NUREG/CR-2306, ORNL/CSD/TM-160, Oak Ridge National Laboratory (1982).

16. N. M. GREENE and L. M. PETRIE, "XSDRNPM-S: A One-Dimensional Discrete-Ordinates Code for Transport Analysis," SCALE, Book IV, NUREG/CR-0200, Vol. 2, Sec. F3, ORNL/NUREG/CSD-2/V2/R1, Oak Ridge National Laboratory (1983).

17. R. T. PRIMM III, "Cross-Section Processing Methodology Used to Design the Advanced Neutron Source Reactor," Trans. Am. Nucl. Soc., 57, 292 (1988).

18. D. R. VONDY, T. B. FOWLER, and G. W. CUNNINGHAM III, "The Bold Venture Computation System for Nuclear Reactor Core Analysis, Version III," ORNL-5711, Oak Ridge National Laboratory (1981).

19. Y. Y. AZMY and F. C. DIFILIPPO, "Comparison of the Diffusion and Transport Calculations for the Advanced Neutron Source Reactor," Proc. Topl. Mtg. Reactor Physics, Jackson, WY, September 18-22, 1988, Vol. II, p. 183 (1988).

20. J. A. McCLURE, "A Two-Dimensional, Time-Dependent Heat Conduction Program," IDO-17227, Idaho National Engineering Laboratory (1967).

21. M. L. GRIEBENOW and K. D. RICHERT, "MACABRE II," IN-1107, Idaho National Engineering Laboratory (1967)

22. H. A. McLAIN, "HFIR Fuel Element Steady State Heat Transfer Analysis, Revised Version," ORNL/TM-1904, Oak Ridge National Laboratory (1967).

23. W. R. GAMBILL, "Thermal-Hydraulic Constraints on Water-Cooled Research Reactor Performance," Nucl. Inst. Meth., A249, 53 (1986).

24. W. R. GAMBILL and T. MOCHIZUKI, "Advanced Neutron Source Design: Burnout Heat Flux Correlation Development," Trans. Am. Nucl. Soc., 57, 298 (1988).

25. R. J. BRISSENDEN and A. R. GARLICK, "Biases in the Estimation of K_{eff} and Its Error by Monte Carlo Methods," Annals of Nuclear Energy, No. 2, 63 (1986).

26. A. F. HENRY, Nuclear-Reactor Analysis, The MIT Press, Cambridge, MA, 1975.

APPENDIX A

SAMPLE ANS MCNP INPUT DECK

```
ans?? - INPUT DECK FOR MCNP FOR THE ADVANCED NEUTRON SOURCE
c       The model was set up by
c             Everett Redmond II
c             EG&G Idaho Inc.
c             PO Box 1625
c             Idaho Falls , ID  83415-3515
c             (208)526-2831
c             This model was set up in partial fulfillment of the
c             requirements for the degree of MASTER OF SCIENCE
c             at the Massachusetts Institute of Technology
c
c       This is a MCNP model of the Advanced Neutron Source. The
c       model contains homogenous fuel zones with graded U-235
c       concentrations.  The geometry representation is almost
c       identical to John Ryskamp's PDQ model number DD460. There
c       are 13.48 g of B-10 and 15 kg of U-235 in this model.
c
c       ***SPECIFIC RUN INFORMATION***
c       there is no hafnium in this run so that we may  compare the
c       this is the base case for comparison to ans80
c
c       CELL SPECIFICATIONS
c
c       This section of the input is the cell specification section.
c       The first entry is the cell number, the second entry is the
c       material number for that cell, the third number is the total
c       concentration of nuclides in that cell in atoms/(barn-cm). If
c       the third entry is negative then concentration is in  g/cc.
c       The other entries on the cell cards are surface numbers used
c       to define the cell. The number 0 in the material entry
c       signifies a void in that cell and hence no concentration is
c       specified.  The imp: cards signify the relative importance of

c       neutrons and photons in the cell. The tmp entry gives the
c       thermal temperature of the cell for the free gas thermal
c       treatment. All D2O is represented at 300K except D2O HOT
c       which is at 350K. All Al and fuel is at 350K.
c
c
c       THIS IS A DRAWING OF THE ANS TO SHOW THE POSITIONS OF THE
c       VARIOUS SECTIONS AND WHAT THEY INCLUDE
c
c       ***************************************************************
c       |     .               |    <- SECTION 1 ->                    *
c       |-----------------------------------------------------------*
c       |          --------   |                                       *
c       |          |  F   |   |                                       *
c       |          |  U   |   C                                       *
c       |          |  E   |   P    <- SECTION 2 ->                    *
c       |          |  L   |   B                                       *
c       |          |      |   T                                       *
c       |          --------   |                                       *
c       |-----------------------------------------------------------*
```

```
c       C                    |    <- SECTION 3 ->                          *
c       /--------------------------------------------------------------------*
c       L                    |    <- SECTION 4 ->                          *
c       |--------------------------------------------------------------------*
c       |  --------          |                                             *
c       |  |  F   |          |                                             *
c       |  |  U   |          |                                             *
c       |  |  E   |          |    <- SECTION 5 ->                          *
c       |  |  L   |          |                                             *
c       |  |      |          |                                             *
c       |  --------          |                                             *
c       |--------------------------------------------------------------------*
c       |                    |                                             *
c       |                    |    <- SECTION 6 ->                          *
c       |                    |                                             *
c       ********************************************************************
c
c       H2O POOL AND AL6061 TANK
c
c                          <-planes-> <-cylinders->
c
1100    1  0.1003       -1      2     -91      93   $ H2O pool
1101    1  0.1003      -89     90     -91      93   $ H2O pool
1102    1  0.1003       -1      2     -93      98   $ H2O pool
1103    1  0.1003      -89     90     -93      98   $ H2O pool
1104    1  0.1003       -1      2     -98      99   $ H2O pool
1105    1  0.1003      -89     90     -98      99   $ H2O pool
1106    1  0.1003       -1      2     -99     100   $ H2O pool
1107    1  0.1003      -89     90     -99     100   $ H2O pool
1108    1  0.1003       -1      2    -100     120   $ H2O pool
1109    1  0.1003      -89     90    -100     120   $ H2O pool
1110    1  0.1003       -1      2    -120     140   $ H2O pool
1111    1  0.1003      -89     90    -120     140   $ H2O pool
1112    1  0.1003       -1      2    -140           $ H2O pool
1113    1  0.1003      -89     90    -140           $ H2O pool
1114    1  0.1003       -2     15     -91      92   $ H2O pool
1115    1  0.1003      -15     16     -91      92   $ H2O pool
1116    1  0.1003      -16     17     -91      92   $ H2O pool
1117    1  0.1003      -17     20     -91      92   $ H2O pool
1118    1  0.1003      -20     45     -91      92   $ H2O pool
1119    1  0.1003      -45     70     -91      92   $ H2O pool
1120    1  0.1003      -70     74     -91      92   $ H2O pool
1121    1  0.1003      -74     75     -91      92   $ H2O pool
1122    1  0.1003      -75     76     -91      92   $ H2O pool
1123    1  0.1003      -76     89     -91      92   $ H2O pool
1124    6  6.0034-2     -2      3     -92      98   $ Al-6061
1125    6  6.0034-2    -88     89     -92      98   $ Al-6061
1126    6  6.0034-2     -2      3     -98      99   $ Al-6061
1127    6  6.0034-2    -88     89     -98      99   $ Al-6061
1128    6  6.0034-2     -2      3     -99     100   $ Al-6061
1129    6  6.0034-2    -88     89     -99     100   $ Al-6061
1130    6  6.0034-2     -2      3    -100     120   $ Al-6061
1131    6  6.0034-2    -88     89    -100     120   $ Al-6061
```

```
1132    6  6.0034-2    -2     3   -120    140   $ Al-6061
1133    6  6.0034-2   -88    89   -120    140   $ Al-6061
1134    6  6.0034-2    -2     3   -140          $ Al-6061
1135    6  6.0034-2   -88    89   -140          $ Al-6061
1136    6  6.0034-2    -3    15    -92     93   $ Al-6061
1137    6  6.0034-2   -15    16    -92     93   $ Al-6061
1138    6  6.0034-2   -16    17    -92     93   $ Al-6061
1139    6  6.0034-2   -17    20    -92     93   $ Al-6061
1140    6  6.0034-2   -20    45    -92     93   $ Al-6061
1141    6  6.0034-2   -45    70    -92     93   $ Al-6061
1142    6  6.0034-2   -70    74    -92     93   $ Al-6061
1143    6  6.0034-2   -74    75    -92     93   $ Al-6061
1144    6  6.0034-2   -75    76    -92     93   $ Al-6061
1145    6  6.0034-2   -76    88    -92     93   $ Al-6061
c
c       SECTION 1
c
100     6  6.0034-2    -3    15   -180    184   $ Al-6061 INNER TUBE
101     3  9.6972-2    -3    15   -170    180   $ D2O hot
102     3  9.6972-2    -3    15   -160    170   $ D2O hot
103     3  9.6972-2    -3    15   -150    160   $ D2O hot
104     3  9.6972-2    -3    15   -149    150   $ D2O hot
105     3  9.6972-2    -3    15   -145    149   $ D2O hot
106     6  6.0034-2    -3    15   -140    145   $ Al-6061  CPBT
107     2  9.8855-2    -3    15   -120    140   $ D2O REFLECTOR
108     2  9.8855-2    -3    15   -100    120   $ D2O REFLECTOR
109     2  9.8855-2    -3    15    -99    100   $ D2O REFLECTOR
110     2  9.8855-2    -3    15    -98     99   $ D2O REFLECTOR
111     2  9.8855-2    -3    15    -93     98   $ D2O REFLECTOR
120     6  6.0034-2   -15    16   -180    184   $ Al-6061 INNER TUBE
121     3  9.6972-2   -15    16   -170    180   $ D2O hot
122     3  9.6972-2   -15    16   -160    170   $ D2O hot
123     3  9.6972-2   -15    16   -150    160   $ D2O hot
124     3  9.6972-2   -15    16   -149    150   $ D2O hot
125     3  9.6972-2   -15    16   -145    149   $ D2O hot
126     6  6.0034-2   -15    16   -140    145   $ Al-6061  CPBT
127     2  9.8855-2   -15    16   -120    140   $ D2O REFLECTOR
128     2  9.8855-2   -15    16   -100    120   $ D2O REFLECTOR
129     2  9.8855-2   -15    16    -99    100   $ D2O REFLECTOR
130     2  9.8855-2   -15    16    -98     99   $ D2O REFLECTOR
131     2  9.8855-2   -15    16    -93     98   $ D2O REFLECTOR
140     6  6.0034-2   -16    17   -180    184   $ Al-6061 INNER TUBE
141     3  9.6972-2   -16    17   -170    180   $ D2O hot
142     3  9.6972-2   -16    17   -160    170   $ D2O hot
143     3  9.6972-2   -16    17   -150    160   $ D2O hot
144     3  9.6972-2   -16    17   -149    150   $ D2O hot
145     3  9.6972-2   -16    17   -145    149   $ D2O hot
146     6  6.0034-2   -16    17   -140    145   $ Al-6061  CPBT
147     2  9.8855-2   -16    17   -120    140   $ D2O REFLECTOR
148     2  9.8855-2   -16    17   -100    120   $ D2O REFLECTOR
149     2  9.8855-2   -16    17    -99    100   $ D2O REFLECTOR
150     2  9.8855-2   -16    17    -98     99   $ D2O REFLECTOR
151     2  9.8855-2   -16    17    -93     98   $ D2O REFLECTOR
```

```
160     6  6.0034-2    -17     20    -180     184   $ Al-6061 INNER TUBE
161     3  9.6972-2    -17     20    -170     180   $ D20 hot
162     3  9.6972-2    -17     18    -160     170   $ D20 hot
163     3  9.6972-2    -17     19    -150     160   $ D20 hot
164     3  9.6972-2    -17     18    -149     150   $ D20 hot
165     3  9.6972-2    -17     19    -145     149   $ D20 hot
166     6  6.0034-2    -17     19    -140     145   $ Al-6061  CPBT
167     2  9.8855-2    -17     20    -130     140   $ D20 REFLECTOR
168     2  9.8855-2    -17     20    -120     130   $ D20 REFLECTOR
169     2  9.8855-2    -17     20    -110     120   $ D20 REFLECTOR
170     2  9.8855-2    -17     20    -100     110   $ D20 REFLECTOR
171     2  9.8855-2    -17     20     -99     100   $ D20 REFLECTOR
172     2  9.8855-2    -17     20     -98      99   $ D20 REFLECTOR
173     2  9.8855-2    -17     20     -93      98   $ D20 REFLECTOR
c
c       SECTION 2
c
200     6  6.0034-2    -20     40    -180     184   $ Al-6061 INNER TUBE
201     3  9.6972-2    -20     40    -174     180   $ D20 hot
202    38  9.3324-2    -20     40    -170     174   $ D20 hot
203     6  6.0034-2    -18     40    -160     170   $ Al-6061 SIDE PLATE
204     5  7.9403-2    -19     20    -150     160   $ AL FUEL ENDCAP
205     6  6.0034-2    -18     41    -149     150   $ Al-6061 SIDE PLATE
206     4  9.9005-2    -19     40    -145     149   $ D20 cold
207     6  6.0034-2    -19     40    -140     145   $ Al-6061  CPBT
210     2  9.8855-2    -20    700    -130     140   $ D20 REFLECTOR
211     2  9.8855-2   -700    701    -130     140   $ D20 REFLECTOR
212     2  9.8855-2   -701    702    -130     140   $ D20 REFLECTOR
213     2  9.8855-2   -702     25    -130     140   $ D20 REFLECTOR
214     2  9.8855-2    -25    703    -130     140   $ D20 REFLECTOR
215     2  9.8855-2   -703    704    -130     140   $ D20 REFLECTOR
216     2  9.8855-2   -704    705    -130     140   $ D20 REFLECTOR
217     2  9.8855-2   -705     40    -130     140   $ D20 REFLECTOR
218     2  9.8855-2    -40     45    -130     140   $ D20 REFLECTOR
220     2  9.8855-2    -20    700    -120     130   $ D20 REFLECTOR
221     2  9.8855-2   -700    701    -120     130   $ D20 REFLECTOR
222     2  9.8855-2   -701    702    -120     130   $ D20 REFLECTOR
223     2  9.8855-2   -702     25    -120     130   $ D20 REFLECTOR
224     2  9.8855-2    -25    703    -120     130   $ D20 REFLECTOR
225     2  9.8855-2   -703    704    -120     130   $ D20 REFLECTOR
226     2  9.8855-2   -704    705    -120     130   $ D20 REFLECTOR
227     2  9.8855-2   -705     40    -120     130   $ D20 REFLECTOR
228     2  9.8855-2    -40     45    -120     130   $ D20 REFLECTOR
230     2  9.8855-2    -20    700    -110     120   $ D20 REFLECTOR
231     2  9.8855-2   -700    701    -110     120   $ D20 REFLECTOR
232     2  9.8855-2   -701    702    -110     120   $ D20 REFLECTOR
233     2  9.8855-2   -702     25    -110     120   $ D20 REFLECTOR
234     2  9.8855-2    -25    703    -110     120   $ D20 REFLECTOR
235     2  9.8855-2   -703    704    -110     120   $ D20 REFLECTOR
236     2  9.8855-2   -704    705    -110     120   $ D20 REFLECTOR
237     2  9.8855-2   -705     40    -110     120   $ D20 REFLECTOR
238     2  9.8855-2    -40     45    -110     120   $ D20 REFLECTOR
240     2  9.8855-2    -20    700    -100     110   $ D20 REFLECTOR
```

```
241     2  9.8855-2   -700    701   -100    110   $ D2O REFLECTOR
242     2  9.8855-2   -701    702   -100    110   $ D2O REFLECTOR
243     2  9.8855-2   -702     25   -100    110   $ D2O REFLECTOR
244     2  9.8855-2    -25    703   -100    110   $ D2O REFLECTOR
245     2  9.8855-2   -703    704   -100    110   $ D2O REFLECTOR
246     2  9.8855-2   -704    705   -100    110   $ D2O REFLECTOR
247     2  9.8855-2   -705     40   -100    110   $ D2O REFLECTOR
248     2  9.8855-2    -40     45   -100    110   $ D2O REFLECTOR
250     2  9.8855-2    -20     25    -99    100   $ D2O REFLECTOR
251     2  9.8855-2    -25     45    -99    100   $ D2O REFLECTOR
260     2  9.8855-2    -20     25    -98     99   $ D2O REFLECTOR
261     2  9.8855-2    -25     45    -98     99   $ D2O REFLECTOR
270     2  9.8855-2    -20     25    -93     98   $ D2O REFLECTOR
271     2  9.8855-2    -25     45    -93     98   $ D2O REFLECTOR
c
c       SECTION 3
c
300     6  6.0034-2    -40     45   -180    184   $ Al-6061 INNER TUBE
301     3  9.6972-2    -40     45   -170    180   $ D2O hot
302     6  6.0034-2    -40     45   -160    170   $ Al-6061 SIDE PLATE
303     5  7.9403-2    -40     41   -150    160   $ AL FUEL ENDCAP
304     4  9.9005-2    -41     45   -150    160   $ D2O cold
305     6  6.0034-2    -41     45   -149    150   $ Al-6061 SIDE PLATE
306     4  9.9005-2    -40     45   -145    149   $ D2O cold
307     6  6.0034-2    -40     45   -140    145   $ Al-6061  CPBT
c
c       SECTION 4
c
400     6  6.0034-2    -45     50   -180    184   $ Al-6061 INNER TUBE
401     4  9.9005-2    -45     49   -170    180   $ D2O cold
402     7  7.9648-2    -49     50   -170    180   $ AL FUEL ENDCAP
403     6  6.0034-2    -45     49   -160    170   $ Al-6061 SIDE PLATE
404     4  9.9005-2    -45     50   -150    160   $ D2O cold
405     6  6.0034-2    -45     49   -149    150   $ Al-6061 SIDE PLATE
406     4  9.9005-2    -45     50   -145    149   $ D2O cold
407     6  6.0034-2    -45     50   -140    145   $ Al-6061  CPBT
c
c       SECTION 5
c
500     6  6.0034-2    -50     70   -180    184   $ Al-6061 INNER TUBE
501     6  6.0034-2    -49     72   -160    170   $ Al-6061 SIDE PLATE
502    39  9.5155-2    -50     70   -156    160   $ D2O cold
503     4  9.9005-2    -50     70   -150    156   $ D2O cold
504     4  9.9005-2    -49     71   -149    150   $ D2O cold
505     4  9.9005-2    -50     71   -145    149   $ D2O cold
506     6  6.0034-2    -50     71   -140    145   $ Al-6061  CPBT
510     2  9.8855-2    -45     50   -130    140   $ D2O REFLECTOR
511     2  9.8855-2    -50    706   -130    140   $ D2O REFLECTOR
512     2  9.8855-2   -706    707   -130    140   $ D2O REFLECTOR
513     2  9.8855-2   -707    708   -130    140   $ D2O REFLECTOR
514     2  9.8855-2   -708     55   -130    140   $ D2O REFLECTOR
515     2  9.8855-2    -55    709   -130    140   $ D2O REFLECTOR
516     2  9.8855-2   -709    730   -130    140   $ D2O REFLECTOR
```

```
517     2  9.8855-2   -730    731   -130    140   $ D2O REFLECTOR
518     2  9.8855-2   -731     70   -130    140   $ D2O REFLECTOR
520     2  9.8855-2    -45     50   -120    130   $ D2O REFLECTOR
521     2  9.8855-2    -50    706   -120    130   $ D2O REFLECTOR
522     2  9.8855-2   -706    707   -120    130   $ D2O REFLECTOR
523     2  9.8855-2   -707    708   -120    130   $ D2O REFLECTOR
524     2  9.8855-2   -708     55   -120    130   $ D2O REFLECTOR
525     2  9.8855-2    -55    709   -120    130   $ D2O REFLECTOR
526     2  9.8855-2   -709    730   -120    130   $ D2O REFLECTOR
527     2  9.8855-2   -730    731   -120    130   $ D2O REFLECTOR
528     2  9.8855-2   -731     70   -120    130   $ D2O REFLECTOR
530     2  9.8855-2    -45     50   -110    120   $ D2O REFLECTOR
531     2  9.8855-2    -50    706   -110    120   $ D2O REFLECTOR
532     2  9.8855-2   -706    707   -110    120   $ D2O REFLECTOR
533     2  9.8855-2   -707    708   -110    120   $ D2O REFLECTOR
534     2  9.8855-2   -708     55   -110    120   $ D2O REFLECTOR
535     2  9.8855-2    -55    709   -110    120   $ D2O REFLECTOR
536     2  9.8855-2   -709    730   -110    120   $ D2O REFLECTOR
537     2  9.8855-2   -730    731   -110    120   $ D2O REFLECTOR
538     2  9.8855-2   -731     70   -110    120   $ D2O REFLECTOR
540     2  9.8855-2    -45     50   -100    110   $ D2O REFLECTOR
541     2  9.8855-2    -50    706   -100    110   $ D2O REFLECTOR
542     2  9.8855-2   -706    707   -100    110   $ D2O REFLECTOR
543     2  9.8855-2   -707    708   -100    110   $ D2O REFLECTOR
544     2  9.8855-2   -708     55   -100    110   $ D2O REFLECTOR
545     2  9.8855-2    -55    709   -100    110   $ D2O REFLECTOR
546     2  9.8855-2   -709    730   -100    110   $ D2O REFLECTOR
547     2  9.8855-2   -730    731   -100    110   $ D2O REFLECTOR
548     2  9.8855-2   -731     70   -100    110   $ D2O REFLECTOR
550     2  9.8855-2    -45     55    -99    100   $ D2O REFLECTOR
551     2  9.8855-2    -55     70    -99    100   $ D2O REFLECTOR
560     2  9.8855-2    -45     55    -98     99   $ D2O REFLECTOR
561     2  9.8855-2    -55     70    -98     99   $ D2O REFLECTOR
570     2  9.8855-2    -45     55    -93     98   $ D2O REFLECTOR
571     2  9.8855-2    -55     70    -93     98   $ D2O REFLECTOR
c
c       SECTION 6
c
600     6  6.0034-2    -70     74   -180    184   $ Al-6061 INNER TUBE
601     5  7.9403-2    -70     71   -170    180   $ AL FUEL ENDCAP
602     4  9.9005-2    -71     72   -170    180   $ D2O cold
603     4  9.9005-2    -70     72   -150    160   $ D2O cold
604     4  9.9005-2    -71     74   -149    150   $ D2O cold
605     4  9.9005-2    -72     74   -150    180   $ D2O cold
606     4  9.9005-2    -71     74   -145    149   $ D2O cold
607     6  6.0034-2    -71     74   -140    145   $ Al-6061  CPBT
608     2  9.8855-2    -70     74   -130    140   $ D2O REFLECTOR
609     2  9.8855-2    -70     74   -120    130   $ D2O REFLECTOR
610     2  9.8855-2    -70     74   -110    120   $ D2O REFLECTOR
611     2  9.8855-2    -70     74   -100    110   $ D2O REFLECTOR
612     2  9.8855-2    -70     74    -99    100   $ D2O REFLECTOR
613     2  9.8855-2    -70     74    -98     99   $ D2O REFLECTOR
614     2  9.8855-2    -70     74    -93     98   $ D2O REFLECTOR
```

```
620     6  6.0034-2    -74     75   -180    184   $ Al-6061 INNER TUBE
621     4  9.9005-2    -74     75   -149    150   $ D2O cold
622     4  9.9005-2    -74     75   -150    180   $ D2O cold
623     4  9.9005-2    -74     75   -145    149   $ D2O cold
624     6  6.0034-2    -74     75   -140    145   $ Al-6061  CPBT
625     2  9.8855-2    -74     75   -120    140   $ D2O REFLECTOR
626     2  9.8855-2    -74     75   -100    120   $ D2O REFLECTOR
627     2  9.8855-2    -74     75    -99    100   $ D2O REFLECTOR
628     2  9.8855-2    -74     75    -98     99   $ D2O REFLECTOR
629     2  9.8855-2    -74     75    -93     98   $ D2O REFLECTOR
640     6  6.0034-2    -75     76   -180    184   $ Al-6061 INNER TUBE
641     4  9.9005-2    -75     76   -149    150   $ D2O cold
642     4  9.9005-2    -75     76   -150    180   $ D2O cold
643     4  9.9005-2    -75     76   -145    149   $ D2O cold
644     6  6.0034-2    -75     76   -140    145   $ Al-6061  CPBT
645     2  9.8855-2    -75     76   -120    140   $ D2O REFLECTOR
646     2  9.8855-2    -75     76   -100    120   $ D2O REFLECTOR
647     2  9.8855-2    -75     76    -99    100   $ D2O REFLECTOR
648     2  9.8855-2    -75     76    -98     99   $ D2O REFLECTOR
649     2  9.8855-2    -75     76    -93     98   $ D2O REFLECTOR
660     6  6.0034-2    -76     88   -180    184   $ Al-6061 INNER TUBE
661     4  9.9005-2    -76     88   -149    150   $ D2O cold
662     4  9.9005-2    -76     88   -150    180   $ D2O cold
663     4  9.9005-2    -76     88   -145    149   $ D2O cold
664     6  6.0034-2    -76     88   -140    145   $ Al-6061  CPBT
665     2  9.8855-2    -76     88   -120    140   $ D2O REFLECTOR
666     2  9.8855-2    -76     88   -100    120   $ D2O REFLECTOR
667     2  9.8855-2    -76     88    -99    100   $ D2O REFLECTOR
668     2  9.8855-2    -76     88    -98     99   $ D2O REFLECTOR
669     2  9.8855-2    -76     88    -93     98   $ D2O REFLECTOR
c
c       UPPER FUEL ELEMENT
c
700    21 7.7042-2    -20     21    160   -158   $ UPPER FUEL ELEMENT
701    21 7.7042-2    -20     21    158   -157   $ UPPER FUEL ELEMENT
702    21 7.7042-2    -20     21    157   -155   $ UPPER FUEL ELEMENT
703    21 7.7042-2    -20     21    155   -154   $ UPPER FUEL ELEMENT
704    23 7.7212-2    -20     21    154   -153   $ UPPER FUEL ELEMENT
705    23 7.7212-2    -20     21    153   -152   $ UPPER FUEL ELEMENT
706    24 7.7296-2    -20     21    152   -151   $ UPPER FUEL ELEMENT
707    24 7.7296-2    -20     21    151   -150   $ UPPER FUEL ELEMENT
708    21 7.7042-2    -21     22    160   -158   $ UPPER FUEL ELEMENT
709    20 7.6958-2    -21     22    158   -157   $ UPPER FUEL ELEMENT
710    20 7.6958-2    -21     22    157   -155   $ UPPER FUEL ELEMENT
711    20 7.6958-2    -21     22    155   -154   $ UPPER FUEL ELEMENT
712    21 7.7042-2    -21     22    154   -153   $ UPPER FUEL ELEMENT
713    22 7.7127-2    -21     22    153   -152   $ UPPER FUEL ELEMENT
714    23 7.7212-2    -21     22    152   -151   $ UPPER FUEL ELEMENT
715    24 7.7296-2    -21     22    151   -150   $ UPPER FUEL ELEMENT
716    20 7.6958-2    -22     23    160   -158   $ UPPER FUEL ELEMENT
717    20 7.6958-2    -22     23    158   -157   $ UPPER FUEL ELEMENT
718    20 7.6958-2    -22     23    157   -155   $ UPPER FUEL ELEMENT
719    20 7.6958-2    -22     23    155   -154   $ UPPER FUEL ELEMENT
```

```
720     20 7.6958-2    -22     23     154    -153   $ UPPER FUEL ELEMENT
721     22 7.7127-2    -22     23     153    -152   $ UPPER FUEL ELEMENT
722     23 7.7212-2    -22     23     152    -151   $ UPPER FUEL ELEMENT
723     24 7.7296-2    -22     23     151    -150   $ UPPER FUEL ELEMENT
724     20 7.6958-2    -23     24     160    -158   $ UPPER FUEL ELEMENT
725     20 7.6958-2    -23     24     158    -157   $ UPPER FUEL ELEMENT
726     20 7.6958-2    -23     24     157    -155   $ UPPER FUEL ELEMENT
727     20 7.6958-2    -23     24     155    -154   $ UPPER FUEL ELEMENT
728     20 7.6958-2    -23     24     154    -153   $ UPPER FUEL ELEMENT
729     22 7.7127-2    -23     24     153    -152   $ UPPER FUEL ELEMENT
730     23 7.7212-2    -23     24     152    -151   $ UPPER FUEL ELEMENT
731     24 7.7296-2    -23     24     151    -150   $ UPPER FUEL ELEMENT
732     20 7.6958-2    -24     25     160    -158   $ UPPER FUEL ELEMENT
733     20 7.6958-2    -24     25     158    -157   $ UPPER FUEL ELEMENT
734     20 7.6958-2    -24     25     157    -155   $ UPPER FUEL ELEMENT
735     20 7.6958-2    -24     25     155    -154   $ UPPER FUEL ELEMENT
736     20 7.6958-2    -24     25     154    -153   $ UPPER FUEL ELEMENT
737     22 7.7127-2    -24     25     153    -152   $ UPPER FUEL ELEMENT
738     23 7.7212-2    -24     25     152    -151   $ UPPER FUEL ELEMENT
739     23 7.7212-2    -24     25     151    -150   $ UPPER FUEL ELEMENT
740     20 7.6958-2    -25     26     160    -158   $ UPPER FUEL ELEMENT
741     20 7.6958-2    -25     26     158    -157   $ UPPER FUEL ELEMENT
742     20 7.6958-2    -25     26     157    -155   $ UPPER FUEL ELEMENT
743     20 7.6958-2    -25     26     155    -154   $ UPPER FUEL ELEMENT
744     20 7.6958-2    -25     26     154    -153   $ UPPER FUEL ELEMENT
745     22 7.7127-2    -25     26     153    -152   $ UPPER FUEL ELEMENT
746     23 7.7212-2    -25     26     152    -151   $ UPPER FUEL ELEMENT
747     23 7.7212-2    -25     26     151    -150   $ UPPER FUEL ELEMENT
748     20 7.6958-2    -26     27     160    -158   $ UPPER FUEL ELEMENT
749     20 7.6958-2    -26     27     158    -157   $ UPPER FUEL ELEMENT
750     20 7.6958-2    -26     27     157    -155   $ UPPER FUEL ELEMENT
751     20 7.6958-2    -26     27     155    -154   $ UPPER FUEL ELEMENT
752     20 7.6958-2    -26     27     154    -153   $ UPPER FUEL ELEMENT
753     22 7.7127-2    -26     27     153    -152   $ UPPER FUEL ELEMENT
754     23 7.7212-2    -26     27     152    -151   $ UPPER FUEL ELEMENT
755     24 7.7296-2    -26     27     151    -150   $ UPPER FUEL ELEMENT
756     21 7.7042-2    -27     28     160    -158   $ UPPER FUEL ELEMENT
757     20 7.6958-2    -27     28     158    -157   $ UPPER FUEL ELEMENT
758     20 7.6958-2    -27     28     157    -155   $ UPPER FUEL ELEMENT
759     20 7.6958-2    -27     28     155    -154   $ UPPER FUEL ELEMENT
760     21 7.7042-2    -27     28     154    -153   $ UPPER FUEL ELEMENT
761     22 7.7127-2    -27     28     153    -152   $ UPPER FUEL ELEMENT
762     23 7.7212-2    -27     28     152    -151   $ UPPER FUEL ELEMENT
763     24 7.7296-2    -27     28     151    -150   $ UPPER FUEL ELEMENT
764     22 7.7127-2    -28     29     160    -158   $ UPPER FUEL ELEMENT
765     21 7.7042-2    -28     29     158    -157   $ UPPER FUEL ELEMENT
766     21 7.7042-2    -28     29     157    -155   $ UPPER FUEL ELEMENT
767     21 7.7042-2    -28     29     155    -154   $ UPPER FUEL ELEMENT
768     22 7.7127-2    -28     29     154    -153   $ UPPER FUEL ELEMENT
769     23 7.7212-2    -28     29     153    -152   $ UPPER FUEL ELEMENT
770     24 7.7296-2    -28     29     152    -151   $ UPPER FUEL ELEMENT
771     24 7.7296-2    -28     29     151    -150   $ UPPER FUEL ELEMENT
772     23 7.7212-2    -29     40     160    -158   $ UPPER FUEL ELEMENT
```

```
773     23 7.7212-2    -29     40     158    -157    $ UPPER FUEL ELEMENT
774     23 7.7212-2    -29     40     157    -155    $ UPPER FUEL ELEMENT
775     23 7.7212-2    -29     40     155    -154    $ UPPER FUEL ELEMENT
776     24 7.7296-2    -29     40     154    -153    $ UPPER FUEL ELEMENT
777     24 7.7296-2    -29     40     153    -152    $ UPPER FUEL ELEMENT
778     24 7.7296-2    -29     40     152    -151    $ UPPER FUEL ELEMENT
779     24 7.7296-2    -29     40     151    -150    $ UPPER FUEL ELEMENT
c
c       LOWER FUEL ELEMENT
c
900     22 7.7127-2    -50     51     180    -179    $ LOWER FUEL ELEMENT
901     21 7.7042-2    -50     51     179    -178    $ LOWER FUEL ELEMENT
902     21 7.7042-2    -50     51     178    -177    $ LOWER FUEL ELEMENT
903     21 7.7042-2    -50     51     177    -176    $ LOWER FUEL ELEMENT
904     23 7.7212-2    -50     51     176    -175    $ LOWER FUEL ELEMENT
905     24 7.7296-2    -50     51     175    -172    $ LOWER FUEL ELEMENT
906     24 7.7296-2    -50     51     172    -171    $ LOWER FUEL ELEMENT
907     24 7.7296-2    -50     51     171    -170    $ LOWER FUEL ELEMENT
908     21 7.7042-2    -51     52     180    -179    $ LOWER FUEL ELEMENT
909     20 7.6958-2    -51     52     179    -178    $ LOWER FUEL ELEMENT
910     20 7.6958-2    -51     52     178    -177    $ LOWER FUEL ELEMENT
911     20 7.6958-2    -51     52     177    -176    $ LOWER FUEL ELEMENT
912     20 7.6958-2    -51     52     176    -175    $ LOWER FUEL ELEMENT
913     22 7.7127-2    -51     52     175    -172    $ LOWER FUEL ELEMENT
914     23 7.7212-2    -51     52     172    -171    $ LOWER FUEL ELEMENT
915     24 7.7296-2    -51     52     171    -170    $ LOWER FUEL ELEMENT
916     20 7.6958-2    -52     53     180    -179    $ LOWER FUEL ELEMENT
917     20 7.6958-2    -52     53     179    -178    $ LOWER FUEL ELEMENT
918     20 7.6958-2    -52     53     178    -177    $ LOWER FUEL ELEMENT
919     20 7.6958-2    -52     53     177    -176    $ LOWER FUEL ELEMENT
920     20 7.6958-2    -52     53     176    -175    $ LOWER FUEL ELEMENT
921     21 7.7042-2    -52     53     175    -172    $ LOWER FUEL ELEMENT
922     23 7.7212-2    -52     53     172    -171    $ LOWER FUEL ELEMENT
923     24 7.7296-2    -52     53     171    -170    $ LOWER FUEL ELEMENT
924     20 7.6958-2    -53     54     180    -179    $ LOWER FUEL ELEMENT
925     20 7.6958-2    -53     54     179    -178    $ LOWER FUEL ELEMENT
926     20 7.6958-2    -53     54     178    -177    $ LOWER FUEL ELEMENT
927     20 7.6958-2    -53     54     177    -176    $ LOWER FUEL ELEMENT
928     20 7.6958-2    -53     54     176    -175    $ LOWER FUEL ELEMENT
929     21 7.7042-2    -53     54     175    -172    $ LOWER FUEL ELEMENT
930     23 7.7212-2    -53     54     172    -171    $ LOWER FUEL ELEMENT
931     24 7.7296-2    -53     54     171    -170    $ LOWER FUEL ELEMENT
932     20 7.6958-2    -54     55     180    -179    $ LOWER FUEL ELEMENT
933     20 7.6958-2    -54     55     179    -178    $ LOWER FUEL ELEMENT
934     20 7.6958-2    -54     55     178    -177    $ LOWER FUEL ELEMENT
935     20 7.6958-2    -54     55     177    -176    $ LOWER FUEL ELEMENT
936     20 7.6958-2    -54     55     176    -175    $ LOWER FUEL ELEMENT
937     20 7.6958-2    -54     55     175    -172    $ LOWER FUEL ELEMENT
938     23 7.7212-2    -54     55     172    -171    $ LOWER FUEL ELEMENT
939     23 7.7212-2    -54     55     171    -170    $ LOWER FUEL ELEMENT
940     20 7.6958-2    -55     56     180    -179    $ LOWER FUEL ELEMENT
941     20 7.6958-2    -55     56     179    -178    $ LOWER FUEL ELEMENT
942     20 7.6958-2    -55     56     178    -177    $ LOWER FUEL ELEMENT
```

```
943     20 7.6958-2    -55     56    177    -176   $ LOWER FUEL ELEMENT
944     20 7.6958-2    -55     56    176    -175   $ LOWER FUEL ELEMENT
945     20 7.6958-2    -55     56    175    -172   $ LOWER FUEL ELEMENT
946     22 7.7127-2    -55     56    172    -171   $ LOWER FUEL ELEMENT
947     23 7.7212-2    -55     56    171    -170   $ LOWER FUEL ELEMENT
948     20 7.6958-2    -56     57    180    -179   $ LOWER FUEL ELEMENT
949     20 7.6958-2    -56     57    179    -178   $ LOWER FUEL ELEMENT
950     20 7.6958-2    -56     57    178    -177   $ LOWER FUEL ELEMENT
951     20 7.6958-2    -56     57    177    -176   $ LOWER FUEL ELEMENT
952     20 7.6958-2    -56     57    176    -175   $ LOWER FUEL ELEMENT
953     21 7.7042-2    -56     57    175    -172   $ LOWER FUEL ELEMENT
954     22 7.7127-2    -56     57    172    -171   $ LOWER FUEL ELEMENT
955     24 7.7296-2    -56     57    171    -170   $ LOWER FUEL ELEMENT
956     20 7.6958-2    -57     58    180    -179   $ LOWER FUEL ELEMENT
957     20 7.6958-2    -57     58    179    -178   $ LOWER FUEL ELEMENT
958     20 7.6958-2    -57     58    178    -177   $ LOWER FUEL ELEMENT
959     20 7.6958-2    -57     58    177    -176   $ LOWER FUEL ELEMENT
960     20 7.6958-2    -57     58    176    -175   $ LOWER FUEL ELEMENT
961     21 7.7042-2    -57     58    175    -172   $ LOWER FUEL ELEMENT
962     22 7.7127-2    -57     58    172    -171   $ LOWER FUEL ELEMENT
963     24 7.7296-2    -57     58    171    -170   $ LOWER FUEL ELEMENT
964     21 7.7042-2    -58     59    180    -179   $ LOWER FUEL ELEMENT
965     20 7.6958-2    -58     59    179    -178   $ LOWER FUEL ELEMENT
966     20 7.6958-2    -58     59    178    -177   $ LOWER FUEL ELEMENT
967     20 7.6958-2    -58     59    177    -176   $ LOWER FUEL ELEMENT
968     20 7.6958-2    -58     59    176    -175   $ LOWER FUEL ELEMENT
969     21 7.7042-2    -58     59    175    -172   $ LOWER FUEL ELEMENT
970     23 7.7212-2    -58     59    172    -171   $ LOWER FUEL ELEMENT
971     24 7.7296-2    -58     59    171    -170   $ LOWER FUEL ELEMENT
972     23 7.7212-2    -59     70    180    -179   $ LOWER FUEL ELEMENT
973     21 7.7042-2    -59     70    179    -178   $ LOWER FUEL ELEMENT
974     21 7.7042-2    -59     70    178    -177   $ LOWER FUEL ELEMENT
975     21 7.7042-2    -59     70    177    -176   $ LOWER FUEL ELEMENT
976     23 7.7212-2    -59     70    176    -175   $ LOWER FUEL ELEMENT
977     23 7.7212-2    -59     70    175    -172   $ LOWER FUEL ELEMENT
978     24 7.7296-2    -59     70    172    -171   $ LOWER FUEL ELEMENT
979     24 7.7296-2    -59     70    171    -170   $ LOWER FUEL ELEMENT
c
c       CONTROL RODS
c
c
c       FIRST
CONTROL ROD c
1204    4  9.9005-2    -3 15       -184           $ D2O COLD CEN HOLE
1205    4  9.9005-2   -15 16       -184           $ D2O COLD CEN HOLE
1206    4  9.9005-2   -16 17       -184           $ D2O COLD CEN HOLE
c
c       SECOND CONTROL ROD
c
1214    4  9.9005-2   -17 20       -184           $ D2O COLD CEN HOLE
1215    4  9.9005-2   -20 45       -184           $ D2O COLD CEN HOLE
1216    4  9.9005-2   -45 70       -184           $ D2O COLD CEN HOLE
c
```

```
c       THIRD CONTROL ROD
c
1224    4  9.9005-2   -70 74      -184            $ D2O COLD CEN HOLE
1225    4  9.9005-2   -74 75      -184            $ D2O COLD CEN HOLE
1226    4  9.9005-2   -75 76      -184            $ D2O COLD CEN HOLE

c       FOURTH CONTROL ROD
c
1234    4  9.9005-2   -76 88      -184            $ D2O COLD CEN HOLE
c
c       SAFETY RODS
c
c       1300    6  6.0034-2    -13     88    -401    400    $ AL6061
c       1301    51 -13.3       -13     73    -402    401    $ HAFNIUM
c       c
c       1305    6  6.0034-2    -13     88    -406    405    $ AL6061
c       1306    51 -13.3       -13     73    -407    406    $ HAFNIUM
c       c
c       1310    6  6.0034-2    -13     88    -411    410    $ AL6061
c       1311    51 -13.3       -13     73    -412    411    $ HAFNIUM
c       c
c       1315    6  6.0034-2    -13     88    -416    415    $ AL6061
c       1316    51 -13.3       -13     73    -417    416    $ HAFNIUM
c       c
c       1320    6  6.0034-2    -13     88    -421    420    $ AL6061
c       1321    51 -13.3       -13     73    -422    421    $ HAFNIUM
c       c
c       1325    6  6.0034-2    -13     88    -426    425    $ AL6061
c       1326    51 -13.3       -13     73    -427    426    $ HAFNIUM
c       c
c       1330    6  6.0034-2    -13     88    -431    430    $ AL6061
c       1331    51 -13.3       -13     73    -432    431    $ HAFNIUM
c       c
c       1335    6  6.0034-2    -13     88    -436    435    $ AL6061
c       1336    51 -13.3       -13     73    -437    436    $ HAFNIUM
c
c       EVERYTHING ELSE OUTSIDE THE H2O POOL
c
2000    0       1:91:-90

c
c       SURFACE SPECIFICATIONS
c
c       In this core model the z axis is the axis of rotation for the
c       fuel elements. Z = 0.0 is at the core midplane. (x,y)=(0.0,0.0)
c       is centered axially between the fuel elements.
c       The first entry in the section is the surface number.
c       The second entry is the surface type,
c       pz=plane perpendicular to z axis cz=cylinder with z axis as its
c       axis. The third entry is either the position of the plane on
c       the z axis or the radius of the cylinder - all comments are
c       made with reference to the core midplane.
c       All dimensions are in cm. Excess surfaces can be in the
```

```
c       problem, however warning messages will result.
c
1       pz       223.9    $ plane at top of h2o pool
2       pz       203.9    $ plane at top of al tank separating d2o & h2o
3       pz       200.9    $ plane at top of d2o REFLECTOR or and bottom
                            of al tank
5       pz       180.0    $ TOP OF CONTROL ROD FULLY OUT
7       pz       150.0    $ TOP OF CONTROL ROD 1/4 INSERTED
9       pz       120.0    $ TOP OF CONTROL ROD 1/2 INSERTED
11      pz        90.0    $ TOP OF CONTROL ROD 3/4 INSERTED
13      pz        60.0    $ top of control rod fully inserted
15      pz       163.4    $ plane for weight windows
16      pz       125.9    $ plane for weight windows
17      pz        88.4    $ plane for weight windows
18      pz        53.9    $ plane at top of al side plate on top fuel
                            element
19      pz        50.9    $ plane at top of al end plate on top fuel
                            element
20      pz        49.9    $ plane at top of top fuel element
21      pz       48.1     $ plane in fuel for fuel grading
22      pz       45.7     $ plane in fuel for fuel grading
23      pz       41.5     $ plane in fuel for fuel grading
24      pz       35.2     $ plane in fuel for fuel grading
25      pz       26.2     $ plane in fuel for fuel grading
26      pz       17.2     $ plane in fuel for fuel grading
27      pz       10.9     $ plane in fuel for fuel grading
28      pz        6.7     $ plane in fuel for fuel grading
29      pz        4.3     $ plane in fuel for fuel grading
30      pz       30.0     $ BOTTOM OF CONTROL ROD 1/4 INSERTED
40      pz        2.5     $ plane at bottom of top fuel element
41      pz        1.5     $ plane at bottom of al end plate on top fuel
                            element
45      pz        0.0     $ plane at core midplane
49      pz       -1.5     $ plane at top of al end plate on bottom fuel
                            element
50      pz       -2.5     $ plane at top of bottom fuel element
51      pz       -4.3     $ plane in fuel for fuel grading
52      pz       -6.7     $ plane in fuel for fuel grading
53      pz      -10.9     $ plane in fuel for fuel grading
54      pz      -17.2     $ plane in fuel for fuel grading
55      pz      -26.2     $ plane in fuel for fuel grading
56      pz      -35.2     $ plane in fuel for fuel grading
57      pz      -41.5     $ plane in fuel for fuel grading
58      pz      -45.7     $ plane in fuel for fuel grading
59      pz      -48.1     $ plane in fuel for fuel grading
60      pz      -30.0     $ BOTTOM OF CONTROL ROD 3/4 INSERTED
70      pz      -49.9     $ plane at bottom of bottom fuel element
71      pz      -50.9     $ plane at bottom of al end plate on bottom
                            fuel element
72      pz      -53.9     $ plane at bottom of al side plate on bottom
                            fuel element
73      pz      -60.0     $ BOTTOM OF CONTROL ROD FULLY INSERTED
74      pz      -88.4     $ plane for weight windows
```

```
75      pz    -125.9    $ plane for weight windows
76      pz    -163.4    $ plane for weight windows
88      pz    -200.9    $ plane at bottom of d2o REFLECTOR
89      pz    -203.9    $ plane at bottom of al tank separating d2o
                          and h2o
90      pz    -223.9    $ plane at bottom of h2o pool
91      cz    199.55    $ outer radius of h2o pool
92      cz    179.55    $ inner radius of h2o pool and outer radius of
                          al tank
93      cz    176.55    $ inner rad. of al tank and out radius of d2o
                          REFLECTOR
94      cz    161.05    $ surf in d20 refl for importance modelling
98      cz    145.55    $ surf in d20 refl for importance modelling
95      cz    129.55    $ surf in d20 refl for importance modelling
99      cz    113.55    $ surf in d20 refl for importance modelling
96      cz     97.55    $ surf in d20 refl for importance modelling
100     cz     81.55    $ surf in d2o refl sim to pdq model for cell
                          separation
110     cz     64.05    $ surf in d20 refl for importance modelling
111     cz     56.55    $ surf in d20 refl for importance modelling
120     cz      46.55   $ surf in d2o refl sim to pdq model for cell
                          separation
130     cz      36.55   $ surf in d20 refl for importance modelling
140     cz      26.55   $ outer radius of core pressure boundary tube
145     cz      25.3    $ inner radius of core pressure boundary tube
149     cz      24.8    $ outer radius of side plate on top fuel
                          element
150     cz      24.1    $ outer radius of top fuel element
151     cz      23.7    $ surf in fuel for fuel grading
152     cz      23.1    $ surf in fuel for fuel grading
153     cz      22.1    $ surf in fuel for fuel grading
154     cz      20.9    $ surf in fuel for fuel grading
155     cz      19.7    $ surf in fuel for fuel grading
156     cz      19.3    $ o.r. for irradiation pos next to bottom fuel
                          element
157     cz      18.5    $ surf in fuel for fuel grading
158     cz      17.9    $ surf in fuel for fuel grading
160     cz      17.5    $ i.r. of top fuel and o.r of side plate on
                          bot fuel
170     cz      16.8    $ o.r. of bottom fuel element
171     cz      16.4    $ surf in fuel for fuel grading
172     cz      15.8    $ surf in fuel for fuel grading
174     cz      15.2    $ i.r. for irradiation pos next to top fuel
                          element
175     cz      14.8    $ surf in fuel for fuel grading
176     cz      13.6    $ surf in fuel for fuel grading
177     cz      12.4    $ surf in fuel for fuel grading
178     cz      11.2    $ surf in fuel for fuel grading
179     cz      10.6    $ surf in fuel for fuel grading
180     cz      10.2    $ inner radius of bottom fuel element
184     cz       9.5    $ inner radius of side plate on bottom fuel
                          element
```

```
188     cz       7.5     $ surf in cent hole sim to pdq model for cell
                           sep
190     cz       3.5     $ surf in cent hole sim to pdq model for cell
                           sep
c
c       CONTROL ROD SURFACE NUMBERS
c
300     c/z      6.4      0.0      0.985   $ I.R. OF ZIRCALOY
301     c/z      6.4      0.0      1.25    $ I.R. OF AL6061
302     c/z      6.4      0.0      2.1     $ I.R. OF HF
303     c/z      6.4      0.0      2.7     $ O.R. OF HF
304     px       6.4                       $ PLANE FOR TALLYING
310     c/z     -6.4      0.0      0.985   $ I.R. OF ZIRCALOY
311     c/z     -6.4      0.0      1.25    $ I.R. OF AL6061
312     c/z     -6.4      0.0      2.1     $ I.R. OF HF
313     c/z     -6.4      0.0      2.7     $ O.R. OF HF
314     px      -6.4                      $ PLANE FOR TALLYING
320     c/z      0.0      6.4      0.985   $ I.R. OF ZIRCALOY
321     c/z      0.0      6.4      1.25    $ I.R. OF AL6061
322     c/z      0.0      6.4      2.1     $ I.R. OF HF
323     c/z      0.0      6.4      2.7     $ O.R. OF HF
324     py       6.4                      $ PLANE FOR TALLYING
330     c/z      0.0     -6.4      0.985   $ I.R. OF ZIRCALOY
331     c/z      0.0     -6.4      1.25    $ I.R. OF AL6061
332     c/z      0.0     -6.4      2.1     $ I.R. OF HF
333     c/z      0.0     -6.4      2.7     $ O.R. OF HF
334     py      -6.4                      $ PLANE FOR TALLYING
350     p        1       -1     0   0     $ SURFACE TO BREAK CEN HOLE
351     p        1        1     0   0     $ SURFACE TO BREAK CEN HOLE
c
c       SAFETY ROD SURFACE NUMBERS
c
400     c/z     34.88964      12.01346      2.5     $ I.R. OF AL6061
401     c/z     34.88964      12.01346      3.2     $ I.R. OF HAFNIUM
402     c/z     34.88964      12.01346      3.5     $ O.R. OF HAFNIUM
405     c/z     20.09718      30.94694      2.5     $ I.R. OF AL6061
406     c/z     20.09718      30.94694      3.2     $ I.R. OF HAFNIUM
407     c/z     20.09718      30.94694      3.5     $ O.R. OF HAFNIUM
410     c/z     34.88964     -12.01346      2.5     $ I.R. OF AL6061
411     c/z     34.88964     -12.01346      3.2     $ I.R. OF HAFNIUM
412     c/z     34.88964     -12.01346      3.5     $ O.R. OF HAFNIUM
415     c/z     20.09718     -30.94694      2.5     $ I.R. OF AL6061
416     c/z     20.09718     -30.94694      3.2     $ I.R. OF HAFNIUM
417     c/z     20.09718     -30.94694      3.5     $ O.R. OF HAFNIUM
420     c/z    -34.88964      12.01346      2.5     $ I.R. OF AL6061
421     c/z    -34.88964      12.01346      3.2     $ I.R. OF HAFNIUM
422     c/z    -34.88964      12.01346      3.5     $ O.R. OF HAFNIUM
425     c/z    -20.09718      30.94694      2.5     $ I.R. OF AL6061
426     c/z    -20.09718      30.94694      3.2     $ I.R. OF HAFNIUM
427     c/z    -20.09718      30.94694      3.5     $ O.R. OF HAFNIUM
430     c/z    -34.88964     -12.01346      2.5     $ I.R. OF AL6061
431     c/z    -34.88964     -12.01346      3.2     $ I.R. OF HAFNIUM
432     c/z    -34.88964     -12.01346      3.5     $ O.R. OF HAFNIUM
```

```
435     c/z    -20.09718      -30.94694     2.5     $ I.R. OF AL6061
436     c/z    -20.09718      -30.94694     3.2     $ I.R. OF HAFNIUM
437     c/z    -20.09718      -30.94694     3.5     $ O.R. OF HAFNIUM
c
c       D2O REGION DIVISOR SURFACES
c
700     pz      43.975
701     pz      38.05
702     pz      32.125
703     pz      20.275
704     pz      14.35
705     pz       8.425
706     pz      -8.425
707     pz     -14.35
708     pz     -20.275
709     pz     -32.125
730     pz     -38.05
731     pz     -43.975
710     cz      29.05
711     cz      31.55
712     cz      34.05
713     cz      36.55
714     cz      39.05
715     cz      41.55
716     cz      44.05
717     cz      49.05
718     cz      51.55
719     cz      54.05
720     cz      56.55
721     cz      59.05
722     cz      61.55

c       MCNP CONTROL INFORMATION
c
c       This run contains neutron and/or  photon production.
c
mode    n
c
c       This is the kcode card that tells MCNP to do a k-effecitve
c       calculation. The first number is the number of neutrons
c       per cycle. The second number is the guess for k-eff.
c       The third number is the number of cycles to skip before
c       tallying. The fourth number is the total number of
c       cycles to be run.
c       A warning message will occur with this kcode card telling the
c       the user that the tallies are normed to the number of neutrons
c       produced in the fission process.
kcode   3000    1.0      4      14
c
c       These are source points for fission production. If a source
c       tape from a previous run is to be used simply comment out or
c       remove these cards. The file 'srctp' must be present and will be
c       used.
```

```
c
c       ksrc    19.0  0.0  24.0  0.0 19.0  24.0  -19.0  0.0  24.0
c                0.0  -19.0  24.0  13.0  0.0  -24.0  0.0  13.0  -24.0
c                -13.0  0.0  -24.0  0.0  -13.0  -24.0
c                19.0  0.0  47.0  0.0 19.0  47.0  -19.0  0.0  47.0
c                0.0  -19.0  47.0  13.0  0.0  -47.0  0.0  13.0  -47.0
c                -13.0  0.0  -47.0  0.0  -13.0  -47.0
c                19.0  0.0   5.0  0.0 19.0   5.0  -19.0  0.0   5.0
c                0.0  -19.0   5.0  13.0  0.0  -5.0  0.0  13.0  -5.0
c                -13.0  0.0  -5.0  0.0  -13.0  -5.0
c                19.0  0.0  36.0  0.0 19.0  36.0  -19.0  0.0  36.0
c                0.0  -19.0  36.0  13.0  0.0  -36.0  0.0  13.0  -36.0
c                -13.0  0.0  -36.0  0.0  -13.0  -36.0
c                19.0  0.0  12.0  0.0 19.0  12.0  -19.0  0.0  12.0
c                0.0  -19.0  12.0  13.0  0.0 -12.0  0.0  13.0 -12.0
c                -13.0  0.0 -12.0  0.0  -13.0 -12.0
c
c       The energy cutoff for the problem is 17 MeV similar to pdq
c       where the cross section sets have a maximum energy of 16.9 MeV.
c       The second number is the energy point below which MCNP will
c       use analog capture, usually a thermal energy.
c
phys:n  17 0.0
c
c
c       MATERIAL SPECIFICATIONS
c
c       isotope          identifier      file
c
c       U-235            92235.50c       rmccs2
c       U-238            92238.50c       rmccs2
c       Si               14000.50c       endf5p2
c       Al-27            13027.50c       rmccs2
c       Mn               25055.50c       endf5u2
c       Fe               26000.55c       rmccs2
c       Cr               24000.50c       rmccs2
c       Mg               12000.50c       endf5u2
c       Cu               29000.50c       rmccs2
c       H                 1001.50c       rmccs2
c       D                 1002.55c       rmccs2
c       O                 8016.50c       rmccs2
c       B-10              5010.50c       rmccs2
c       Hf               72000.50c       newxs2
c       Zr               40000.50c       endf5p2
c       light water thermal (300K)  lwtr.01t   tmccs2
c       heavy water thermal (300K)  hwtr.01t   tmccs2
c       heavy water thermal (400K)  hwtr.02t   tmccs2
c
c       These are the material cards. The number next to the nuclide
c       identifier is the nuclide's fraction of the total concentra-
c       tion.A   mt card gives the associated thermal library for that
c       material.
```

```
c
c       MATERIAL 1 - H2O pool total conc = 0.1003
c
m1      1001.50c  0.66667  8016.50c  0.33333
c
c       MATERIAL 2 - D2O REFLECTORor total conc = 9.8855-2
c
m2      1001.50c  1.6671-3  1002.55c  6.6502-1  8016.50c  3.3332-1
c
c       MATERIAL 3 - D2O hot total conc = 9.6972-2
c
m3      1001.50c  1.6665-3  1002.55c  6.6494-1  8016.50c  3.334-1
c
c       MATERIAL 4 - D2O cold total conc = 9.9005-2
c
m4      1001.50c  1.6666-3  1002.55c  6.6502-1  8016.50c  3.3332-1
c
c       MATERIAL 5 - Al end caps on fuel elements total conc = 7.9166-2
c                    without boron
c
c        m5   1001.50c  1.027-3  1002.55c  4.1091-1  8016.50c  2.0596-1
c             25055.50c  2.83938-4  26000.55c  1.30353-3
c             24000.50c  5.01863-4  12000.50c  4.27849-3
c             14000.50c  2.22136-3  29000.50c  4.50011-4
c             13027.50c  3.73069-1
c
c       MATERIAL 5 - Al end caps on fuel elements total conc = 7.9403-2
c                    with boron
c
m5      1001.50c  1.0239-3  1002.55c  4.0968-1  8016.50c  2.0535-1
        25055.50c  2.83090-4  26000.55c  1.29960-3
        24000.50c  5.00370-4  12000.50c  4.26570-3
        14000.50c  2.21470-3  29000.50c  4.48670-4
        13027.50c  3.71960-1  5010.50c   2.9772-3
c
c       MATERIAL 6 - Al 6061 total conc = 6.0034-2
c
m6      25055.50c  7.4308-4  26000.55c  3.4114-3  14000.50c  5.8134-3
        24000.50c  1.3134-3  12000.50c  1.1197-2  29000.50c  1.1777-3
        13027.50c  9.7634-1
c
c       MATERIAL 7 - Al end caps on fuel elements total conc = 7.9648-2
c                       this is the endcap on the top of the bot element
c                       with boron
c
m7      1001.50c  1.0207-3  1002.55c  4.0842-1  8016.50c  2.0471-1
        25055.50c  2.82220-4  26000.55c  1.29560-3
        24000.50c  4.98830-4  12000.50c  4.25260-3
        14000.50c  2.20790-3  29000.50c  4.47290-4
        13027.50c  3.70810-1  5010.50c   6.0502-3
c
c       MATERIAL 20 - Fuel total conc = 7.6958-2
```

```
c
m30     92235.50c 1.0
m20     92235.50c  9.2853-3   92238.50c  6.9013-4  14000.50c  7.5554-3
         1001.50c  1.0625-3    1002.55c  4.2397-1   8016.50c  2.1252-1
        13027.50c  3.42150-1  25055.50c  1.15680-4
        26000.55c  5.31050-4  24000.50c  2.04460-4
        12000.50c  1.74300-3  29000.50c  1.83330-4
c
c       MATERIAL 21 - Fuel total conc = 7.7042-2
c
m21     92235.50c  7.4202-3   92238.50c  5.5150-4  14000.50c  6.21848-3
         1001.50c  1.0614-3    1002.55c  4.2351-1   8016.50c  2.1229-1
        13027.50c  3.46180-1  25055.50c  1.15550-4
        26000.55c  5.30470-4  24000.50c  2.04230-4
        12000.50c  1.74110-3  29000.50c  1.83130-4
c
c       MATERIAL 22 - Fuel total conc = 7.7127-2
c
m22     92235.50c  5.5590-3   92238.50c  4.1317-4  14000.50c  4.8845-3
         1001.50c  1.0602-3    1002.55c  4.2304-1   8016.50c  2.1205-1
        13027.50c  3.50220-1  25055.50c  1.15420-4
        26000.55c  5.29890-4  24000.50c  2.04010-4
        12000.50c  1.73920-3  29000.50c  1.82930-4
c
c       MATERIAL 23 - Fuel total conc = 7.7212-2
c
m23     92235.50c  3.7019-3   92238.50c  2.7514-4  14000.50c  3.5534-3
         1001.50c  1.0591-3    1002.55c  4.2258-1   8016.50c  2.1182-1
        13027.50c  3.54240-1  25055.50c  1.15300-4
        26000.55c  5.29310-4  24000.50c  2.03797-4
        12000.50c  1.73730-3  29000.50c  1.82730-4
c
c       MATERIAL 24 - Fuel total conc = 7.7296-2
c
m24     92235.50c  1.8490-3   92238.50c  1.3742-4  14000.50c  2.2253-3
         1001.50c  1.0579-3    1002.55c  4.2212-1   8016.50c  2.1159-1
        13027.50c  3.58250-1  25055.50c  1.15170-4
        26000.55c  5.28730-4  24000.50c  2.03560-4
        12000.50c  1.73540-3  29000.50c  1.82530-4
c
c       MATERIAL 38 - upper irradiation target total conc = 9.3324-2
c
m38      1001.50c  1.5584-3    1002.55c  6.2183-1   8016.50c  3.1178-1
        13027.50c  6.32940-2  25055.50c  4.81720-5
        26000.55c  2.21150-4  24000.50c  8.51450-5 14000.50c  3.7687-4
        12000.50c  7.25880-4  29000.50c  7.63480-5
c
c       MATERIAL 39 - lower irradiation target total conc =   9.5155-2
c
m39      1001.50c  1.5606-3    1002.55c  6.2273-1   8016.50c   3.1212-1
        13027.50c  6.20770-2  25055.50c  4.72460-5
        26000.55c  2.16900-4  24000.50c  8.35070-5 14000.50c  3.6962-4
        12000.50c  7.11920-4  29000.50c  7.48790-5
```

```
c
c       MATERIAL 50 - Zircaloy in the control rods density is 6.4 g/cc
c
m50     40000.50c 1.0
c
c       MATERIAL 51 - Natural Hafnium the gram density is 13.3 g/cc
c
m51     72000.50c 1.0
mt4     hwtr.01t
mt3     hwtr.01t
mt2     hwtr.01t
mt1     lwtr.01t
mt39    hwtr.01t
mt38    hwtr.01t
mt24    hwtr.01t
mt23    hwtr.01t
mt22    hwtr.01t
mt21    hwtr.01t
mt20    hwtr.01t
mt7     hwtr.01t
mt5     hwtr.01t
c
c       TEMPERATURE AND IMPORTANCE CARDS
c
#           tmp1            imp:p    imp:n
 100        3.0160e-08      1.0      1.0
 101        3.0160e-08      1.0      1.0
 102        3.0160e-08      1.0      1.0
 103        3.0160e-08      1.0      1.0
 104        3.0160e-08      1.0      1.0
 105        3.0160e-08      1.0      1.0
 106        3.0160e-08      1.0      1.0
 107        2.5851e-08      1.0      1.0
 108        2.5851e-08      1.0      1.0
 109        2.5851e-08      1.0      1.0
 110        2.5851e-08      1.0      1.0
 111        2.5851e-08      1.0      1.0
 120        3.0160e-08      1.0      1.0
 121        3.0160e-08      1.0      1.0
 122        3.0160e-08      1.0      1.0
 123        3.0160e-08      1.0      1.0
 124        3.0160e-08      1.0      1.0
 125        3.0160e-08      1.0      1.0
 126        3.0160e-08      1.0      1.0
 127        2.5851e-08      1.0      1.0
 128        2.5851e-08      1.0      1.0
 129        2.5851e-08      1.0      1.0
 130        2.5851e-08      1.0      1.0
 131        2.5851e-08      1.0      1.0
 140        3.0160e-08      1.0      1.0
 141        3.0160e-08      1.0      1.0
 142        3.0160e-08      1.0      1.0
 143        3.0160e-08      1.0      1.0
```

144	3.0160e-08	1.0	1.0
145	3.0160e-08	1.0	1.0
146	3.0160e-08	1.0	1.0
147	2.5851e-08	1.0	1.0
148	2.5851e-08	1.0	1.0
149	2.5851e-08	1.0	1.0
150	2.5851e-08	1.0	1.0
151	2.5851e-08	1.0	1.0
160	3.0160e-08	1.0	1.0
161	3.0160e-08	1.0	1.0
162	3.0160e-08	1.0	1.0
163	3.0160e-08	1.0	1.0
164	3.0160e-08	1.0	1.0
165	3.0160e-08	1.0	1.0
166	3.0160e-08	1.0	1.0
167	2.5851e-08	1.0	1.0
168	2.5851e-08	1.0	1.0
169	2.5851e-08	1.0	1.0
170	2.5851e-08	1.0	1.0
171	2.5851e-08	1.0	1.0
172	2.5851e-08	1.0	1.0
173	2.5851e-08	1.0	1.0
200	3.0160e-08	1.0	1.0
201	3.0160e-08	1.0	1.0
202	3.0160e-08	1.0	1.0
203	3.0160e-08	1.0	1.0
204	3.0160e-08	1.0	1.0
205	3.0160e-08	1.0	1.0
206	2.5851e-08	1.0	1.0
207	3.0160e-08	1.0	1.0
210	2.5851e-08	1.0	1.0
211	2.5851e-08	1.0	1.0
212	2.5851e-08	1.0	1.0
213	2.5851e-08	1.0	1.0
214	2.5851e-08	1.0	1.0
215	2.5851e-08	1.0	1.0
216	2.5851e-08	1.0	1.0
217	2.5851e-08	1.0	1.0
218	2.5851e-08	1.0	1.0
220	2.5851e-08	1.0	1.0
221	2.5851e-08	1.0	1.0
222	2.5851e-08	1.0	1.0
223	2.5851e-08	1.0	1.0
224	2.5851e-08	1.0	1.0
225	2.5851e-08	1.0	1.0
226	2.5851e-08	1.0	1.0
227	2.5851e-08	1.0	1.0
228	2.5851e-08	1.0	1.0
230	2.5851e-08	1.0	1.0
231	2.5851e-08	1.0	1.0
232	2.5851e-08	1.0	1.0
233	2.5851e-08	1.0	1.0
234	2.5851e-08	1.0	1.0

235	2.5851e-08	1.0	1.0
236	2.5851e-08	1.0	1.0
237	2.5851e-08	1.0	1.0
238	2.5851e-08	1.0	1.0
240	2.5851e-08	1.0	1.0
241	2.5851e-08	1.0	1.0
242	2.5851e-08	1.0	1.0
243	2.5851e-08	1.0	1.0
244	2.5851e-08	1.0	1.0
245	2.5851e-08	1.0	1.0
246	2.5851e-08	1.0	1.0
247	2.5851e-08	1.0	1.0
248	2.5851e-08	1.0	1.0
250	2.5851e-08	1.0	1.0
251	2.5851e-08	1.0	1.0
260	2.5851e-08	1.0	1.0
261	2.5851e-08	1.0	1.0
270	2.5851e-08	1.0	1.0
271	2.5851e-08	1.0	1.0
300	3.0160e-08	1.0	1.0
301	3.0160e-08	1.0	1.0
302	3.0160e-08	1.0	1.0
303	3.0160e-08	1.0	1.0
304	2.5851e-08	1.0	1.0
305	3.0160e-08	1.0	1.0
306	2.5851e-08	1.0	1.0
307	3.0160e-08	1.0	1.0
400	3.0160e-08	1.0	1.0
401	2.5851e-08	1.0	1.0
402	3.0160e-08	1.0	1.0
403	3.0160e-08	1.0	1.0
404	2.5851e-08	1.0	1.0
405	3.0160e-08	1.0	1.0
406	2.5851e-08	1.0	1.0
407	3.0160e-08	1.0	1.0
500	3.0160e-08	1.0	1.0
501	3.0160e-08	1.0	1.0
502	2.5851e-08	1.0	1.0
503	2.5851e-08	1.0	1.0
504	2.5851e-08	1.0	1.0
505	2.5851e-08	1.0	1.0
506	3.0160e-08	1.0	1.0
510	2.5851e-08	1.0	1.0
511	2.5851e-08	1.0	1.0
512	2.5851e-08	1.0	1.0
513	2.5851e-08	1.0	1.0
514	2.5851e-08	1.0	1.0
515	2.5851e-08	1.0	1.0
516	2.5851e-08	1.0	1.0
517	2.5851e-08	1.0	1.0
518	2.5851e-08	1.0	1.0
520	2.5851e-08	1.0	1.0
521	2.5851e-08	1.0	1.0

522	2.5851e-08	1.0	1.0
523	2.5851e-08	1.0	1.0
524	2.5851e-08	1.0	1.0
525	2.5851e-08	1.0	1.0
526	2.5851e-08	1.0	1.0
527	2.5851e-08	1.0	1.0
528	2.5851e-08	1.0	1.0
530	2.5851e-08	1.0	1.0
531	2.5851e-08	1.0	1.0
532	2.5851e-08	1.0	1.0
533	2.5851e-08	1.0	1.0
534	2.5851e-08	1.0	1.0
535	2.5851e-08	1.0	1.0
536	2.5851e-08	1.0	1.0
537	2.5851e-08	1.0	1.0
538	2.5851e-08	1.0	1.0
540	2.5851e-08	1.0	1.0
541	2.5851e-08	1.0	1.0
542	2.5851e-08	1.0	1.0
543	2.5851e-08	1.0	1.0
544	2.5851e-08	1.0	1.0
545	2.5851e-08	1.0	1.0
546	2.5851e-08	1.0	1.0
547	2.5851e-08	1.0	1.0
548	2.5851e-08	1.0	1.0
550	2.5851e-08	1.0	1.0
551	2.5851e-08	1.0	1.0
560	2.5851e-08	1.0	1.0
561	2.5851e-08	1.0	1.0
570	2.5851e-08	1.0	1.0
571	2.5851e-08	1.0	1.0
600	3.0160e-08	1.0	1.0
601	3.0160e-08	1.0	1.0
602	2.5851e-08	1.0	1.0
603	2.5851e-08	1.0	1.0
604	2.5851e-08	1.0	1.0
605	2.5851e-08	1.0	1.0
606	2.5851e-08	1.0	1.0
607	3.0160e-08	1.0	1.0
608	2.5851e-08	1.0	1.0
609	2.5851e-08	1.0	1.0
610	2.5851e-08	1.0	1.0
611	2.5851e-08	1.0	1.0
612	2.5851e-08	1.0	1.0
613	2.5851e-08	1.0	1.0
614	2.5851e-08	1.0	1.0
620	3.0160e-08	1.0	1.0
621	2.5851e-08	1.0	1.0
622	2.5851e-08	1.0	1.0
623	2.5851e-08	1.0	1.0
624	3.0160e-08	1.0	1.0
625	2.5851e-08	1.0	1.0
626	2.5851e-08	1.0	1.0

627	2.5851e-08	1.0	1.0
628	2.5851e-08	1.0	1.0
629	2.5851e-08	1.0	1.0
640	3.0160e-08	1.0	1.0
641	2.5851e-08	1.0	1.0
642	2.5851e-08	1.0	1.0
643	2.5851e-08	1.0	1.0
644	3.0160e-08	1.0	1.0
645	2.5851e-08	1.0	1.0
646	2.5851e-08	1.0	1.0
647	2.5851e-08	1.0	1.0
648	2.5851e-08	1.0	1.0
649	2.5851e-08	1.0	1.0
660	3.0160e-08	1.0	1.0
661	2.5851e-08	1.0	1.0
662	2.5851e-08	1.0	1.0
663	2.5851e-08	1.0	1.0
664	3.0160e-08	1.0	1.0
665	2.5851e-08	1.0	1.0
666	2.5851e-08	1.0	1.0
667	2.5851e-08	1.0	1.0
668	2.5851e-08	1.0	1.0
669	2.5851e-08	1.0	1.0
700	3.0160e-08	1.0	1.0
701	3.0160e-08	1.0	1.0
702	3.0160e-08	1.0	1.0
703	3.0160e-08	1.0	1.0
704	3.0160e-08	1.0	1.0
705	3.0160e-08	1.0	1.0
706	3.0160e-08	1.0	1.0
707	3.0160e-08	1.0	1.0
708	3.0160e-08	1.0	1.0
709	3.0160e-08	1.0	1.0
710	3.0160e-08	1.0	1.0
711	3.0160e-08	1.0	1.0
712	3.0160e-08	1.0	1.0
713	3.0160e-08	1.0	1.0
714	3.0160e-08	1.0	1.0
715	3.0160e-08	1.0	1.0
716	3.0160e-08	1.0	1.0
717	3.0160e-08	1.0	1.0
718	3.0160e-08	1.0	1.0
719	3.0160e-08	1.0	1.0
720	3.0160e-08	1.0	1.0
721	3.0160e-08	1.0	1.0
722	3.0160e-08	1.0	1.0
723	3.0160e-08	1.0	1.0
724	3.0160e-08	1.0	1.0
725	3.0160e-08	1.0	1.0
726	3.0160e-08	1.0	1.0
727	3.0160e-08	1.0	1.0
728	3.0160e-08	1.0	1.0
729	3.0160e-08	1.0	1.0

730	3.0160e-08	1.0	1.0
731	3.0160e-08	1.0	1.0
732	3.0160e-08	1.0	1.0
733	3.0160e-08	1.0	1.0
734	3.0160e-08	1.0	1.0
735	3.0160e-08	1.0	1.0
736	3.0160e-08	1.0	1.0
737	3.0160e-08	1.0	1.0
738	3.0160e-08	1.0	1.0
739	3.0160e-08	1.0	1.0
740	3.0160e-08	1.0	1.0
741	3.0160e-08	1.0	1.0
742	3.0160e-08	1.0	1.0
743	3.0160e-08	1.0	1.0
744	3.0160e-08	1.0	1.0
745	3.0160e-08	1.0	1.0
746	3.0160e-08	1.0	1.0
747	3.0160e-08	1.0	1.0
748	3.0160e-08	1.0	1.0
749	3.0160e-08	1.0	1.0
750	3.0160e-08	1.0	1.0
751	3.0160e-08	1.0	1.0
752	3.0160e-08	1.0	1.0
753	3.0160e-08	1.0	1.0
754	3.0160e-08	1.0	1.0
755	3.0160e-08	1.0	1.0
756	3.0160e-08	1.0	1.0
757	3.0160e-08	1.0	1.0
758	3.0160e-08	1.0	1.0
759	3.0160e-08	1.0	1.0
760	3.0160e-08	1.0	1.0
761	3.0160e-08	1.0	1.0
762	3.0160e-08	1.0	1.0
763	3.0160e-08	1.0	1.0
764	3.0160e-08	1.0	1.0
765	3.0160e-08	1.0	1.0
766	3.0160e-08	1.0	1.0
767	3.0160e-08	1.0	1.0
768	3.0160e-08	1.0	1.0
769	3.0160e-08	1.0	1.0
770	3.0160e-08	1.0	1.0
771	3.0160e-08	1.0	1.0
772	3.0160e-08	1.0	1.0
773	3.0160e-08	1.0	1.0
774	3.0160e-08	1.0	1.0
775	3.0160e-08	1.0	1.0
776	3.0160e-08	1.0	1.0
777	3.0160e-08	1.0	1.0
778	3.0160e-08	1.0	1.0
779	3.0160e-08	1.0	1.0
900	3.0160e-08	1.0	1.0
901	3.0160e-08	1.0	1.0
902	3.0160e-08	1.0	1.0

903	3.0160e-08	1.0	1.0
904	3.0160e-08	1.0	1.0
905	3.0160e-08	1.0	1.0
906	3.0160e-08	1.0	1.0
907	3.0160e-08	1.0	1.0
908	3.0160e-08	1.0	1.0
909	3.0160e-08	1.0	1.0
910	3.0160e-08	1.0	1.0
911	3.0160e-08	1.0	1.0
912	3.0160e-08	1.0	1.0
913	3.0160e-08	1.0	1.0
914	3.0160e-08	1.0	1.0
915	3.0160e-08	1.0	1.0
916	3.0160e-08	1.0	1.0
917	3.0160e-08	1.0	1.0
918	3.0160e-08	1.0	1.0
919	3.0160e-08	1.0	1.0
920	3.0160e-08	1.0	1.0
921	3.0160e-08	1.0	1.0
922	3.0160e-08	1.0	1.0
923	3.0160e-08	1.0	1.0
924	3.0160e-08	1.0	1.0
925	3.0160e-08	1.0	1.0
926	3.0160e-08	1.0	1.0
927	3.0160e-08	1.0	1.0
928	3.0160e-08	1.0	1.0
929	3.0160e-08	1.0	1.0
930	3.0160e-08	1.0	1.0
931	3.0160e-08	1.0	1.0
932	3.0160e-08	1.0	1.0
933	3.0160e-08	1.0	1.0
934	3.0160e-08	1.0	1.0
935	3.0160e-08	1.0	1.0
936	3.0160e-08	1.0	1.0
937	3.0160e-08	1.0	1.0
938	3.0160e-08	1.0	1.0
939	3.0160e-08	1.0	1.0
940	3.0160e-08	1.0	1.0
941	3.0160e-08	1.0	1.0
942	3.0160e-08	1.0	1.0
943	3.0160e-08	1.0	1.0
944	3.0160e-08	1.0	1.0
945	3.0160e-08	1.0	1.0
946	3.0160e-08	1.0	1.0
947	3.0160e-08	1.0	1.0
948	3.0160e-08	1.0	1.0
949	3.0160e-08	1.0	1.0
950	3.0160e-08	1.0	1.0
951	3.0160e-08	1.0	1.0
952	3.0160e-08	1.0	1.0
953	3.0160e-08	1.0	1.0
954	3.0160e-08	1.0	1.0
955	3.0160e-08	1.0	1.0

956	3.0160e-08	1.0	1.0
957	3.0160e-08	1.0	1.0
958	3.0160e-08	1.0	1.0
959	3.0160e-08	1.0	1.0
960	3.0160e-08	1.0	1.0
961	3.0160e-08	1.0	1.0
962	3.0160e-08	1.0	1.0
963	3.0160e-08	1.0	1.0
964	3.0160e-08	1.0	1.0
965	3.0160e-08	1.0	1.0
966	3.0160e-08	1.0	1.0
967	3.0160e-08	1.0	1.0
968	3.0160e-08	1.0	1.0
969	3.0160e-08	1.0	1.0
970	3.0160e-08	1.0	1.0
971	3.0160e-08	1.0	1.0
972	3.0160e-08	1.0	1.0
973	3.0160e-08	1.0	1.0
974	3.0160e-08	1.0	1.0
975	3.0160e-08	1.0	1.0
976	3.0160e-08	1.0	1.0
977	3.0160e-08	1.0	1.0
978	3.0160e-08	1.0	1.0
979	3.0160e-08	1.0	1.0
1204	2.5851e-08	1.0	1.0
1205	2.5851e-08	1.0	1.0
1206	2.5851e-08	1.0	1.0
1214	2.5851e-08	1.0	1.0
1215	2.5851e-08	1.0	1.0
1216	2.5851e-08	1.0	1.0
1224	2.5851e-08	1.0	1.0
1225	2.5851e-08	1.0	1.0
1226	2.5851e-08	1.0	1.0
1234	2.5851e-08	1.0	1.0
2000	0.0	0.0	0.0
1100	2.5851e-08	1.0	1.0
1101	2.5851e-08	1.0	1.0
1102	2.5851e-08	1.0	1.0
1103	2.5851e-08	1.0	1.0
1104	2.5851e-08	1.0	1.0
1105	2.5851e-08	1.0	1.0
1106	2.5851e-08	1.0	1.0
1107	2.5851e-08	1.0	1.0
1108	2.5851e-08	1.0	1.0
1109	2.5851e-08	1.0	1.0
1110	2.5851e-08	1.0	1.0
1111	2.5851e-08	1.0	1.0
1112	2.5851e-08	1.0	1.0
1113	2.5851e-08	1.0	1.0
1114	2.5851e-08	1.0	1.0
1115	2.5851e-08	1.0	1.0
1116	2.5851e-08	1.0	1.0
1117	2.5851e-08	1.0	1.0

```
1118        2.5851e-08      1.0       1.0
1119        2.5851e-08      1.0       1.0
1120        2.5851e-08      1.0       1.0
1121        2.5851e-08      1.0       1.0
1122        2.5851e-08      1.0       1.0
1123        2.5851e-08      1.0       1.0
1124        3.0160e-08      1.0       1.0
1125        3.0160e-08      1.0       1.0
1126        3.0160e-08      1.0       1.0
1127        3.0160e-08      1.0       1.0
1128        3.0160e-08      1.0       1.0
1129        3.0160e-08      1.0       1.0
1130        3.0160e-08      1.0       1.0
1131        3.0160e-08      1.0       1.0
1132        3.0160e-08      1.0       1.0
1133        3.0160e-08      1.0       1.0
1134        3.0160e-08      1.0       1.0
1135        3.0160e-08      1.0       1.0
1136        3.0160e-08      1.0       1.0
1137        3.0160e-08      1.0       1.0
1138        3.0160e-08      1.0       1.0
1139        3.0160e-08      1.0       1.0
1140        3.0160e-08      1.0       1.0
1141        3.0160e-08      1.0       1.0
1142        3.0160e-08      1.0       1.0
1143        3.0160e-08      1.0       1.0
1144        3.0160e-08      1.0       1.0
1145        3.0160e-08      1.0       1.0
c
c       THESE ARE THE CELLS FOR TALLIES
c       CHOOSE THE TALLIES AS YOU WISH
c
c       OUTER H2O POOL ANS AL6061 TANK
c       1100 1101 1102 1103 1104 1105 1106 1107 1108 1109
c       1110 1111 1112 1113 1114 1115 1116 1117 1118 1119
c       1120 1121 1122 1123 1124 1125 1126 1127 1128 1129
c       1130 1131 1132 1133 1134 1135 1136 1137 1138 1139
c       1140 1141 1142 1143 1144 1145
c       CPBT ANS ALL AL6061 AND D2O REGIONS INSIDE INCLUDING ENDCAPS
c       100 101 102 103 104 105 106 120 121 122 123 124 125
c       126 140 141 142 143 144 145 146 160 161 162 163 164
c       165 166 200 201 202 203 204 205 206 207 300 301 302
c       303 304 305 306 307 400 401 402 403 404 405 406 407
c       500 501 502 503 504 505 506 600 601 602 603 604 605
c       606 607 620 621 622 623 624 640 641 642 643 644 660
c       661 662 663 664
c       D2O REFLECTOR REGIONS
c       107 108 109 110 111 127 128 129 130 131 147 148 149
c       150 151 167 168 169 170 171 172 173 210 211 212 213
c       214 215 216 217 218 220 221 222 223 224 225 226 227
c       228 230 231 232 233 234 235 236 237 238 240 241 242
c       243 244 245 246 247 248 250 251 260 261 270 271 510
```

```
c       511 512 513 514 515 516 517 518 520 521 522 523 524
c       525 526 527 528 530 531 532 533 534 535 536 537 538
c       540 541 542 543 544 545 546 547 548 550 551 560 561
c       570 571 608 609 610 611 612 613 614 625 626 627 628
c       629 645 646 647 648 649 665 666 667 668 669
c       FUEL REGIONS
c       D2O REFLECTOR REGIONS
f34:n   210 211 212 213 214 215 216 217 218
        510 511 512 513 514 515 516 517 518
fs34    -710 -711 -712 t
e34     6.83-7  5.531-3  0.821  17.0
f44:n   220 221 222 223 224 225 226 227 228
        520 521 522 523 524 525 526 527 528
fs44    -714 -715 -716 t
e44     6.83-7  5.531-3  0.821  17.0
f54:n   230 231 232 233 234 235 236 237 238
        530 531 532 533 534 535 536 537 538
fs54    -717 -718 -719 -720 -721 -722 t
e54     6.83-7  5.531-3  0.821  17.0
f64:n   210 211 212 213 214 215 216 217 218
        510 511 512 513 514 515 516 517 518
fs64    -710 -711 -712 t
e64     6.25-7  1.0-4  0.1      17.0
f74:n   220 221 222 223 224 225 226 227 228
        520 521 522 523 524 525 526 527 528
fs74    -714 -715 -716 t
e74     6.25-7  1.0-4  0.1      17.0
f84:n   230 231 232 233 234 235 236 237 238
        530 531 532 533 534 535 536 537 538
fs84    -717 -718 -719 -720 -721 -722 t
e84     6.25-7  1.0-4  0.1      17.0
f24:n   107 108 109 110 111 127 128 129 130 131 147 148 149
        150 151 167 168 169 170 171 172 173 210 211 212 213
        214 215 216 217 218 220 221 222 223 224 225 226 227
        228 230 231 232 233 234 235 236 237 238 240 241 242
        243 244 245 246 247 248 250 251 260 261 270 271 510
        511 512 513 514 515 516 517 518 520 521 522 523 524
        525 526 527 528 530 531 532 533 534 535 536 537 538
        540 541 542 543 544 545 546 547 548 550 551 560 561
        570 571 608 609 610 611 612 613 614 625 626 627 628
        629 645 646 647 648 649 665 666 667 668 669
e24     6.83-7  5.531-3  0.821  17.0
fq24     e f
c       FUEL REGIONS
f7:n    700 701 702 703 704 705 706 707 708 709 710 711 712 713 714
        715 716 717 718 719 720 721 722 723 724 725 726 727 728 729
        730 731 732 733 734 735 736 737 738 739 740 741 742 743 744
        745 746 747 748 749 750 751 752 753 754 755 756 757 758 759
        760 761 762 763 764 765 766 767 768 769 770 771 772 773 774
        775 776 777 778 779
        900 901 902 903 904 905 906 907 908 909 910 911 912 913 914
        915 916 917 918 919 920 921 922 923 924 925 926 927 928 929
        930 931 932 933 934 935 936 937 938 939 940 941 942 943 944
```

```
        945 946 947 948 949 950 951 952 953 954 955 956 957 958 959
        960 961 962 963 964 965 966 967 968 969 970 971 972 973 974
        975 976 977 978 979
c
fq7     e f
f17:n   (700 701 702 703 704 705 706 707 708 709 710 711 712 713 714
        715 716 717 718 719 720 721 722 723 724 725 726 727 728 729
        730 731 732 733 734 735 736 737 738 739 740 741 742 743 744
        745 746 747 748 749 750 751 752 753 754 755 756 757 758 759
        760 761 762 763 764 765 766 767 768 769 770 771 772 773 774
        775 776 777 778 779)
        (900 901 902 903 904 905 906 907 908 909 910 911 912 913 914
        915 916 917 918 919 920 921 922 923 924 925 926 927 928 929
        930 931 932 933 934 935 936 937 938 939 940 941 942 943 944
        945 946 947 948 949 950 951 952 953 954 955 956 957 958 959
        960 961 962 963 964 965 966 967 968 969 970 971 972 973 974
        975 976 977 978 979)
c
fq17     e f
f4:n    700 701 702 703 704 705 706 707 708 709 710 711 712 713 714
        715 716 717 718 719 720 721 722 723 724 725 726 727 728 729
        730 731 732 733 734 735 736 737 738 739 740 741 742 743 744
        745 746 747 748 749 750 751 752 753 754 755 756 757 758 759
        760 761 762 763 764 765 766 767 768 769 770 771 772 773 774
        775 776 777 778 779
        900 901 902 903 904 905 906 907 908 909 910 911 912 913 914
        915 916 917 918 919 920 921 922 923 924 925 926 927 928 929
        930 931 932 933 934 935 936 937 938 939 940 941 942 943 944
        945 946 947 948 949 950 951 952 953 954 955 956 957 958 959
        960 961 962 963 964 965 966 967 968 969 970 971 972 973 974
        975 976 977 978 979
e4      6.83-7  5.531-3  0.821  17.0
fq4     e f
c
f14:n   700 701 702 703 704 705 706 707 708 709 710 711 712 713 714
        715 716 717 718 719 720 721 722 723 724 725 726 727 728 729
        730 731 732 733 734 735 736 737 738 739 740 741 742 743 744
        745 746 747 748 749 750 751 752 753 754 755 756 757 758 759
        760 761 762 763 764 765 766 767 768 769 770 771 772 773 774
        775 776 777 778 779
        900 901 902 903 904 905 906 907 908 909 910 911 912 913 914
        915 916 917 918 919 920 921 922 923 924 925 926 927 928 929
        930 931 932 933 934 935 936 937 938 939 940 941 942 943 944
        945 946 947 948 949 950 951 952 953 954 955 956 957 958 959
        960 961 962 963 964 965 966 967 968 969 970 971 972 973 974
        975 976 977 978 979
c
fm14    1.0 30 (-2) (-6)
e14     6.83-7  5.531-3  0.821  17.0
fq14    e m
c
c       THIS CARD GIVES ADDITIONAL PRINTING INFORMATION IN THE OUTPUT
c
print
```

APPENDIX B

MCNP AND PDQ CALCULATIONS PERFORMED

Run	Description	Core Multiplication Factor
DD462	PDQ-7 calculation of graded fuel core model containing boron in the fuel end caps.	1.1608
DD470	PDQ-7 calculation of graded fuel core model without boron in the fuel end caps.	1.2994
DD478	PDQ-7 calculation of graded fuel core model containing boron in the fuel end caps. Homogenized hafnium was present in the central hole to the core midplane.	1.0301
ANS34	MCNP calculation of graded fuel core model without boron in the fuel end caps. The D_2O $S(\alpha,\beta)$ thermal library used was evaluated at 300 K.	1.2595 ± 0.0050[a]
ANS36	MCNP calculation of graded fuel core model containing boron in the fuel end caps. The D_2O $S(\alpha,\beta)$ thermal library used was evaluated at 300 K. All four control rods were fully inserted in the central hole.	0.9014 ± 0.0032
ANS38	MCNP calculation of graded fuel core model containing boron in the fuel end caps. The D_2O $S(\alpha,\beta)$ thermal library used was evaluated at 400 K.	1.1368 ± 0.0040
ANS39	MCNP calculation of graded fuel core model containing boron in the fuel end caps. The D_2O $S(\alpha,\beta)$ thermal library used was evaluated at 300 K.	1.1205 ± 0.0045
ANS41	MCNP calculation of graded fuel core model containing boron in the fuel end caps. The D_2O $S(\alpha,\beta)$ thermal library used was evaluated at 300 K. The region above the bottom fuel element and next to the top fuel element was a void.	1.0962 ± 0.0044

Run	Description	Core Multiplication Factor
ANS42	MCNP calculation of graded fuel core model containing boron in the fuel end caps. The D_2O $S(\alpha,\beta)$ thermal library used was evaluated at 300 K. The coolant channels in both fuel elements were voided.	1.0661 ± 0.0042
ANS43	MCNP calculation of graded fuel core model containing boron in the fuel end caps. There was no $S(\alpha,\beta)$ thermal library used in this calculation.	1.1343 ± 0.0033
ANS45	MCNP calculation of graded fuel core model containing boron in the fuel end caps. The D_2O $S(\alpha,\beta)$ thermal library used was evaluated at 300 K. All four control rods are at the fully removed position (100 mm above the top element).	1.1162 ± 0.0040
ANS46	MCNP calculation of graded fuel core model containing boron in the fuel end caps. All eight safety rods were fully inserted. The D_2O $S(\alpha,\beta)$ thermal library used was evaluated at 300 K.	0.8568 ± 0.0030
ANS48	MCNP calculation of graded fuel core model containing boron in the fuel end caps. The D_2O $S(\alpha,\beta)$ thermal library used was evaluated at 300 K. Four voided beam tubes were modeled.	1.1302 ± 0.0033
ANS49	MCNP calculation of graded fuel core model containing boron in the fuel end caps. All four control rods were inserted to core midplane. The entire central hole was voided. The D_2O $S(\alpha,\beta)$ thermal library used was evaluated at 300 K.	0.9453 ± 0.0043
ANS50	MCNP calculation of graded fuel core model containing boron in the fuel end caps. All four control rods were inserted to core midplane. The D_2O $S(\alpha,\beta)$ thermal library used was evaluated at 300 K.	1.0036 ± 0.0040

Run	Description	Core Multiplication Factor
ANS51	MCNP calculation of graded fuel core model containing boron in the fuel end caps. All four control rods were inserted to core midplane. No D_2O $S(\alpha,\beta)$ thermal library was used. Analog capture was used below 0.625 eV and importance weighting was begun 55 cm into the reflector.	0.9942 ± 0.0039
ANS52	MCNP calculation of graded fuel core model containing boron in the fuel end caps. All four control rods were inserted to core midplane. No D_2O $S(\alpha,\beta)$ thermal library was used. Importance weighting was begun 55 cm into the reflector.	0.9981 ± 0.0034
ANS53	MCNP calculation of graded fuel core model containing boron in the fuel end caps. There was no $S(\alpha,\beta)$ thermal library used in this calculation. The free gas temperature used was 300 K for all liquid except the D_2O above the fuel elements which was 350 K. The free gas temperature of the fuel and all Al-6061 was 350 K.	1.1232 ± 0.0033
ANS59	MCNP calculation of graded fuel core model containing boron in the fuel end caps. The D_2O $S(\alpha,\beta)$ thermal library used was evaluated at 300 K. Control rods were inserted to core midplane. The weight window generator was used to optimize a flux tally in the fuel and optimize the fast energy group within this tally.	0.9951 ± 0.0028
ANS60	MCNP calculation of graded fuel core model containing boron in the fuel end caps. The D_2O $S(\alpha,\beta)$ thermal library used was evaluated at 300 K. The weight windows from ANS59 were used in this problem.	1.0155 ± 0.0133

Run	Description	Core Multiplication Factor
ANS62	MCNP calculation of graded fuel core model containing boron in the fuel end caps. There was no S(α,β) thermal library used in this calculation. Analog capture was used in the thermal region. Spatial weight windows were generated. The flux tally in the fuel was optimized. Control rods were inserted to core midplane.	1.0005 ± 0.0053
ANS63	MCNP calculation of graded fuel core model containing boron in the fuel end caps. There was no S(α,β) thermal library used in this calculation. Analog capture was used in the thermal region. Energy-dependent weight windows were generated over 9 energy groups. The thermal energy group of the flux tally in the fuel was optimized. Control rods were inserted to core midplane.	1.0017 ± 0.0039
ANS64	MCNP calculation of graded fuel core model containing boron in the fuel end caps. The D_2O S(α,β) thermal library used was evaluated at 300 K. The weight windows from ANS62 were used in this problem. Control rods were inserted to core midplane.	1.0136 ± 0.0101
ANS65	MCNP calculation of graded fuel core model containing boron in the fuel end caps. The D_2O S(α,β) thermal library used was evaluated at 300 K. The weight windows from ANS63 were used in this problem. Control rods were inserted to core midplane.	1.0007 ± 0.0052
ANS66	MCNP calculation of graded fuel core model containing boron in the fuel end caps. There was no D_2O S(α,β) thermal library used. Analog capture was used in the thermal region. Energy-dependent weight windows were generated optimizing the thermal group in a D_2O reflector cell. The cell position was Z = -499.0 to 499.0 mm, R = 265.5 to 365.5 mm. Control rods were inserted to core midplane.	1.0113 ± 0.0039

Run	Description	Core Multiplication Factor
ANS67	MCNP calculation of graded fuel core model containing boron in the fuel end caps. The D_2O $S(\alpha,\beta)$ thermal library used was evaluated at 300 K. Control rods were inserted to core midplane. Weight windows from ANS63 were used a KSRC card was used instead of a SRCTP.	0.966 ± 0.0109
ANS69	MCNP calculation of graded fuel core model containing boron in the fuel end caps. The D_2O $S(\alpha,\beta)$ thermal library used was evaluated at 300 K. Control rods were inserted to core midplane. Weight windows from ANS66 were used.	1.0007 ± 0.0140
ANS70	MCNP calculation of graded fuel core model containing boron in the fuel end caps. No D_2O $S(\alpha,\beta)$ thermal library was used in this calculation. Analog capture was used in the thermal region. Energy-dependent weight windows were generated optimizing the thermal group in the fuel regions. No control rods were present.	1.1290 ± 0.0035
ANS71	MCNP calculation of graded fuel core model containing boron in the fuel end caps. The D_2O $S(\alpha,\beta)$ thermal library used was evaluated at 300 K. Control rods were inserted to core midplane. Weight windows from ANS70 were used.	1.0002 ± 0.0036
ANS72	MCNP calculation of graded fuel core model containing boron in the fuel end caps. The D_2O $S(\alpha,\beta)$ thermal library used was evaluated at 300 K. Control rods were inserted to core midplane. Weight windows from ANS70 were used. The U-235 and U-238 cross sections were evaluated at 600 K.	0.9953 ± 0.0052

Run	Description	Core Multiplication Factor
ANS73	MCNP calculation of graded fuel core model containing boron in the fuel end caps. The D_2O $S(\alpha,\beta)$ thermal library used was evaluated at 300 K. Control rods were inserted to core midplane. Weight windows from ANS70 were used. The U-235 and U-238 cross sections were evaluated at 900 K.	0.9938 ± 0.0053
ANS74	MCNP calculation of graded fuel core model containing boron in the fuel end caps. The D_2O $S(\alpha,\beta)$ thermal library used was evaluated at 300 K. Control rods were inserted to core midplane.	1.0002 ± 0.0037
ANS75	MCNP calculation of graded fuel core model containing boron in the fuel end caps. The D_2O $S(\alpha,\beta)$ thermal library used was evaluated at 300 K. Analog capture was used in the thermal region. Control rods were inserted to core midplane.	1.0014 ± 0.0078
ANS76	MCNP calculation of graded fuel core model containing boron in the fuel end caps. No D_2O $S(\alpha,\beta)$ thermal library was used in this calculation. Control rods were inserted to core midplane.	1.0145 ± 0.0046
ANS77	MCNP calculation of graded fuel core model containing boron in the fuel end caps. The D_2O $S(\alpha,\beta)$ thermal library used was evaluated at 300 K. Control rods were inserted to core midplane. Importance modelling was performed in the reflector.	0.9974 ± 0.0080
ANS80	MCNP calculation of graded fuel core model containing boron in the fuel end caps. The D_2O $S(\alpha,\beta)$ thermal library used was evaluated at 300 K. Weight windows from ANS70 were used. No control rods were present.	1.1319 ± 0.0045

Run	Description	Core Multiplication Factor
ANS81	MCNP calculation of graded fuel core model containing boron in the fuel end caps. The D_2O $S(\alpha,\beta)$ thermal library used was evaluated at 300 K. No control rods were present.	1.1308 ± 0.0031

a. The statistical uncertainties reported with all MCNP calculations represent one standard deviation.